ANALYSIS OF A PARALLEL ARRAY OF WAVEGUIDE OR CAVITY-BACKED RECTANGULAR SLOT ANTENNAS

Thesis for the Degree of Ph. D.
MICHIGAN STATE UNIVERSITY
SATNAM PRASAD MATHUR
1974

This is to certify that the

thesis entitled

ANALYSIS OF A PARALLEL ARRAY OF WAVEGUIDE
OR CAVITY-BACKED RECTANGULAR SLOT ANTENNAS

presented by

Satnam Prasad Mathur

has been accepted towards fulfillment
of the requirements for

Ph.D. degree in Electrical Engineering and System Science

Dennis P. Nyquist
Major professor

Date April 22, 1974

O-7639

W—004

ABSTRACT

ANALYSIS OF A PARALLEL ARRAY OF WAVEGUIDE OR CAVITY-BACKED RECTANGULAR SLOT ANTENNAS

By

Satnam Prasad Mathur

The circuit and radiation properties of a finite parallel array of N transverse, waveguide-backed, rectangular slot antennas are investigated in this thesis. A theoretical analysis is based upon a rigorous integral equation approach, and the theoretically predicted results are compared with experimental measurements.

An array of flush-mounted slot antennas consists of N parallel, transverse slots cut in an infinitesimally thin ground plane of large lateral extent and backed by a rectangular waveguide or cavity. Two modes of array excitation are considered: first by an incident dominant-mode wave in the backing waveguide and secondly by impressed driving currents maintained at the centers of one (or more) slots by a system of input currents.

In the theoretical investigations, a system of N coupled, Hallén-type integral equations for the N unknonw slot field distributions in the apertures of the array elements, maintained by either type of excitation, are formulated. These equations are solved numerically when the array is excited by an incident, dominant-mode wave in the backing waveguide and by an approximate analytical method (new, extended King-Sandler array theory) when the array is driven by a system of input currents.

Numerical results for either type of array excitation indicate (for appropriate slot and waveguide dimensions) the existence of a slow wave along the array aperture. It is also demonstrated that the phase velocity of the traveling wave along the array aperture can be controlled by varying the width of the backing waveguide (if the array is excited by a dominant-mode wave) and that scanning of radiation beam is consequently possible. No such beam scanning can be achieved by variation of waveguide width when the array is excited by a system of input currents, indicating a behavior similar to that for a Yagi-Uda slot array cut in a ground plane in an otherwise unbounded space. Phase velocity of the aperture field along the array is also sensitive to slot lengths and element spacings. Optimum slot dimensions to achieve endfire radiation of maximum directivity with reasonable side and back lobe levels are determined.

Impedance characteristics of the array are studied for both types of excitation. For the array excited by an incident wave, the SWR in the driving waveguide is relatively insensitive to backing waveguide width while it is quite sensitive to slot parameters (dimensions and spacings). Impedance of the Yagi-Uda parasitic, waveguide-backed slot array behaves essentially as that of a complementary dipole array except for a shift in resonant length of the driven element.

An experimental investigation of slot field distributions, the distribution of aperture field along the array, the SWR in the transmission system exciting the array, and the array radiation field is carried out. Excellent agreement between experimental results and those of the numerical, analytical solution is obtained for the array excited by an incident waveguide mode. It is indicated that the new, approximate parasitic array theory for waveguide-backed slots predicts accurate results for arrays of narrow slots having deep backing waveguides or cavities.

ANALYSIS OF A PARALLEL ARRAY OF WAVEGUIDE OR CAVITY-BACKED RECTANGULAR SLOT ANTENNAS

By

Satnam Prasad Mathur

A THESIS

Submitted to
Michigan State University
in partial fulfillment of the requirements
for the degree of

DOCTOR OF PHILOSOPHY

Department of Electrical Engineering and System Science

1974

ACKNOWLEDGMENT

The author wishes to express his sincere appreciation to his major professor, Dr. D.P. Nyquist, for his guidance and assistance throughout this study. His active participation in the project and his willingness to discuss problems as they arose made working with him a rewarding experience. Thanks also go to Dr. J. Asmussen and Dr. J.S. Frame for their many suggestions and technical advice on problems encountered in the research. He wishes to thank other members of his guidance committee for their time and interest in this study: Dr. B. Ho and Dr. K.M. Chen.

The research reported in this thesis was supported, in parts, by Division of Engineering Research, Michigan State University.

Finally, special thanks go to Mr. Marc Butler and Mr. R. Kotsch for their help and encouragement throughout this study.

TABLE OF CONTENTS

LIST OF TABLES

LIST OF FIGURES

Figure Page

Figure Page

CHAPTER 1

INTRODUCTION

A theoretical and experimental investigation on the circuit and radiation properties of a finite, waveguide-backed slot array is performed. The slot array consists of a system of narrow slots cut in a thin conducting ground plane of large lateral extent and backed by a waveguide designed to support the dominant TE_{10}-mode wave. The slots are cut transversely through the broad wall of the waveguide, which can be arbitrarily terminated at each of its ends. Two methods of array excitation are investigated: 1) an incident dominant-mode wave in the backing waveguide and 2) an impressed current between the edges of one or more slots at their centers. Such slot arrays are popular for aerospace applications due to their inherent adaptability to flush mounting.

It has been demonstrated by Burton and King(1) that a slow wave can be excited along a parallel array of appropriately spaced, resonant-length slots cut in a large, thin ground plane. Since such a slot array is the complementary antenna to a parallel array of cylindrical dipoles, the existence of a slow wave along the slotted ground plane is also suggested by the results of investigations by Mailloux(2), (3) on the excitation of a traveling surface waves along long Yagi-Uda dipole arrays. It has also been demonstrated by Coe and Held(4) that a similar slow wave aperture field is obtained when each individual slot is backed by a rectangular cavity.

If the slot array is backed by a waveguide on one side of the ground plane, it may be possible to control the phase velocity of the traveling wave along the array aperture by adjusting the phase velocity of the fast, dominant wave in the backing waveguide. It has been demonstrated by Hyneman$^{(5)}$, using an approximate variational method, that, for an infinite array of closely spaced transverse slots, two useful means of radiation pattern control involve either adjusting the transverse geometry of the backing waveguide or varying the element spacing in the slot array. It is, therefore, possible to excite a slow wave in the array aperture and consequently achieve endfire radiation. By appropriately controlling suitable array parameters or the backing waveguide dimensions, some degree of control can be achieved over the phase velocity of the traveling wave aperture field with a consequent capability to scan the direction of the radiation beam. This phenomenon is studied in detail in the present research.

Elliott$^{(6)}$ investigated (using an approximate variational technique) a serrated waveguide of infinite length where infinitesimally spaced transverse slots are cut into, and extended completely across the broad waveguide wall of variable thickness. Elliott concluded from his study of the serrated waveguide that the fundamental mode in the waveguide and along the array aperture has a complex propagation constant, which is insensitive to frequency but modestly sensitive to wall thickness. It was also found that the phase velocity of the fundamental mode wave along the serrated waveguide can be varied by controlling the serration width to spacing ratio or serration length (which is equal to the broad wall width).

From the experimental investigations by Kelly and Elliott(7) of the same serrated waveguide it was confirmed that the phase velocity can be effectively controlled by varying the wall thickness. However, thick-walled serrated waveguide presented practical problems in its construction, while it was found that varying serration width to spacing ratio was ineffective insofar as the variation of complex propagation constant in the serrated waveguide was concerned. In summary, only the thin-walled, serrated waveguide provided least mechanical problems in its construction while a reasonable variation of leakage (attenuation) was achieved as the length of serrations was varied (while phase constant remained relatively insensitive to such variations). Among effective methods for wide control over phase constant (phase velocity) were found to be the variation of serrated waveguide width and the properties of its dielectric loading.

In light of the above observations, it was decided to study more rigorously the radiation and circuit properties of a finite parallel array of N waveguide-backed, rectangular slot antennas cut transversely through the infinitesimally thin broad wall of a backing waveguide. It is assumed that the slots are backed by a waveguide of variable width "a" which is terminated by arbitrary reflection coefficients Γ_1 and Γ_2 at its two ends. It is further assumed that the array is excited either by a dominant-mode incident wave in the backing waveguide or by means of impressed (input) currents at the centers of any number of the array elements. A rigorous integral equation technique is used to determine the slot fields in the elements of the finite array. In terms of these slot fields, the circuit and radiation characteristics of the array are determined for various slot parameters and backing waveguide dimensions to optimize the array design and to determine the feasibility of scanning the radiation beam from endfire to off-endfire. A set of experimental measurements is made to confirm the theoretical predictions.

Using a technique similar to those reported by Galejs(8), (9) for the analysis of single, cavity-backed slots, a system of N coupled, Hallén type integral equations for the N unknown slot field distributions in the apertures of the array elements is formulated as indicated in Chapter 2. These equations are solved both numerically by Harrington's moment method(10) and analytically (approximate) by a modification and extension of the King-Sandler dipole array theory(11) to the waveguide-backed slot array. The radiation field of the array as well as its circuit properties can be readily calculated in terms of the known slot fields.

The numerical solution for the slot fields in the aperture of the array excited by a dominant-mode-incident wave is indicated in Chapter 3. Numerical results presented in Chapter 3 for five and ten element arrays indicate the existence of a slow wave aperture field for an optimal set of array parameters, with resultant endfire radiation. The feasibility of scanning the radiation beam of the array by varying the phase velocity of the traveling wave in its aperture through variations of the backing waveguide width is demonstrated.

Chapter 4 develops an approximate, analytical solution for the slot fields in the array excited by impressed δ-function currents at the centers of one (or more) of its elements. Results presented in Chapter 4 indicate the existence of a slow wave along the array aperture, and hence the existence of endfire radiation, for an optimal choice of array parameters in five, ten and twenty-five element arrays. The new, extended King-Sandler array theory also predicts accurate results for an array of slots cut in a ground screen immersed in otherwise unbounded free-space (complementary to a dipole array) and for a single slot backed by a rectangular cavity; the new predictions agree well with the published results by Galejs(8) and by King, Mack and Sandler(12). It is also pointed out in Chapter 4 that this new array theory does not predict accurate results for an array of wide slots or for array backed by a shallow waveguide (or a cavity).

Experimental results are compared with corresponding predicted theoretical results in Chapter 5. It is found that the numerical solution predicts accurate results (agrees well with experiments) for an eight-element, waveguide-backed slot array excited by a TE_{10}-mode incident wave. However, the new theory for a waveguide-backed, Yagi-Uda slot array excited by an impressed current predicts accurate results (agrees relatively well with experiment) only for an array of narrow slots.

The circuit properties of the slot array excited by a dominant-mode-incident wave in the backing waveguide indicates a reasonably good match between the antenna input terminals and the standard waveguide circuitory which is employed to excite the array i.e., the SWR is relatively low. As the slot lengths exceed their resonant lengths, the SWR in the backing waveguide increases sharply. As the width of the backing waveguide is reduced (to vary the phase velocity of the aperture field) so its dominant mode approaches cut off, the SWR also rises, although not as sharply as might be anticipated.

If the slot array is driven by an impressed current, the input admittance to the driven element passes through a resonance when the length of that element lies between 0.22 λ_o and 0.23 λ_o for both five- and ten-element arrays. The ten-element Yagi-Uda slot array displays a band width of approximately 400 MHz for a design where its input admittance passes through resonance at the center frequency of 3.0 GHZ.

A brief summary as well as conclusions are included in Chapter 6.

CHAPTER 2

FORMULATION OF BASIC THEORY FOR THE WAVEGUIDE-BACKED SLOT ARRAY

2.1 Geometry and Statement of the Problem:

In this chapter a system of Hallén-type integral equations will be developed for the voltage distribution in the elements of a parallel array of N waveguide-backed, rectangular slot antennas. The final expressions for E-plane and H-plane radiation fields of the array and its circuit properties are then calculated in terms of these slot fields.

The geometrical structure of the array of N waveguide-backed slots is shown in Figure (2.1). N slots of width 2ϵ with centers at $x = \frac{a}{2}$ are cut parallel to the x-axis in a large conducting ground plane at locations $z = z_1$, $z = z_2$, $z = z_3, \ldots,$ $z = z_k, \ldots, z = z_N$. The slots are backed by a rectangular waveguide of width "a" and height "b" which is terminated by reflection coefficients Γ_1 and Γ_2, respectively, at $z = 0$ and $z = c$. The kth element of the array has length $2h_k$ and is center-driven by an input current I_k; an approximately one-dimensional slot field $E_{kz}(x)$ is excited in its aperture by I_k and its coupling to other elements of the array. When the array is excited alternatively by an incident dominant-mode wave in the backing waveguide, then $I_k = 0$, for all k. In section 2.2, a theory encompassing both modes of excitation is presented.

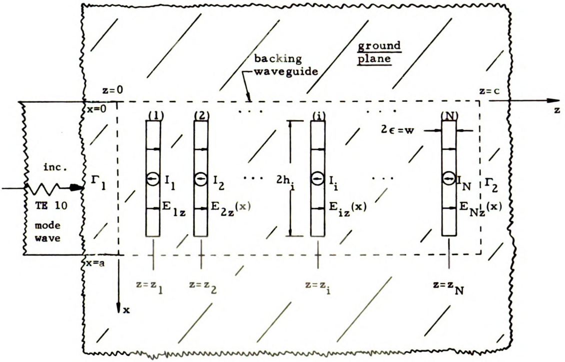

a. Top view of waveguide (or cavity) backed slot array.

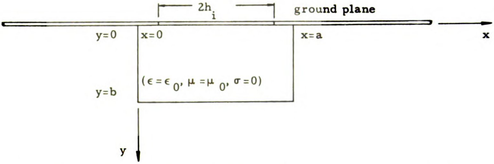

b. Side view (in a cross section at $z=z_i$) of waveguide (or cavity) backed slot array.

Figure 2.1. Geometrical structure of a waveguide (or cavity) backed parallel array of N rectangular slots.

2.2 Integral Equations for the Slot Field Distribution:

The system of integral equations for the electric field distributions in the rectangular slots is based upon the boundary condition for the tangential components of magnetic field at their apertures. A harmonic time dependence of the form $e^{j\omega t}$ is presumed throughout the development. Let $\vec{H}^o(x,y = 0^-,z)$ be the magnetic field at a point just outside the aperture in the exterior region, $y < 0$ and $\vec{H}^i(x,y = 0^+,z)$ be that at a point just inside the aperture in the interior region $y > 0$, then the boundary condition for the tangential magnetic field at the aperture of the kth slot requires that

$$\hat{n} \times [\vec{H}^i_k(x,y = 0^+,z) - \vec{H}^o_k(x,y = 0^-,z)] = \vec{K}^e_k(x,z) \tag{2.1}$$

where $\hat{n} = \hat{y}$ is the unit normal vector to the aperture pointing from the exterior region $(y < 0)$ into the interior region $(y > 0)$, and $\vec{K}^e_k(x,z)$ is the impressed electric surface current maintained in the kth slot. In all expressions, subscripts refer to a specific element in the array.

It is assumed that each slot is in general driven by a current I_k of angular frequency ω flowing in a wire of infinitesimal thickness at the center $(x = \frac{a}{2})$ of the slot. Therefore, $\vec{K}^e_k(x,z)$ can be expressed as

$$\vec{K}^e_k(x,z) = -\hat{z}\ I_k \delta(x - \frac{a}{2}) \tag{2.2}$$

where $\delta(x - \frac{a}{2})$ is the Dirac delta function.

The scalar component equations from expression (2.1) are

$$\left.\begin{aligned} H^{i}_{kx}(x,y=0^{+},z) - H^{o}_{kx}(x,y=0^{-},z) &= I_{k}\delta(x-\tfrac{a}{2}) \\ H^{i}_{kz}(x,y=0^{+},z) &= H^{o}_{kz}(x,y=0^{-},z)\ . \end{aligned}\right\} \qquad (2.3)$$

For narrow slots with $h_k \gg \varepsilon$ and $2\varepsilon/\lambda_0 \ll 1$, where λ_0 is the free-space wavelength, it is well known that(9), (13)

$$H^{i}_{kz}(x,y=0^{+},z) \approx 0 \quad \text{and} \quad H^{o}_{kz}(x,y=0^{-},z) \approx 0\ .$$

The basic boundary condition to be satisfied at $y = 0$ therefore takes the form:

$$H^{i}_{kx}(x,\ 0^{+},z) - H^{o}_{kx}(x,\ 0^{-},z) = I_{k}\delta(x - a/2)\,. \qquad (2.4)$$

2.2.1 Magnetic Field in the Interior Region ($y > 0$):

The EM field in the interior of the backing waveguide or cavity can be regarded (by linear superposition) as having two distinct sources of excitation, namely:

(i) the EM field radiated into the interior region through the aperture of the kth slot with its impressed surface current $\vec{K}^{e}_{k}(x,z)$, $(k = 1,2,\ldots,N)$ and

(ii) the EM field of an incident dominant-mode wave in the backing waveguide. It is assumed that the backing waveguide supports only the TE_{10} dominant-mode as a propagating wave.

In general, excitation is provided by the simultaneous application of an incident TE_{10} wave and the impressed surface currents $\vec{K}^{e}_{k}(x,z)$; in practical implementation of the array, however, only one or the other of the two excitations is utilized.

The interior magnetic field can be expressed as the superposition of the magnetic field of the TE_{10} wave incident at $z = 0$

with arbitrary reflection coefficients Γ_1 and Γ_2 at $z = 0$ and $z = c$ respectively, and that radiated by the aperture fields of the kth slot (which involves the impressed surface current $\vec{K}_k^e(x,z)$).

As illustrated in Figure (2.2b), which considers the backing waveguide with a load Z_L at $z = c$ corresponding to reflection coefficient Γ_2 and a TE_{10} wave incident at $z = 0$, the interior field consists of traveling TE_{10} waves propagating in the $\pm$ z directions.

It can be shown$^{(14)}$ that the transverse fields for such a wave are:

$$\left.\begin{aligned} \vec{E}_t &= E_o\vec{e}_1^{\,h}(1 + \Gamma_2 e^{2j\beta_{10}^h z})e^{-j\beta_{10}^h z} \\ \text{and}\qquad \vec{H}_t &= \frac{E_o}{Z_{10}^h}(\hat{z}\times\vec{e}_1^{\,h})(1 - \Gamma_2 e^{2j\beta_{10}^h z})e^{-j\beta_{10}^h z} \end{aligned}\right\} \qquad (2.5)$$

where $\Gamma_2 = \left(\frac{Z_L - Z_1^h}{Z_L + Z_1^h}\right)e^{-2j\beta_1^h c}$,

$Z_{10}^h = \frac{k_o\zeta_o}{\beta_{10}^h}$ = wave impedance for TE_{10} mode,

$\beta_{10}^h = \sqrt{k_o^2 - (\pi/a)^2}$ = phase constant of TE_{10} mode,

$\zeta_o = 120\pi$ = intrinsic impedance of free space,

$k_o = w\sqrt{\mu_o\varepsilon_o} = \frac{2\pi}{\lambda_o}$ = free-space wave number,

and E_o = arbitrary amplitude constant for incident TE_{10} mode.

$\vec{e}_1^{\,h}$ and $\vec{h}_1^{\,h} = \frac{1}{Z_{10}^h}(\hat{z}\times\vec{e}_1^{\,h})$ are the dominant, transverse mode fields with the assumed normalization condition

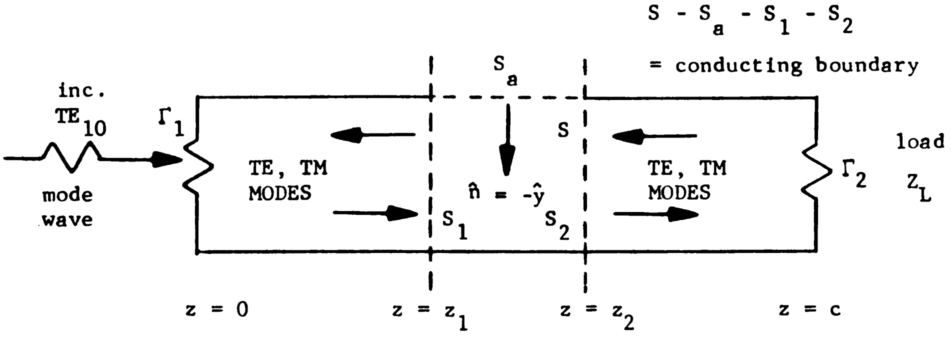

(a) General Problem.

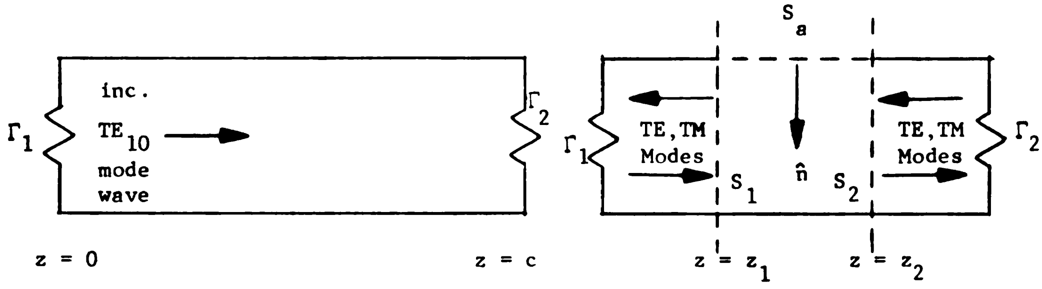

(b) Field maintained by incident TE_{10} mode only.

(c) Field maintained by slot fields in aperture S_a.

Figure 2.2. Illustration of principle of superposition for the determination of interior magnetic field.

$$\int_{c.s.} (\vec{e}_1^{\,h} \times \vec{h}_1^{\,h}) \cdot \hat{z}ds = 1$$

and can be expressed as

$$\vec{e}_1^{\,h} = -\hat{y}\sqrt{\frac{2Z_{10}^h}{ab}}\ \sin(\frac{\pi x}{a})$$

$$\vec{h}_1^{\,h} = (\frac{1}{Z_{10}^h})(\hat{z} \times \vec{e}_1^{\,h}) = \hat{x}\sqrt{\frac{2}{ab\ Z_{10}^h}}\ \sin(\frac{\pi x}{a})\ .$$

Expressions (2.5) can now be rewritten as:

$$\left.\begin{aligned} \vec{E}_t(x,z) &= -\hat{y}\ E_o\sqrt{\frac{2Z_{10}^h}{ab}}\ (1 + \Gamma_2 e^{2j\beta_{10}^h z})e^{-j\beta_{10}^h z}\ \sin(\frac{\pi x}{a}) \\ \vec{H}_t(x,z) &= \hat{x}\ E_o\sqrt{\frac{2}{abZ_{10}^h}}\ (1 - \Gamma_2 e^{2j\beta_{10}^h z})e^{-j\beta_{10}^h z}\ \sin(\frac{\pi x}{a}) \end{aligned}\right\} . \qquad (2.6)$$

As illustrated in Figure (2.2c), the interior field excited by the slot fields in the apertures of the array elements (which are ultimately related to the impressed surface current $\vec{K}_k^e(x,z)$ in the kth slot) will consist of both TE_q as well as TM_q modes beyond the cross-sectional planes at $z = z_1$ and $z = z_2$. In general, these fields can be expressed by modal expansions(14) as:

$$\left.\begin{aligned} \vec{E} &= \sum_q [A_q \vec{E}_q^- + B_q \vec{E}_q^+] \\ \vec{H} &= \sum_q [A_q \vec{H}_q^- + B_q \vec{H}_q^+] \end{aligned}\right\} \ldots \quad \text{for} \quad z \le z_1$$

and

$$\left.\begin{aligned} \vec{E} &= \sum_q [C_q \vec{E}_q^+ + D_q \vec{E}_q^-] \\ \vec{H} &= \sum_q [C_q \vec{H}_q^+ + D_q \vec{H}_q^-] \end{aligned}\right\} \ldots \quad \text{for} \quad z \ge z_2$$

where summations over q include all TE as well as all TM modes, and the modal fields are(14)

$$\vec{E}_q^{\pm} = [\vec{e}_q(x,y) \pm \vec{e}_{zq}(x,y)]e^{\mp \gamma_q z}$$

$$\vec{H}_q^{\pm} = [\pm \frac{1}{Z_q}\, \hat{z} \times e_q(x,y) + \vec{h}_{zq}(x,y)]e^{\mp \gamma_q z} .$$

γ_q is the propagation constant of the qth guided wave mode. Reflection coefficients Γ_{1q} and Γ_{2q} are defined as

$$\Gamma_{1q} \equiv \frac{B_q}{A_q} = \left.\frac{\text{amplitude of qth mode wave incident upon } z = 0}{\text{amplitude of qth mode wave reflected from } z = 0}\right|_{z=0}$$

and

$$\Gamma_{2q} = \frac{D_q}{C_q} = \left.\frac{\text{amplitude of qth mode wave incident upon } z = c}{\text{amplitude of qth mode wave reflected from } z = c}\right|_{z=c} .$$

Therefore, the modal expansions can be rewritten as

$$\left.\begin{aligned} \vec{E} &= \sum_q A_q[\vec{E}_q^- + \Gamma_{1q}\, \vec{E}_q^+] \\ \vec{H} &= \sum_q A_q[\vec{H}_q^- + \Gamma_{1q}\, \vec{H}_q^+] \end{aligned}\right\} \ldots \quad \text{for} \quad z \le z_1 \tag{2.7a}$$

and

$$\left.\begin{aligned} \vec{E} &= \sum_q C_q[\vec{E}_q^+ + \Gamma_{2q}\, \vec{E}_q^-] \\ \vec{H} &= \sum_q C_q[\vec{H}_q^+ + \Gamma_{2q}\, \vec{H}_q^-] \end{aligned}\right\} \ldots \quad \text{for} \quad z \ge z_2 \ . \tag{2.7b}$$

Let the following surfaces be defined:

S = closed surface consisting of waveguide boundaries and transverse cross-sectional planes through $z = z_1$ and $z = z_2$.

S_a = aperture surface consisting of the slots which comprise the array elements.

S_1 = cross-sectional surface through $z = z_1$.

S_2 = cross-sectional surface through $z = z_2$.

The boundary conditions to be applied at the waveguide boundary surface $S - S_1 - S_2$ are:

$\hat{n} \times \vec{E}(\vec{r}) = 0$ ... in the surface $S - S_1 - S_2 - S_a$ outside the aperture (on the conducting boundaries)

$\hat{n} \times \vec{E}(\vec{r}) \neq 0$ ... in the surface S_a of the array (on the aperture surface) .

Making use of the Lorentz Lemma and the normalization condition

$$\int_{c.s.} (\vec{e}_q \times \vec{h}_q) \cdot \hat{z} ds = 1 \quad \text{... for all } q$$

where c.s. = any waveguide cross-section, it can be shown(15) that constants A_q and C_q are given as

$$A_q = \frac{I_q^{(+)} + \Gamma_{2q} I_q^{(-)}}{2(\Gamma_{1q}\,\Gamma_{2q} - 1)} \tag{2.8}$$

and

$$C_q = \frac{I_q^{(-)} + \Gamma_{1q}\, I_q^{(+)}}{2(\Gamma_{1q}\,\Gamma_{2q} - 1)} \tag{2.9}$$

where aperture integrals have been defined as

$$I_q^{(\pm)} = \int_{S_a} \hat{n} \cdot (\vec{E}^s \times \vec{H}_q^{(\pm)}) ds$$

and $\vec{E}^s$ is the slot field in the array aperture and $\hat{n} = -\hat{y}$.

At points in the aperture of the narrow slots, the slot field $\vec{E}^s$ can be approximated by the one-dimensional expression

$$\vec{E}^s \approx \hat{z}\, E_z^s(x,z) .$$

The integrand of $I_q^{(\pm)}$ can be rewritten as

$$\hat{n} \cdot (\vec{E}^s \times \vec{H}_q^{(\pm)}) = -\hat{y} \cdot (\hat{z}\, E_z^s \times \vec{H}_q^{(\pm)}) = E_z^s(\hat{x} \cdot \vec{H}_q^{(\pm)})$$

therefore the aperture integral becomes

$$I_q^{(\pm)} = \pm \int_{S_a} E_z^s(x',z')h_{xq}(x',0,z')e^{\mp\gamma_q z'}\, dx'dz'$$

or

$$I_q^{(\pm)} = \pm \sum_{i=1}^{N} \int_{S_{ia}} E_{iz}^s(x',z')h_{xq}(x',0,z')e^{\mp\gamma_q z'}\, dx'dz' \tag{2.10}$$

where S_{ia} is the aperture of ith slot in the N-element array.

The x-component of magnetic field can now be expressed as

$$\left.\begin{aligned} H_x(x,y,z) &= \sum_q A_q h_{xq}(x',z')[-e^{\gamma_q z} + \Gamma_{1q} e^{-\gamma_q z}] \quad \ldots \text{ for } \quad z \le z_1 \\ H_x(x,y,z) &= \sum_q C_q h_{xq}(x',z')[e^{-\gamma_q z} - \Gamma_{2q} e^{\gamma_q z}] \quad \ldots \text{ for } \quad z \ge z_2 \end{aligned}\right\} \tag{2.11}$$

The normal mode magnetic fields are$^{(14)}$

$$\left.\begin{aligned} (h_x)_{nm} &= \frac{1}{(k_c)_{nm}} \sqrt{\frac{\epsilon_m \epsilon_n}{abZ_{nm}^h}}\, (\frac{n\pi}{a})\ \sin(\frac{n\pi x}{a})\ \cos(\frac{m\pi y}{b}) \quad \ldots \text{ TE Modes} \\ (h_x)_{nm} &= \frac{1}{(k_c)_{nm}} \sqrt{\frac{\epsilon_m \epsilon_n}{abZ_{nm}^e}}\, (\frac{m\pi}{b})\ \sin(\frac{n\pi x}{a})\ \cos(\frac{m\pi y}{b}) \quad \ldots \text{ TM Modes} \end{aligned}\right\} \tag{2.12}$$

where

$(k_c)_{nm} = \sqrt{\gamma_{nm}^2 + k^2}$ = cut off wave number of nmth mode,

$$\epsilon_m = \begin{cases} 1 & \ldots \text{ for } \quad m = 0 \\ 2 & \ldots \text{ for } \quad m \neq 0 \end{cases}, \text{ and}$$

$Z_{nm}^{h,e}$ = wave impedance of (TE,TM) modes.

The above expressions of $(h_x)_q$ satisfy the ortho-normalization condition:

$$\int_{c.s.} \hat{z} \cdot (\vec{e}_p \times \vec{h}_q) ds = \delta_p^q = \begin{cases} 0 \ \ldots \ \text{for} \ \ p \neq q \\ 1 \ \ldots \ \text{for} \ \ p = q \ . \end{cases}$$

(p,q) are general indices which include all TE_{nm} and TM_{nm} modes.

If relations (2.9), (2.10) and (2.12) are used, then equations (2.11) can be expressed as:

$$H_x(x,y,z) = \frac{1}{\omega\mu_o}\left[\frac{\partial^2}{\partial x^2} + k_o^2\right]\int_{S_a} E_z^s(x',z')G^i(x,y,z,x',z')dx'dz' \ , \qquad (2.13a)$$

where the interior Green's function G^i is given by

$$G^i(x,y,z,x',z') = \frac{1}{ab}\sum_{n=1}^{\infty}\sum_{m=0}^{\infty} \frac{\epsilon_m}{\gamma_{nm}[1 - (\Gamma_1)_{nm}(\Gamma_2)_{nm}]}$$

$$\sin(\frac{n\pi x}{a})\sin(\frac{n\pi x'}{a})\cos(\frac{m\pi y}{b}) f_{nm}(z,z') \qquad (2.13b)$$

with

$$f_{nm}(z,z') = e^{-\gamma_{nm}|z-z'|} - (\Gamma_1)_{nm}e^{-\gamma_{nm}(z+z')} - (\Gamma_2)_{nm}e^{\gamma_{nm}(z+z')}$$

$$+ (\Gamma_1)_{nm}(\Gamma_2)_{nm}e^{\gamma_{nm}|z-z'|} \qquad (2.13c)$$

and in summary $\int_{S_a} = \sum_{i=1}^{N}\int_{S_{ia}}$,

$$(k_c)_{nm}^2 = k_o^2 + \gamma_{nm}^2 = k_x^2 + k_y^2 = (\frac{n\pi}{a})^2 + (\frac{m\pi}{b})^2$$

$$\gamma_{nm} = \begin{cases} \sqrt{k_x^2 + k_y^2 - k_o^2} & \ldots \ \text{for} \ \ k_o < (k_x^2 + k_y^2) \\ j\sqrt{k_o^2 - k_x^2 - k_y^2} & \ldots \ \text{for} \ \ k_o > (k_x^2 + k_y^2) \ . \end{cases}$$

$(\Gamma_1)_{nm}$ and $(\Gamma_2)_{nm}$ must be specified for various assumed terminations.

Expressions (2.6) along with equations (2.13) result in a total interior magnetic field at aperture surface $y = 0^+$ as:

$$H_x^i(x,z) = \frac{1}{\omega\mu_o}\left[\frac{\partial^2}{\partial x^2} + k_o^2\right]\int_{S_a} E_z^s(x',z')G^i(x,z,x',z')dx'dz'$$

$$+ E_o\sqrt{\frac{2}{abZ_{10}^h}}\,[1 - (\Gamma_2)_{10}e^{2j\beta_{10}^h z}]e^{-j\beta_{10}^h z}\sin(\frac{\pi x}{a}) \qquad (2.14a)$$

and equation (2.13b) gives

$$G^i(x,z,x',z') = \frac{1}{ab}\sum_{n=1}^{\infty}\sum_{m=0}^{\infty}\frac{\epsilon_m}{\gamma_{nm}[1 - (\Gamma_1)_{nm}(\Gamma_2)_{nm}]}\sin(\frac{n\pi x}{a})$$

$$\sin(\frac{n\pi x'}{a})f_{nm}(z,z'). \qquad (2.14b)$$

In equation (2.14a) $\int_{S_a}$ can be replaced by $\sum_{i=1}^{N}\int_{S_{ia}}$ where S_{ia} is defined as the aperture of ith slot

$$S_{ia} = \text{the slot surface} = \begin{cases} \frac{a}{2} - h_i \le x \le \frac{a}{2} + h_i \\ z_i - \epsilon \le z \le z_i + \epsilon . \end{cases}$$

Therefore, the interior magnetic field just inside the aperture of the kth slot at $y = 0^+$ is

$$H_{kx}^i(x,0^+,z) = \frac{1}{\omega\mu_o}\left[\frac{\partial^2}{\partial x^2} + k_o^2\right]\sum_{i=1}^{N}\int_{S_{ia}} E_{iz}^s(x',z')G^i(x,z,x',z')$$

$$dx'dz' + E_o\sqrt{\frac{2}{abZ_{10}^h}}\,[1 - (\Gamma_2)_{10}e^{2j\beta_{10}^h z}]\,e^{-j\beta_{10}^h z}\sin(\frac{\pi x}{a})$$

$$\ldots \text{ for } (x,z) \in S_{ka}. \qquad (2.15)$$

2.2.2 Magnetic Field in the Exterior Region $(y < 0)$:

It is well known that(16) a solution to Maxwell's equations for the EM field $\vec{E}(\vec{r})$, $\vec{B}(\vec{r})$ at any point in (otherwise unbounded) free space can be expressed in terms of its values on a closed surface S which encloses all the electric sources which maintain the field as

$$\vec{E}(\vec{r}) = -\oint_S \{j\omega\epsilon_o[\hat{n} \times \vec{H}(\vec{r}')]G(\vec{r},\vec{r}') + [\hat{n} \cdot \vec{E}(\vec{r}')]\nabla G(\vec{r},\vec{r}') + [\hat{n} \times \vec{E}(\vec{r}')] \times \nabla G(\vec{r},\vec{r}')\}ds' \quad (2.16)$$

$$\vec{H}(\vec{r}) = -\oint_S \{[\hat{n} \times \vec{H}(\vec{r}')] \times \nabla G(\vec{r},\vec{r}') - j\omega\epsilon_o[\hat{n} \times \vec{E}(\vec{r}')]G(\vec{r},\vec{r}') + [\hat{n} \cdot \vec{H}(\vec{r}')]\nabla G(\vec{r},\vec{r}')\}ds' \quad (2.17)$$

where $G(\vec{r},\vec{r}')$ is the Green's function for unbounded free-space

$$G(\vec{r},\vec{r}') = \frac{e^{-jk_o|\vec{r} - \vec{r}'|}}{4\pi|\vec{r} - \vec{r}'|},$$

$$k_o = \omega\sqrt{\mu_o\epsilon_o} = \text{free-space wave number},$$

and $\hat{n}$ is the outward directed unit normal vector to S. Jackson(16) has demonstrated that when the closed surface S assumes the form of an infinitesimally thin (plane) pancake shaped surface of infinite lateral extent which separates two half-space regions, then the EM field in either half-space can be expressed in terms of fields which are maintained on its plane boundary S_o as:

$$\vec{E}(\vec{r}) = -\int_{S_o} [\hat{n} \times \vec{E}(\vec{r}')] \times \nabla G^o(\vec{r},\vec{r}')ds' \quad (2.18)$$

$$\vec{H}(\vec{r}) = -\int_{S_o} \{-j\omega\epsilon_o[\hat{n} \times \vec{E}(\vec{r}\,')]G^o(\vec{r},\vec{r}\,') - [\hat{n} \cdot \vec{H}(\vec{r}\,')] \nabla G^o(\vec{r},\vec{r}\,')\}ds' \tag{2.19}$$

when $\hat{n}$ is the unit normal vector to the half-space boundary S_o which is directed into the field region of interest and $G^o(\vec{r},\vec{r}\,')$ is the free-space Green's function for a half-space

$$G^o(\vec{r},\vec{r}\,') = \frac{e^{-jk_o|\vec{r} - \vec{r}\,'|}}{2\pi|\vec{r} - \vec{r}\,'|} .$$

The boundary conditions at the surface S_o in the $y = 0$ plane are:

$$\left.\begin{array}{l} \hat{n} \times \vec{E}(\vec{r}\,') \neq 0 \\ \hat{n} \cdot \vec{H}(\vec{r}\,') \neq 0 \end{array}\right\} \text{... in the aperture surface } S_a \text{ of the array, and}$$

$$\left.\begin{array}{l} \hat{n} \times \vec{E}(\vec{r}\,') = 0 \\ \hat{n} \cdot \vec{H}(\vec{r}\,') = 0 \end{array}\right\} \text{... in the plane conducting surface } S_o - S_a \text{ outside the slot apertures.}$$

The integration over surface S_o in equation (2.19) therefore reduces to an integration over aperture surface S_a (in the $y' = 0$ plane) of the slot array as

$$\vec{H}(\vec{r}) = -\int_{S_a} \{-j\omega\epsilon_o[\hat{n} \times \vec{E}(\vec{r}\,')]G^o(\vec{r},\vec{r}\,') + [\hat{n} \cdot \vec{H}(\vec{r}\,')]\nabla G^o(\vec{r},\vec{r}\,')\}ds'. \tag{2.20}$$

In the array aperture surface S_a, $\hat{n} = -\hat{y}$ and $ds' = dx'dz'$ and for narrow slots

$$\begin{aligned} &\vec{E}(\vec{r}\,') = \vec{E}^s(\vec{r}\,') \approx \hat{z}\, E_z^s(\vec{r}\,') \\ &E_x^s(\vec{r}\,') \approx 0 \text{ and } \frac{\partial E_x^s}{\partial z} \approx 0. \end{aligned} \tag{2.21}$$

From the Maxwell equation

$$\nabla \times \vec{E} = -j\omega\mu_o\vec{H} ,$$

$$\hat{n} \cdot \vec{H}(\vec{r}') \approx \frac{j}{\omega\mu_o}\frac{\partial E_z^s}{\partial x'} . \tag{2.22}$$

Substituting equations (2.21) and (2.22) into equation (2.20) yields

$$H_x(x,0^-,z) = -\int_{S_a} \{j\omega\epsilon_o E_z^s(x',z')G^o(x,z,x',z') + \frac{j}{\omega\mu_o}\frac{\partial}{\partial x'} E_z^s(x',z')$$

$$\frac{\partial}{\partial x} G^o(x,z,x',z')\}dx'dz' \quad \ldots \quad \text{for} \quad (x,z) \in S_a \tag{2.23}$$

where

$$G^o(x,z,x',z') = \frac{e^{-jk_o\sqrt{(x-x')^2 + (z-z')^2}}}{2\pi\sqrt{(x-x')^2 + (z-z')^2}} .$$

It is readily verified that

$$\frac{\partial}{\partial x} G^o(x,z,x',z') = -\frac{\partial}{\partial x'} G^o(x,z,x',z')$$

$$\frac{\partial^2}{\partial x^2} G^o(x,z,x',z') = -\frac{\partial^2}{\partial x \partial x'} G^o(x,z,x',z')$$

and the boundary condition on the slot field at $\frac{a}{2} \pm h_k$ requires that

$$E_z^s(x' = \frac{a}{2} \pm h_k, z') = 0 . \tag{2.24}$$

Equation (2.23) can consequently be written as

$$H_{kx}^o(x,0^-,z) = \frac{-j}{\omega\mu_o}\sum_{i=1}^{N}\int_{z_i-\epsilon}^{z_i+\epsilon}\int_{a/2-h_i}^{a/2+h_i}\{\frac{\partial}{\partial x'} E_{iz}^s(x',z')\frac{\partial}{\partial x} G^o(x,z,x',z')$$

$$+ k_o^2 E_z^s(x',z')G^o(x,z,x',z')\}dx'dz' \quad \ldots \quad \text{for} \quad (x,z) \in S_{ka} . \tag{2.25}$$

Upon integrating by parts with respect to x' and making use of equation (2.24), equation (2.25) can finally be expressed as

$$H^o_{kx}(x,0^-,z) = \frac{-j}{\omega\mu_o}\left[\frac{\partial^2}{\partial x^2} + k_o^2\right]\sum_{i=1}^{N}\int_{S_{ia}} E^s_{iz}(x',z')G^o(x,z,x',z')dx'dz' \ \ldots$$

$$\text{for} \quad (x,z) \in S_{ka}. \qquad (2.26)$$

Substituting $H^i_{kx}(x,0^+,z)$ and $H^o_{kx}(x,0^-,z)$ from equations (2.15) and (2.26) into boundary condition (2.4) yields

$$\frac{j}{\omega\mu_o}\left[\frac{\partial^2}{\partial x^2} + k_o^2\right]\sum_{i=1}^{N}\int_{S_{ia}} E^s_{iz}(x',z')G^i(x,z,x',z')dx'dz' +$$
$$E_o\sqrt{\frac{2}{abZ^h_{10}}}\left[1 - (\Gamma_2)_{10}e^{2j\beta^h_{10}z}\right]e^{-j\beta^h_{10}z}\sin\left(\frac{\pi x}{a}\right) +$$
$$\frac{j}{\omega\mu_o}\left[\frac{\partial^2}{\partial x^2} + k_o^2\right]\sum_{i=1}^{N}\int_{S_{ia}} E^s_{iz}(x',z')G^o(x,z,x',z')dx'dz' = I_k\delta(x - a/2)$$

or

$$\left[\frac{\partial^2}{\partial x^2} + k_o^2\right]\sum_{i=1}^{N}\int_{S_{ia}} E^s_{iz}(x',z')G(x,z,x',z')dx'dz' = -j\omega\mu_o I_k\delta(x - a/2) +$$
$$j\omega\mu_o E_o\sqrt{\frac{2}{abZ^h_{10}}}\left[1 - (\Gamma_2)_{10}e^{2j\beta^h_{10}z}\right]e^{-j\beta^h_{10}z}\sin\left(\frac{\pi x}{a}\right) \ \ldots \ \text{for} \quad (x,z) \in S_{ka}$$
$$(2.27)$$

where it has been assumed that $\epsilon = \epsilon_o$ and $\mu = \mu_o$ for the interior region $(y > 0)$ and

$$G(x,z,x',z') = G^i(x,z,x',z') + G^o(x,z,x',z').$$

Let $g(z) = \sqrt{\frac{2}{abZ^h_{10}}}\left[1 - (\Gamma_2)_{10}e^{2j\beta^h_{10}z}\right]e^{-j\beta^h_{10}z}$. Equation (2.27) can then be more conveniently written as

$$\left[\frac{\partial^2}{\partial x^2} + k_o^2\right]\left\{ \sum_{i=1}^{N} \int_{S_{ia}} E^s_{iz}(x',z')G(x,z,x',z')dx'dz' \right\} =$$

$$-jk_o\zeta_o I_k \delta(x - a/2) + jk_o\zeta_o E_o g(z)\sin(\frac{\pi x}{a}) \quad \ldots \text{ for } \quad (x,z) \in S_{ka}. \quad (2.28)$$

Equation (2.28) is the basic integro-differential equation for the unknown slot electric fields, $E^s_{iz}(x,z)$, in individual elements of the array. These slot fields are excited by an incident TE_{10}-mode wave of amplitude E_o as well as the impressed current I_k at the center of the kth slot.

2.3. Conversion to a System of Hallén-Type Integral Equations for Slot Voltage Distributions:

Integro-differential equations (2.28) can be converted to a system of Hallén-type integral equations for the unknown slot field distributions. There are distinct advantages associated with utilization of the Hallén-type integral equations:

(i) direct numerical solutions are relatively easily obtained using the Hallén formulation, and

(ii) an extension of the King-Sandler dipole array theory can be developed for the waveguide-backed slot array. The latter leads to an approximate analytical solution for the slot field distribution that results in a great reduction in computation time.

If a function $A_k(x,z)$ is defined as

$$A_k(x,z) \equiv \sum_{i=1}^{N} \int_{a/2-h_i}^{a/2+h_i} \int_{z_i-\epsilon}^{z_i+\epsilon} E^s_{iz}(x',z')G(x,z,x',z')dx'dz' \qquad (2.29)$$

then equation (2.28) becomes:

$$\left(\frac{\partial^2}{\partial x^2} + k_o^2\right)A_k(x,z) = -jk_o\zeta_o I_k \delta(x-a/2) + jk_o\zeta_o E_o g(z)\sin(\frac{\pi x}{a}). \qquad (2.30)$$

A complementary solution to the inhomogeneous differential equation (2.30) is obtained as

$$A_k^c(x) = A_1 \cos k_o x + A_2 \sin k_o x \tag{2.31}$$

where A_1 and A_2 are arbitrary constants. Since the particular integral for an equation of the form

$$\frac{d^2y}{dx^2} + a^2 y = f(x)$$

is given by

$$y^p(x) = \frac{1}{a} \int_o^x f(s) \sin a(x - s) ds,$$

then equation (2.30) can be shown to have the particular integral

$$A_k^p(x,z) = \frac{-j\zeta_o I_k}{2} \sin k_o |x - a/2| - \frac{jk_o \zeta_o E_o g(z)}{\gamma_{10}^2} \sin(\frac{\pi x}{a}).$$

Another term involving $\sin k_o x$ is also obtained in the particular integral. However, $\sin k_o x$ is already included in equation (2.31) and therefore it is neglected in the expression for the particular integral. The general solution to the equation is thus

$$A_k(x,z) = A_k^c(x) + A_k^p(x,z)$$

$$= A_1 \cos k_o x + A_2 \sin k_o x + A_k^p(x,z). \tag{2.32}$$

Since $E_{iz}^s(x',z')$ is symmetric about $x' = a/2$, i.e.,

$$E_{iz}^s(a/2 - \xi, z') = E_{iz}^s(a/2 + \xi, z'),$$

it follows, by definition of $A_k(x,z)$, that

$$A_k(a/2 - \xi, z) = A_k(a/2 + \xi, z).$$

This requires a relationship between A_1 and A_2 and leads to a final solution to equation (2.30) of the form:

$$A_k(x,z) = C_k\cos k_o(x - a/2) + A_k^p(x,z). \tag{2.33}$$

In terms of definition (2.29) and solution (2.33), a new system of pure integral equations is obtained as

$$\sum_{i=1}^{N} \int_{a/2-h_i}^{a/2+h_i} \int_{z_i-\epsilon}^{z_i+\epsilon} E_{iz}^s(x',z')G(x,z,x',z')dx'dz' = C_k\cos k_o(x - a/2)$$

$$- \frac{j\zeta_o}{2} I_k\sin k_o|x - a/2| - \frac{\frac{jk_o\zeta_o E_o g(z)}{2}}{\gamma_{10}} \sin(\frac{\pi x}{a}) \tag{2.34}$$

$$\ldots \text{ for } (x,z) \in S_{ka} \text{ and } k = 1,2,3,\ldots,N .$$

This is a system of Hallén-type integral equations for the unknown slot field distributions. It must be remembered, however, that in arriving at expressions for interior and exterior magnetic fields, $H_{kx}^i(x,0^+,z)$ and $H_{kx}^o(x,0^-,z)$, respectively, use was made of the assumption that the slots are thin and narrow having $h_k \gg \epsilon$ and $k_o\epsilon \ll 1$; the longitudinal component of the slot field, $E_x^s(x,z)$ could therefore be neglected. For wide slots in which $E_x^s(x,z)$ is not negligible compared to $E_z^s(x,z)$, it is probably not possible to reduce the resulting system of coupled integro-differential equations to a Hallén-type system.

It is permissible, for the assumed narrow slots described above, to use a quasi-static field approximation for the z-dependence of $E_z^s(x,z)$. The electric field in a slot of width 2ϵ cut in a thin, conducting screen of infinite extent has the approximate form(8) (obtained by a conformal mapping technique)

$$E_{iz}^s(x,z) \approx \frac{V_i(x)}{\pi\sqrt{\epsilon^2 - (z-z_i)^2}} \tag{2.35}$$

where $V_i(x)$ is the voltage distribution along the ith slot. This expression is consistent with the definition for the voltage difference between the edges of the ith slot. According to the usual definition for voltage difference an identity is obtained as follows:

$$V_i(x) = -\int_{z_i+\varepsilon}^{z_i-\varepsilon} E^s_{iz}(x,z)dz = \frac{V_i(x)}{\pi}\int_{z_i-\varepsilon}^{z_i+\varepsilon} \frac{dz}{\sqrt{\varepsilon^2 - (z-z_i)^2}} = V_i(x) .$$

Using the above approximation for $E^s_{iz}(x,z)$, equation (2.34) becomes a system of integral equations for the voltage distributions along elements of the slot array as follows:

$$\sum_{i=1}^{N} \int_{a/2-h_i}^{a/2+h_i} \int_{z_i-\varepsilon}^{z_i+\varepsilon} \frac{V_i(x')}{\pi\sqrt{\varepsilon^2 - (z'-z_i)^2}} G(x,z,x',z')dx'dz'$$

$$= C_k\cos k_o(x - a/2) - \frac{j\zeta_o}{2} I_k\sin k_o|x - a/2|$$

$$- \frac{\frac{j\zeta_o k_o}{2}}{\gamma_{10}} E_o g(z)\sin(\frac{\pi x}{a}) \ \ldots \text{ for } (x,z) \in S_{ka} \text{ and } k = 1,2,3,\ldots,N. \quad (2.36)$$

Let equation (2.36) be satisfied for $k = 1,2,\ldots,N$ at centers z_k of the kth slot (this reduction to a one-dimensional system of integral equations is possible since the z-dependence of $E^s_z(x,z)$ has been specified approximately in terms of the square-root edge singularity factor) and let the kernel for the system of integral equations be defined as

$$K(x,x',z') \equiv \frac{G(x,z_k,x',z')}{\pi\sqrt{\varepsilon^2 - (z' - z_i)^2}} = K_{ki}(x,x',z')$$

then

$$\sum_{i=1}^{N} \int_{a/2-h_i}^{a/2+h_i} \int_{z_i-\epsilon}^{z_i+\epsilon} V_i(x')K_{ki}(x,x',z')dx'dz' = C_k \cos k_o(x - a/2)$$

$$- \frac{j\zeta_o}{2} I_k \sin k_o|x - a/2| - \frac{jk_o\zeta_o}{2\,Y_{10}} E_o g(z_k)\sin(\frac{\pi x}{a}) \;\ldots\; \text{for} \quad k = 1,2,3,\ldots,N. \qquad (2.37)$$

Equations (2.37) are a system of N quasi-one-dimensional, coupled, Hallén-type integral equations for the slot voltage distributions, $V_i(x)$, $i = 1,2,3,\ldots,N$. Once this system of equations is solved, either by applying numerical methods or by extension of the King-Sandler dipole array theory, the radiation fields maintained by the slot-voltage distribution along the array aperture as well as the input impedance to the antenna can be calculated. Solutions to the system of integral equations will be obtained in Chapters 3 and 4 by numerical and approximate analytical methods, respectively. In the next section, the E-plane and H-plane radiation fields are determined in terms of the voltage distributions $V_i(x)$.

2.4 Radiation Field Maintained by the Slot Array:

Let the origin of spherical coordinates be located as indicated in Figure (2.3). $\vec{r}$ is the position vector from the origin to any point in space, while $\vec{r}'$ is the position vector locating any source point in the array aperture. The electric field at any point in space is then determined from equation (2.18) as

$$\vec{E}(\vec{r}) = -\int_{S_a} [\hat{n} \times \vec{E}(\vec{r}')] \times \nabla G^o(\vec{r},\vec{r}')dx' . \qquad (2.38)$$

It is noted that

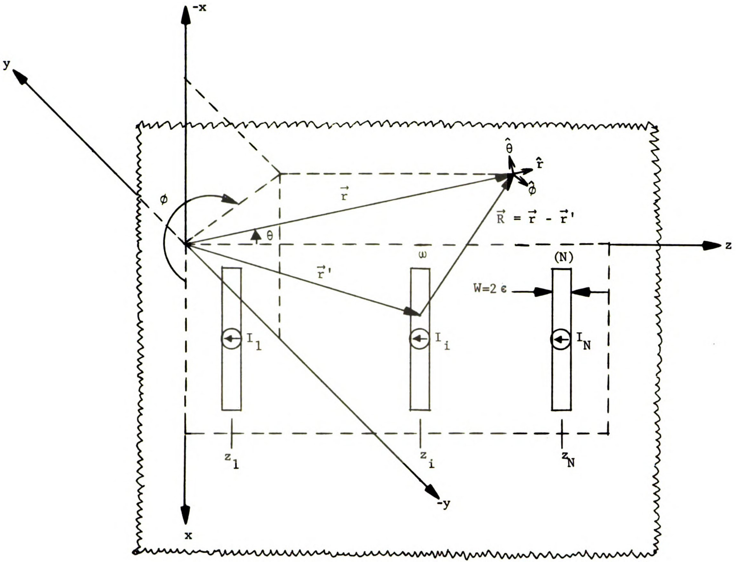

Figure 2.3. Geometry for radiation field calculation.

$$\nabla G^o(\vec{r},\vec{r}\,') = \frac{\partial G^o}{\partial R}\,\nabla R(\vec{r},\vec{r}\,')$$

$$= -\hat{R}\left(\frac{1 + jk_oR}{R}\right)G^o(\vec{r},\vec{r}\,')$$

$$= -\hat{R}\left(\frac{1 + jk_oR}{R}\right)\frac{e^{-jk_oR}}{2\pi R}$$

where $\vec{R} = (\vec{r} - \vec{r}\,')$, $R = |\vec{r} - \vec{r}\,'|$, and $\hat{R} = \frac{\vec{R}}{R}$. Subject to the usual radiation zone $(k_oR >> 1)$ approximations

$$\left.\begin{array}{l} \hat{R} \approx \hat{r} \\ \\ R \approx r - \hat{r}\cdot\vec{r}\,' \end{array}\right\} \text{... for radiation fields,}$$

such that for points in the radiation zone

$$\hat{R}\,\frac{e^{-jk_oR}}{2\pi R} \approx \hat{r}\,\frac{e^{-jk_o(r-\hat{r}\cdot\vec{r}\,')}}{2\pi r} = \hat{r}\,\frac{e^{-jk_or}}{2\pi r}\,e^{jk_o(\hat{r}\cdot\vec{r}\,')}$$

then

$$\nabla G^o(\vec{r},\vec{r}\,') \approx -\hat{r}\,\frac{jk_oe^{-jk_or}}{2\pi r}\,e^{jk_o(\hat{r}\cdot\vec{r}\,')} \quad .$$

For points in the half-space $y < 0$, then $\hat{n} = -\hat{y}$, and at source points in the array aperture

$$\vec{E}(\vec{r}\,') \approx \hat{z}\,E_z^s(x',z')$$

such that the radiation field becomes (for $k_oR >> 1$)

$$\vec{E}^r(\vec{r}) \approx -jk_o\,\frac{e^{-jk_or}}{2\pi r}\int_{S_a} E_z^s(x',z')e^{jk_o(\hat{r}\cdot\vec{r}\,')}\,(\hat{x}\times\hat{r})dx' .$$

Since $\hat{x} = \hat{r}\sin\theta\cos\phi + \hat{\theta}\cos\theta\cos\phi - \hat{\phi}\sin\phi$

while $\hat{r} = \hat{x}\sin\theta\cos\phi + \hat{y}\sin\theta\sin\phi + \hat{z}\cos\theta$, the radiation field takes the form

$$\vec{E}^r(\vec{r}) \approx jk_o \frac{e^{-jk_o r}}{2\pi r}(\hat{\phi}\cos\theta\cos\phi + \hat{\theta}\sin\phi)\sum_{i=1}^{N}\int_{S_{ia}} E^s_{iz}(x',z')\, e^{jk_o(x'\sin\theta\cos\phi + z'\cos\theta)}\,dx'dz'. \tag{2.39}$$

Since $k_o\varepsilon \ll 1$, then

$$e^{jk_o(x'\sin\theta\cos\phi + z'\cos\theta)} \approx e^{jk_o x'\sin\theta\cos\phi}\, e^{jk_o z_i\cos\theta}$$

and using equation (2.35) to express $E^s_{iz}(x',z')$ in terms of the voltage distribution $V_i(x)$ in the ith slot, the radiation field assumes the form

$$\vec{E}^r(\vec{r}) \approx jk_o \frac{e^{-jk_o r}}{2\pi r}(\hat{\phi}\cos\theta\cos\phi + \hat{\theta}\sin\phi)\sum_{i=1}^{N} e^{jk_o z_i\cos\theta} \int_{z_i-\varepsilon}^{z_i+\varepsilon}\int_{a/2-h_i}^{a/2+h_i} \frac{V_i(x')}{\pi\sqrt{\varepsilon^2 - (z'-z_i)^2}}\, e^{jk_o x'\sin\theta\cos\phi}\,dx'dz'. \tag{2.40}$$

The integral over z' evaluates to unity as

$$\int_{z_i-\varepsilon}^{z_i+\varepsilon} \frac{dz'}{\pi\sqrt{\varepsilon^2 - (z'-z_i)^2}} = 1$$

such that equation (2.40) takes the final form

$$\vec{E}^r(\vec{r}) \approx jk_o \frac{e^{-jk_o r}}{2\pi r}(\hat{\phi}\cos\theta\cos\phi + \hat{\theta}\sin\phi)\sum_{i=1}^{N} e^{jk_o z_i\cos\theta} \int_{a/2-h_i}^{a/2+h_i} V_i(x')\, e^{jk_o x'\sin\theta\cos\phi}\,dx' . \tag{2.41}$$

It is convenient to specialize the above expression for the radiation field to the principal planes, namely the E-plane ($\phi = -\pi/2$) and H-plane ($\phi = 0$), to obtain

$$\vec{E}^r_E(\vec{r}) \approx -\hat{\theta}\,\frac{jk_o e^{-jk_o r}}{2\pi r}\sum_{i=1}^{N} e^{jk_o z_i \cos\theta}\int_{a/2-h_i}^{a/2+h_i} V_i(x')\,dx'$$

... E-plane radiation field (2.42)

and

$$\vec{E}^r_H(\vec{r}) \approx \hat{\phi}\,\frac{jk_o e^{-jk_o r}}{2\pi r}\cos\theta\sum_{i=1}^{N} e^{jk_o z_i \cos\theta}\int_{a/2-h_i}^{a/2+h_i} V_i(x')\,e^{jk_o x'\sin\theta}\,dx' \qquad (2.43)$$

... H-plane radiation field.

It is clear that once the slot voltages, $V_i(x')$, have been evaluated by solution of equations (2.37), the radiation fields are readily calculated from expressions (2.42) and (2.43).

CHAPTER 3

SLOT ARRAY EXCITED BY DOMINANT BACKING-WAVEGUIDE MODE: NUMERICAL SOLUTION

3.1 Introductory Remarks:

In this chapter a numerical solution to the system of integral equations (2.37) is discussed. Only one mode of array excitation is considered, namely, that where the impressed field in the array aperture is maintained by a TE_{10} mode incident wave in the backing waveguide. The impressed current (coaxial current generator) mode of array excitation is considered in Chapter 4.

The point matching method, a special case of the method of moments$^{(17)}$ is applied to reduce the system of integral equations to an algebraic matrix equation. The voltage distribution in the ith slot of the array, $V_i(x)$, is first expanded in a series of appropriate functions, after which the integral equations are subsequently point matched to reduce them to a system of linear algebraic equations for the coefficients in the expansion. Numerical processes of integration and matrix inversion are applied to calculate the expansion coefficients; the series for $V_i(x)$ is then summed numerically to reconstruct the voltage distribution. All of the numerical operations are implemented on a high-speed digital computer (CDC 6500 system).

Some simplifications to the system of integral equations (2.37) are discussed in the next section, while sections 3.2 and 3.3

deal with the formulation of the basic matrix equations. Expressions for radiation fields are derived in section 3.4, while section 3.5 deals with the input impedance to the backing waveguide. Numerical results are discussed in section 3.6.

3.2 Simplification of the System of Hallén-type Integral Equations:

Since it is assumed that $I_k \equiv 0$, equations (2.37) can be rewritten as:

$$\sum_{i=1}^{N} \int_{a/2-h_i}^{a/2+h_i} \int_{z_i-\epsilon}^{z_i+\epsilon} V_i(x')K_{ki}(x,x'z')dx'dz' = C_k \cos k_o(x - a/2)$$

$$- \frac{jk_o\zeta_o}{\gamma_{10}^2} E_o g(z_k) \sin(\frac{\pi x}{a}) \quad \ldots \text{ for } \quad k = 1,2,3,\ldots,N. \qquad (3.1)$$

The field components of a TE_{10} mode incident wave, for the given geometry (Fig. 1) of the backing waveguide are given as[14]

$$\left.\begin{aligned} H_z &= \frac{-jE_o}{\zeta_o} (\frac{\lambda_o}{2a}) \sqrt{\frac{2Z_{10}^h}{ab}} \cos(\frac{\pi x}{a}) e^{-j\beta_1^h z} \\ H_x &= E_o \sqrt{\frac{2}{abZ_{10}^h}} \sin(\frac{\pi x}{a}) e^{-j\beta_1^h z} \\ E_y &= -E_o \sqrt{\frac{2Z_{10}^h}{ab}} \sin(\frac{\pi x}{a}) e^{-j\beta_1^h z} \end{aligned}\right\} \qquad (3.2)$$

all other field components being zero. An inspection of equations (3.2) reveals that E_y and H_x components of the TE_{10} wave are symmetric (even functions) about the point $x = a/2$. Recall also that the integral equations for the $V_i(x)$ are based upon the boundary condition (at $y = 0$) for H_x; the incident field component of H_x^i can be regarded as the impressed field which excites the slot fields. Thus the induced field (voltage) in the slots must also be symmetric about $x = a/2$ since the slots are all symmetrically placed about that point. That is

$$V_i(x = a/2 - u) = V_i(x = a/2 + u) \quad \ldots \text{ for } \quad i = 1,2,3,\ldots,N. \qquad (3.3)$$

Utilizing property (3.3), equation (3.1) becomes:

$$\sum_{i=1}^{N} \int_{a/2}^{a/2+h_i} \int_{z_i-\varepsilon}^{z_i+\varepsilon} V_i(x')[K_{ki}(x,x',z') + K_{ki}(x,a-x',z')]dx'dz'$$

$$- C_k \cos k_o(x-a/2) = \frac{-j\zeta_o k_o}{2\gamma_{10}} E_o g(z_k) \sin(\frac{\pi x}{a})$$

$$\ldots \text{ for } \quad k = 1,2,3,\ldots,N, \qquad (3.4)$$

where $K_{ki}(x,x',z') = \dfrac{G(x,z_k,x',z')}{\pi\sqrt{\varepsilon^2-(z'-z_i)^2}}$,

$$K_{ki}(x,a-x',z') = \frac{G(x,z_k,a-x',z')}{\pi\sqrt{\varepsilon^2-(z'-z_i)^2}} .$$

3.3 Numerical Solution Using Pulse Functions and Point-Matching:

Let the upper-half of the ith slot be partitioned into M_i rectangular subsections as shown in Figure (3.1). M_i is any integer and the partitioning of the ith aperture is described as:

$$\left.\begin{array}{l} \Delta x_i = \dfrac{h_i}{M_i} , \\[2ex] x_{im} = \dfrac{a}{2} - \Delta x_i(m - \tfrac{1}{2}) , \ m = 1,2,3,\ldots,M_{i.} , \\[2ex] (\Delta x)_{im} = \text{the interval: } \ x_{im} - \dfrac{\Delta x_i}{2} \le x < x_{im} + \dfrac{\Delta x_i}{2} \end{array}\right\} . \qquad (3.5)$$

Define a set of pulse functions $f_{im}(x)$ as:

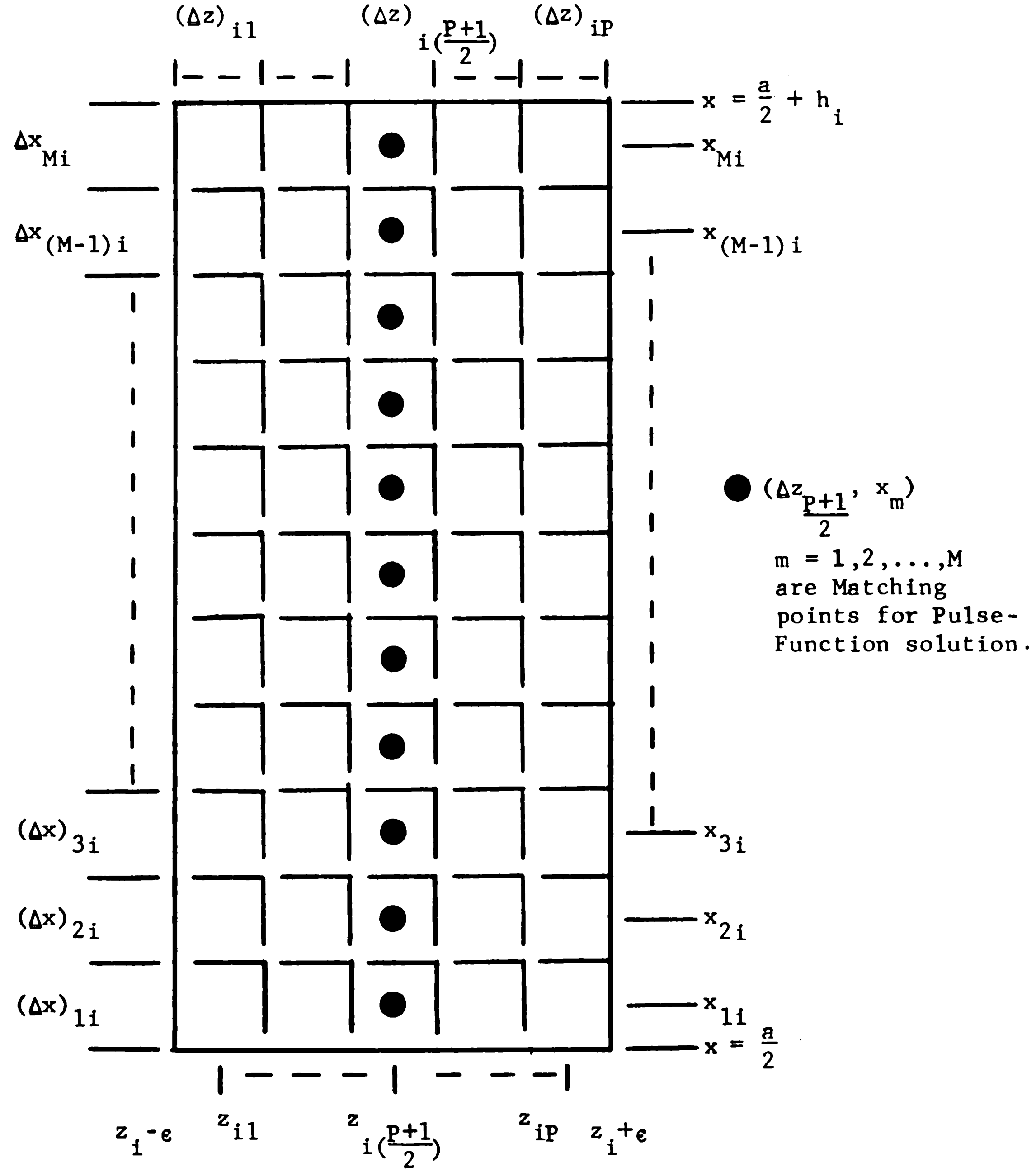

Figure 3.1. Integration Subdivision and Matching Points for Numerical Solution of the Integral Equations.

$$f_{im}(x) = \begin{cases} 1 & \ldots \text{ for } x \in (\Delta x)_{im} \\ 0 & \ldots \text{ for } x \notin (\Delta x)_{im} \, . \end{cases} \tag{3.6}$$

Expression (3.6) defines a set of pulse functions to be associated with the ith slot aperture.

Let the slot voltage distribution in the ith aperture be approximated by a pulse function expression as

$$V_i(x) \approx \sum_{m=1}^{M_i} \alpha_{im} f_{im}(x) \, , \tag{3.7}$$

where the α_{im} are unknown expansion coefficients. Substituting expansion (3.7) into the integral equations (3.4) and point-matching the integral equations at the set of points (x_{kn}, z_k), $k = 1,2,3,\ldots,N$ and $n = 1,2,3,\ldots,M_k$, which locate the center of subsections defined by $(\Delta x)_{kn}$, the system of integral equations (3.4) are reduced to a system of linear algebraic equations

$$\sum_{i=1}^{N} \sum_{m=1}^{M_i} \alpha_{im} I_{im}^{kn} - C_k \cos k_o(x_{kn} - \frac{a}{2}) = \frac{-j\zeta_o k_o}{\frac{2}{\gamma_{10}}} E_o g(z_k) \sin(\frac{\pi x_{kn}}{a}) \, ,$$

$$\ldots \text{ for } k = 1,2,3,\ldots,N, \text{ and } n = 1,2,3,\ldots,M_k, \tag{3.8}$$

where

I_{im}^{kn} = field contribution at the kth slot, nth subsection due to sources in the ith slot, mth subsection,

or

$$I_{im}^{kn} = \int_{z_i-\epsilon}^{z_i+\epsilon} \int_{(\Delta x)_{im}} [K_{ki}(x_{kn}, x', z') + K_{ki}(x_{kn}, a-x', z')] dx' dz' . \tag{3.9}$$

Equation (3.8) can be further simplified by enforcing the boundary condition for $V_i(x)$ at $x = \frac{a}{2} + h_i$, namely,

$$V_i(x = \frac{a}{2} + h_i) = 0$$

which implies that $\alpha_{im} = 0$ for $m = M_i$. Equation (3.8) then becomes:

$$\sum_{i=1}^{N} \sum_{m=1}^{M_i-1} \alpha_{im} I_{im}^{kn} - C_k \cos k_o(x_{kn} - \frac{a}{2}) = \frac{-j\zeta_o k_o}{2\gamma_{10}} E_o g(z_k) \sin(\frac{\pi x_{kn}}{a})$$

$$\ldots \text{ for } k = 1,2,3,\ldots,N, \text{ and } n = 1,2,3,\ldots,M_k . \qquad (3.10)$$

Equation (3.10) is a matrix equation for the α_{im}. The system must still be point matched at subsection $n = M_k$. In the latter matrix equation, the number of equations and unknowns are equal. If, for example, each of the N slots is partitioned into M subsections such that $M_i = M$ for $i = 1,2,3,\ldots,N$, then the total number of equations is NM. The number of unknown coefficients α_{im} is N(M-1) while there exist N unknown constants C_k such that the total number of unknowns is also equal to NM.

3.3.1 Numerical Evaluation of the Various Integrals:

Various integrals involved in equation (3.10) are given by equation (3.9) as

$$I_{im}^{kn} = \int_{z_i-\epsilon}^{z_i+\epsilon} \int_{(\Delta x')_{im}} [K_{ki}(x_{kn},x',z') + K_{ki}(x_{kn},z-x',z')]dx'dz',$$

where

$$K_{ki}(x_{kn},x',z') = \frac{G^i(x_{kn},z_k,x',z') + G^o(x_{kn},z_k,x',z')}{\pi\sqrt{\epsilon^2 - (z'-z_i)^2}}$$

and

$$K_{ki}(x_{kn},a-x',z') = \frac{G^{i}(x_{kn},z_k,a-x',z') + G^{o}(x_{kn},z_k,a-x',z')}{\pi\sqrt{\epsilon^2 - (z'-z_i)^2}} .$$

In order to bring out the nature of singularities that will occur in the evaluation of I^{kn}_{im}, consider the following two cases:

(a) Case $i \neq k$: In this case source-point and field-point are in different slots; as a result G^o is only a slowly varying function of z' during the integration from $z' = z_i - \epsilon$ to $z' = z_i + \epsilon$, and G can be regarded as approximately constant with respect to z' and equal to its value at $z' = z_i$. That is

$$I^{kn}_{im} \approx \int_{(\Delta x')_{im}} [G(x_{kn},z_k,x',z_i) + G(x_{kn},z_k,a-x',z_i)]dx'$$

$$\times \int_{z_i-\epsilon}^{z_i+\epsilon} \frac{dz'}{\pi\sqrt{\epsilon^2 - (z'-z_i)^2}} .$$

However, the integration over z' evaluates to unity, while for sufficiently small Δx_i (large M_i) the x' integral can be approximated, and

$$I^{kn}_{im} \approx [G(x_{kn},z_k,x_{im},z_i) + G(x_{kn},z_k,a-x_{im},z_i)]\Delta x_i . \qquad (3.11)$$

(b) Case $i = k$: This case corresponds to the situation where source-point and field-point both are in the same aperture. Here G^o can vary significantly during integration with respect to z' and a more accurate approximation is needed. Let the ith slot be partitioned along the z-direction as indicated in

Figure (3.1). Let the maximum number of subsections be P, then

$$\Delta z = \frac{2\varepsilon}{P}$$

$$z_{ip} = z_i - \varepsilon + (p - \tfrac{1}{2})\Delta z, \quad p = 1,2,3,\ldots,P,$$

$$(\Delta z)_{ip} = \text{the interval:} \quad z_{ip} - \frac{\Delta z}{2} \le z \le z_{ip} + \frac{\Delta z}{2}. \tag{3.12}$$

With the above partitioning scheme, the expression for I^{kn}_{im} becomes:

$$I^{kn}_{km} \approx \sum_{p=1}^{P} \int_{(\Delta x')_{km}} \int_{(\Delta z')_{kp}} \frac{[G(x_{kn},z_k,x',z') + G(x_{kn},z_k,a-x',z')]dx'dz'}{\pi\sqrt{\varepsilon^2 - (z'-z_k)^2}}. \tag{3.13}$$

Basically, two types of singularities can occur in evaluation of expression (3.13); one when $z' = z_k \pm \varepsilon$ which corresponds to the cases of $p = 1$ or $p = P$, and a second when $p = (\frac{P+1}{2})$ and $m = n$. In the first type (the square root edge singularities), the denominator of (3.13) approaches zero while the second kind involves a Green's function singularity where G^o becomes infinite. These singularities are all integrable, however, and the improper integral (3.13) is convergent. There are, thus, four special cases for the evaluation of (3.13):

(i) <u>Cases excluding $p = 1$, $p = P$, ($p = \frac{P+1}{2}$ and $m = n$)</u>: In this case there is no singularity in the integrand of (3.13) and K_{ki} varies slowly over the region of integration such that for sufficiently small Δx_k and Δz (large M_k and P)

$$\int_{(\Delta x')_{km}} \int_{(\Delta z')_{kp}} [K_{kk}(x_{kn},x',z') + K_{kk}(x_{kn},a-x',z')]dz'dx'$$

$$\approx [K_{kk}(x_{kn},x_{km},z_{kp}) + K_{kk}(x_{kn},a-x_{km},z_{kp})]\Delta z\Delta x_k \ . \tag{3.14}$$

(ii) Case p = 1 (edge singularity): In this case the variation of G over $(\Delta z')_{kp}$ can be neglected, but the edge singularity must be integrated analytically:

$$S_p(k,m,n) \approx \int_{(\Delta x')_{km}} \int_{(\Delta z')_{kp}} [K_{kk}(x_{kn},x',z') + K_{kk}(x_{kn},a-x',z')]dz'dx'$$

$$\approx \int_{(\Delta x')_{km}} [G(x_{kn},z_k,x',z_{k1}) + G(x_{kn},z_k,a-x',z_{k1})]dz'dx'$$

$$\times \int_{z_k-\epsilon}^{z_k-\epsilon+\Delta z} \frac{dz'}{\pi\sqrt{\epsilon^2 - (z'-z_k)^2}} \ .$$

The z' integration evaluates to

$$\int_{z_k-\epsilon}^{z_k-\epsilon+\Delta z} \frac{dz'}{\pi\sqrt{\epsilon^2 - (z'-z_k)^2}} = \frac{1}{\pi}\left[\frac{\pi}{2} + \text{Arc}\ \sin\left(\frac{\Delta z}{\epsilon} - 1\right)\right] \ .$$

Therefore,

$$S_p(k,m,n) \approx \left[\frac{1}{2} + \frac{1}{\pi}\text{Arc}\ \sin\left(\frac{\Delta z}{\epsilon} - 1\right)\right][G(x_{kn},z_k,x_{km},z_{k1})$$

$$+ G(x_{kn},z_k,a-x_{km},z_{k1})]\Delta x_k \ . \tag{3.15}$$

(iii) Case p = P (edge singularity): In this case the variation of G can be ignored, but the second edge singularity must be integrated:

$$\int_{(\Delta x')_{km}} \int_{(\Delta z')_{kp}} [K_{kk}(x_{kn},x',z') + K_{kk}(x_{kn},a-x',z')]dz'dx'$$

$$\approx \int_{(\Delta x')_{km}} [G(x_{kn},z_k,x',z_{kp}) + G(x_{kn},z_k,a-x',z_{kp})]dx'$$

$$\times \int_{z_k+\varepsilon-\Delta z}^{z_k+\varepsilon} \frac{dz'}{\pi\sqrt{\varepsilon^2 - (z'-z_k)^2}} .$$

As before, the z'-integration evaluates to:

$$\int_{z_k+\varepsilon-\Delta z}^{z_k+\varepsilon} \frac{dz'}{\pi\sqrt{\varepsilon^2 - (z'-z_k)^2}} = \frac{1}{\pi}\left[\frac{\pi}{2} - \text{Arc sin}\left(1 - \frac{\Delta z}{\varepsilon}\right)\right]$$

$$= \frac{1}{\pi}\left[\frac{\pi}{2} + \text{Arc sin}\left(\frac{\Delta z}{\varepsilon} - 1\right)\right],$$

and approximated integral becomes:

$$S_p(k,m,n) \approx \left[\frac{1}{2} + \frac{1}{\pi}\text{Arc sin}\left(\frac{\Delta z}{\varepsilon} - 1\right)\right]\left[G(x_{kn},z_k,x_{kn},z_{kP}) + G(x_{kn},z_k,a-x_{km},z_{kp})\right]\Delta x_k . \qquad (3.16)$$

(iv) <u>Case</u> $p = \frac{P+1}{2}$ <u>and $m = n$ (Green's function singularity)</u>:

First, it is to be noted that when $p = \frac{P+1}{2}$ and $m \neq n$, there are no singularities in the integrand of expression (3.13), and its evaluation is given by expression (3.14) with $p = \frac{P+1}{2}$.

In the case when $p = \frac{P+1}{2}$ and $m = n$, then there is singularity in G^o, but the square root edge singularity term remains relatively constant during the integration over $(\Delta z')_k$ and approximately equal to its value at $x' = x_{km}$, $z' = z_{kp}$ such that

$$S_p(k,m,m) \approx \frac{1}{\pi\epsilon} \int_{(\Delta x')_{km}} \int_{(\Delta z')_{kp}} [G(x_{km},z_k,x',z') +$$

$$G(x_{km},z_k,a-x',z')]dz'dx'$$

or

$$S_p(k,m,m) \approx \frac{1}{\pi\epsilon} \int_{(\Delta x')_{km}} \int_{(\Delta z')_{kp}} G^o(x_{km},z_k,x',z')dz'dx' +$$

$$\frac{1}{\pi\epsilon} [G^i(x_{km},z_k,x_{km},z_{kp}) + G(x_{km},z_k,a-x_{km},z_{kp})]\Delta z \ \Delta x_k.$$

The improper integral (whose integrand is singular at $x' = x_{km}$, $z' = z_k$)

$$\int_{(\Delta x')_{km}} \int_{(\Delta z')_{kp}} G^o(x_{km},z_k,x',z')dz'dx'$$

$$= \int_{x_{km}-\Delta x_k/2}^{x_{km}+\Delta x_k/2} \int_{z_k-\Delta z/2}^{z_k+\Delta z/2} \frac{e^{-jk_o\sqrt{(x_{km}-x')^2+(z_k-z')^2}}}{2\pi\sqrt{(x_{km}-x')^2+(z_k-z')^2}} dz'dx',$$

can be evaluated, as shown in Appendix I, to

$$\int_{(\Delta x')_{km}} \int_{(\Delta z')_{kp}} G^o(x_{km},z_k,x',z')dz'dx' \approx \frac{2}{\pi} [\frac{-jk_o\Delta x_k\Delta_z}{4} +$$

$$\frac{\Delta z}{2} \ln(\frac{\Delta x_k}{\Delta z} + \sqrt{1 + (\frac{\Delta x_k}{\Delta z})^2}) + \frac{\Delta x_k}{2} \ln(\frac{\Delta z}{\Delta x_k} + \sqrt{1 + (\frac{\Delta z}{\Delta x_k})^2})],$$

giving the final expression for $S_p(k,m,m)$ as:

$$S_p(k,m,m) \approx \frac{\Delta x_k\Delta z}{\pi\epsilon} \{\frac{1}{\pi} [- \frac{jk_o}{2} + \frac{1}{\Delta x_k} \ln(\frac{\Delta x_k}{\Delta z} + \sqrt{1 + (\frac{\Delta x_k}{\Delta z})^2}) +$$

$$\frac{1}{\Delta z} \ln(\frac{\Delta z}{\Delta x_k} + \sqrt{1 + (\frac{\Delta z}{\Delta x_k})^2})] + G^i(x_{km},z_k,x_{km},z_{kp}) + G(x_{km},z_k,a-x_{km},z_{kp})\}. \tag{3.17}$$

I_{im}^{kn} as defined by expression (3.9) can now be numerically computed using expressions (3.11) through (3.17). Matrix equation (3.10) can subsequently be solved (by numerical matrix methods) for unknown expansion coefficients α_{im}. This consequently leads to the numerical determination of slot voltage distributions $V_i(x)$, $i = 1,2,3,\ldots,N$.

3.4 Radiation Field Maintained by the Slot Array:

It was shown in section 2.4 that the radiation field maintained by the slot array is given by

$$\vec{E}^r(\vec{r}) \approx jk_o \frac{e^{-jk_o r}}{2\pi r} (\hat{\phi} \cos\theta \cos\phi + \hat{\theta} \sin\phi) \sum_{i=1}^{N} e^{jk_o z_i \cos\theta} \int_{a/2-h_i}^{a/2+h_i} V_i(x') e^{jk_o x' \sin\theta \cos\phi} dx'. \tag{2.41}$$

Use of symmetry condition (3.3) leads to the following modification of equation (2.41):

$$\vec{E}^r(\vec{r}) \approx \frac{jk_o e^{-jk_o r}}{2\pi r} (\hat{\phi} \cos\theta \cos\phi + \hat{\theta} \sin\phi) e^{jk_o a/2 \sin\theta\cos\phi} \sum_{i=1}^{N} e^{jk_o z_i \cos\theta} \times \int_{a/2}^{a/2+h_i} V_i(x') \cos[k_o(a/2 - x')\sin\theta \cos\phi] dx'. \tag{3.18}$$

Substituting the pulse function expansion (3.7) for $V_i(x')$ in terms of (now determined) coefficients α_{im} yields for the x'-integral the following expression

$$\int_{a/2}^{a/2+h_i} V_i(x') \cos[k_o(a/2-x')\sin\theta \cos\phi] dx' \approx \int_{a/2}^{a/2+h_i} \sum_{m=1}^{M_i} \alpha_{im} f_{im}(x') \times \cos[k_o(a/2-x')\sin\theta \cos\phi] \approx \sum_{m=1}^{M_i} \alpha_{im} \int_{(\Delta x')_{im}} \cos[k_o(a/2-x')\sin\theta \cos\phi] dx'$$

where for sufficiently small Δx_i (large M_i) the latter integral is readily approximated such that

$$\int_{a/2}^{a/2+h_i} V_i(x')\cos[k_o(a/2-x')\sin\theta\cos\phi]dx'$$

$$\approx \sum_{m=1}^{M_i} \alpha_{im}\cos[k_o(a/2-x_{im})\sin\theta\cos\phi]\Delta x_i .$$

Finally, the expression for the radiation field becomes

$$\vec{E}^r(\vec{r}) \approx \frac{jk_o}{2\pi}\frac{e^{-jk_or}}{r}(\hat{\theta}\sin\phi + \hat{\phi}\cos\theta\cos\phi)e^{jk_oa/2\sin\theta\cos\phi}$$

$$\times \sum_{i=1}^{N} e^{jk_oz_i\cos\theta}\sum_{m=1}^{M_i}\alpha_{im}\cos[k_o(a/2 - x_{im})\sin\theta\cos\phi]\Delta x_i . \quad (3.19)$$

Expression for the radiation fields in the two principal planes, namely the E-plane ($\phi = -\pi/2$) and H-plane ($\phi = 0$) are obtained from equation (3.19) as

$$\vec{E}^r_E(\vec{r}) \approx -\hat{\theta}\,\frac{jk_oe^{-jk_or}}{2\pi r}\sum_{i=1}^{N} e^{jk_oz_i\cos\theta}\sum_{m=1}^{M_i}\alpha_{im}\Delta x_i$$

... for E-plane radiation field, (3.20)

and

$$\vec{E}^r_H(\vec{r}) \approx \hat{\phi}\,\frac{jk_oe^{-jk_or}}{2\pi r}\cos\theta\, e^{jk_oa/2\sin\theta}\sum_{i=1}^{N} e^{jk_oz_i\cos\theta}$$

$$\times \sum_{m=1}^{M_i}\alpha_{im}\cos[k_o(a/2-x_{im})\cos\theta]\Delta x_i$$ ... for H-plane radiation field.

(3.21)

3.5 Input Impedance to Backing Waveguide.

The circuit properties of the slot array, described by the input impedance to backing waveguide; this impedance can be evaluated at an arbitrarily located terminal plane. In this analysis, the input impedance is defined at the $z = 0$ crossectional plane of the backing waveguide (Figure 2.1)). The impedance of the antenna is therefore defined as

$$Z_{in} = - \left. \frac{(E_y^i)_{10}}{(H_x^i)_{10}} \right|_{z=0} , \tag{3.22}$$

where

$(E_y^i)_{10}$ = the y-component of the total interior electric field associated with TE_{10} mode wave,

$(H_x^i)_{10}$ = the x-component of the total interior magnetic field associated with TE_{10} mode wave,

and

Z_{in} = the input impedance of the slot array at $z = 0$.

In section 2.2.1, the EM field in the interior of the backing waveguide was calculated using the principle of linear superposition. Employing the same principle $(E_y^i)_{10}$ and $(H_x^i)_{10}$ can be written as

$$\left. \begin{aligned} (E_y^i)_{10} &= (E_y^{inc})_{10} + (E_y^s)_{10} \\ (H_x^i)_{10} &= (H_x^{inc})_{10} + (H_x^s)_{10} \end{aligned} \right\} \tag{3.23}$$

where superscripts "inc" and "s" indicate, respectively, the incident TE_{10} mode field in the absence of the slots and the TE_{10} mode component of the EM field scattered by the slot array (which was expressed as a modal expansion over all TE_q and TM_q modes). With the above definitions of $(E_y^i)_{10}$ and $(H_x^i)_{10}$, expression

(3.22) becomes

$$Z_{in} = - \left. \frac{(E_y^{inc})_{10} + (E_y^s)_{10}}{(H_x^{inc})_{10} + (H_x^s)_{10}} \right|_{z=0} . \qquad (3.24)$$

A procedure similar to the one followed in determining the interior magnetic field excited by the slot fields in the apertures of the array elements can be used to evaluate $(E_y^s)_q$, where subscript q includes all possible TE and TM scattered modes. It can be shown that such a procedure will yield for E_y^s:

$$E_y^s(x,y,z) = \int_{S_a} E_z^s(x',z')\{ \sum_{n=1}^{\infty} \sum_{m=0}^{\infty} \frac{\epsilon_m}{ab[1 - (\Gamma_1)_{nm}(\Gamma_2)_{nm}]}$$

$$\sin(\frac{n\pi x}{a}) \sin(\frac{n\pi x'}{a}) \cos(\frac{m\pi y}{b}) \cos(\frac{m\pi y'}{b}) [e^{\gamma_{nm}(z-z')} + (\Gamma_1)_{nm}$$

$$e^{-\gamma_{nm}(z+z')} - (\Gamma_2)_{nm} e^{\gamma_{nm}(z+z')} - (\Gamma_1)_{nm}(\Gamma_2)_{nm} e^{-\gamma_{nm}(z-z')}]\}dx'dz'$$

$$\ldots \text{ for } z \leq z_1 . \qquad (3.25)$$

$(E_y^s)_{10}$ is obtained from equation (3.25) by retaining only the $n = 1$, $m = 0$ component term in the double summation. Recalling that for $m = 0$, $\epsilon_m = 1$, $(E_y^s)_{10}$ is given as

$$(E_y^s)_{10} = \sin(\frac{\pi x}{a}) \int_{S_a} E_z^s(x',z')\{ \frac{1}{ab[1 - (\Gamma_1)_{10}(\Gamma_2)_{10}]} \sin(\frac{\pi x'}{a})$$

$$\cdot [e^{j\beta_{10}^h(z-z')} + (\Gamma_1)_{10} e^{-j\beta_{10}^h(z+z')} - (\Gamma_2)_{10} e^{j\beta_{10}^h(z+z')}$$

$$- (\Gamma_1)_{10}(\Gamma_2)_{10} e^{-j\beta_{10}^h(z-z')}]\}dx'dz' \ldots \text{ for } z \leq z_1 . \qquad (3.26)$$

With the above result for $(E_y^s)_{10}$ and equation (2.6) for $(E_y^{inc})_{10}$, the expression for $(E_y^i)_{10}$ can be written as

$$(E_y^i)_{10} = -E_o\sqrt{\frac{2Z_{10}^h}{ab}}\,[1 + (\Gamma_2)_{10}e^{2j\beta_{10}^h z}]e^{-j\beta_{10}^h z}\sin(\frac{\pi x}{a}) +$$

$$\text{expression (3.26)} \quad \ldots \text{ for } \quad z \le z_1. \tag{3.27}$$

The corresponding expression for $(H_y^i)_{10}$ is determined by using Maxwell's equation for curl $\vec{E}$, namely

$$\nabla \times \vec{E}^i = -j\omega\mu_o\vec{H}^i \;,$$

which in component form yields

$$\left.\begin{aligned} H_x^i &= \frac{1}{j\omega\mu_o}\frac{\partial}{\partial z}E_y^i \\ H_z^i &= \frac{-1}{j\omega\mu_o}\frac{\partial}{\partial x}E_y^i \end{aligned}\right\}. \tag{3.28}$$

The first of expressions (3.28) along with equation (3.27) leads to the final expression for $(H_x^i)_{10}$ as

$$(H_x^i)_{10} = \frac{1}{Z_1^h}E_o\sqrt{\frac{2Z_{10}^h}{ab}}\,[1 - (\Gamma_2)_{10}e^{2j\beta_{10}^h z}]e^{-j\beta_{10}^h z}$$

$$\times \sin(\frac{\pi x}{a}) + \frac{1}{Z_{10}^h}\frac{\sin(\frac{\pi x}{a})}{ab[1 - (\Gamma_1)_{10}(\Gamma_2)_{10}]}\int_{S_a} E_z^s(x',z')$$

$$\times \sin(\frac{\pi x'}{a})\{e^{j\beta_{10}^h(z-z')} - (\Gamma_1)_{10}e^{-j\beta_{10}^h(z+z')}$$

$$- (\Gamma_2)_{10}e^{j\beta_{10}^h(z+z')} + (\Gamma_1)_{10}(\Gamma_2)_{10}e^{-j\beta_{10}^h(z-z')}\}dx'dz'$$

$$\ldots \text{ for } \quad z \le z_1. \tag{3.28}$$

Substituting expressions (3.27) and (3.28) into equation (3.22) and simplifying, the following expression for Z_{in} results

$$Z_{in} = Z^h_{10}\left[\frac{1 + (\Gamma_2)_{10} - A\,I_A}{1 - (\Gamma_2)_{10} + B\,I_A}\right] = \text{antenna impedance at } z = 0 \text{ input plane,} \qquad (3.29)$$

where

$$A = \frac{1 + (\Gamma_1)_{10}}{E_o\sqrt{2abZ^h_{10}}\,[1 - (\Gamma_1)_{10}(\Gamma_2)_{10}]} ,$$

$$B = \frac{1 - (\Gamma_1)_{10}}{E_o\sqrt{2abZ^h_{10}}\,[1 - (\Gamma_1)_{10}(\Gamma_2)_{10}]} , \text{ and}$$

$$I_A = \sum_{i=1}^{N}\int\int_{S_{ia}} E^s_{iz}(x',z')[e^{-j\beta^h_{10}z'} - (\Gamma_2)_{10}e^{j\beta^h_{10}z'}]\sin(\frac{\pi x'}{a})\,dx'dz'.$$

A special case of interest is that where there are no slots in the structure. In this situation E^s_{iz} will be identically zero implying I_A will be zero. Thus it is found that

$$Z_{in} = Z^h_{10}\left[\frac{1 + (\Gamma_2)_{10}}{1 - (\Gamma_2)_{10}}\right] ,$$

which is the well known result for an arbitrarily terminated waveguide. This provides a check on the derivation of expression (3.29).

If the quasi-static field approximation, as given by equation (2.35), to the slot field $E^s_{iz}(x',z')$ is used, then

$$I_A = \sum_{i=1}^{N}\int\int_{S_{ia}} \frac{V_i(x')}{\pi\sqrt{\epsilon^2 - (z'-z_i)^2}}\sin(\frac{\pi x'}{a})[e^{-j\beta^h_{10}z'} - (\Gamma_2)_{10}e^{j\beta^h_{10}z'}]dx'dz'. \qquad (3.30)$$

3.5.1 Numerical Evaluation of I_A:

The z'-integrals in expression (3.30) can be evaluated analytically while x'-integrals must be computed numerically in terms of the pulse function expansion for $V_i(x)$ using the same technique described in section 3.3. With the x-partitioning scheme described by expression (3.5) and expansion (3.7) for $V_i(x)$,

$$I_A = \sum_{i=1}^{N} \int_{a/2-h_i}^{a/2+h_i} V_i(x')\sin\left(\frac{\pi x'}{a}\right)dx' \int_{z_i-\varepsilon}^{z_i+\varepsilon} \frac{\left[e^{-j\beta_{10}^h z'} - (\Gamma_2)_{10} e^{j\beta_{10}^h z'}\right]}{\pi\sqrt{\varepsilon^2 - (z'-z_i)^2}}\, dz'$$

or

$$I_A = 2\sum_{i=1}^{N} \sum_{m=1}^{M_i} \alpha_{im} \int_{(\Delta x')_{im}} \sin\left(\frac{\pi x'}{a}\right)dx' \int_{z_i-\varepsilon}^{z_i+\varepsilon} \frac{\left[e^{-j\beta_{10}^h z'} - (\Gamma_2)_{10} e^{j\beta_{10}^h z'}\right]}{\pi\sqrt{\varepsilon^2 - (z'-z_i)^2}}\, dz'.$$

However

$$\int_{z_i-\varepsilon}^{z_i+\varepsilon} \frac{e^{\pm j\beta_{10}^h z'}}{\pi\sqrt{\varepsilon^2 - (z'-z_i)^2}}\, dz' = e^{\pm j\beta_{10}^h z_i} J_o(\beta_{10}^h \varepsilon),$$

where $J_o(\beta_{10}^h\varepsilon)$ is the Bessel function of first kind and order zero with real argument $\beta_{10}^h\varepsilon$, therefore

$$I_A = 2\sum_{i=1}^{N} \left[\left(e^{-j\beta_{10}^h z_i} - (\Gamma_2)_{10} e^{j\beta_{10}^h z_i}\right) J_o(\beta_{10}^h\varepsilon)\right] \cdot \sum_{m=1}^{M_i} \alpha_{im} \sin\left(\frac{\pi x_{im}}{a}\right)\Delta x_i \ . \tag{3.31}$$

Equation (3.31), along with expression (3.29), completely determine input impedance Z_{in}.

3.6 Numerical Results:

In order to solve for the slot voltage distributions, the input impedance of the array and its radiation field, a computer program was developed and implemented on a CDC 6500 system.

As indicated by matrix equation (3.10), the order of the matrix involved is $(NM_i) \times (NM_i)$ if all the M_i are equal. The unknowns involved are the $N(M_i - 1)$ expansion coefficients α_{im} and the N constants C_{kk}. For a 10-element array, for example, and with $M_i = 10$, a matrix of order 100×100 results. It, therefore, becomes clear that initial runs must be made for say, $N = 5$, thus reducing the matrix size and resulting in a considerable saving in computation time. It was found that for $M_i < 10$ the evaluation of various integrals involved in the calculation of I_{im}^{kn} as well as the convergence of the numerical solution might not be satisfactory. Results were thus obtained first for a 5-element slot array with $M_i = 10$ to determine the optimum array dimensions, i.e., the element lengths and element spacings, that give rise to optimal end-fire radiation from the array.

Figure (3.2) shows the relative amplitude and phase distributions of voltage in the element of a 5-element waveguide backed slot array. Various dimensions are identified on the top left hand corner of the figure. In all cases, the double Fourier series, used in the evaluation of G^i was truncated after n_{max} and m_{max} terms (the total number of terms summed is, therefore, equal to $n_{max} \times m_{max}$). The element lengths are fixed at $\frac{h}{\lambda_o} = 0.22$ and element spacings at $\frac{\Delta z}{\lambda_o} = 0.1$. The backing waveguide is matched at both the input and output terminals

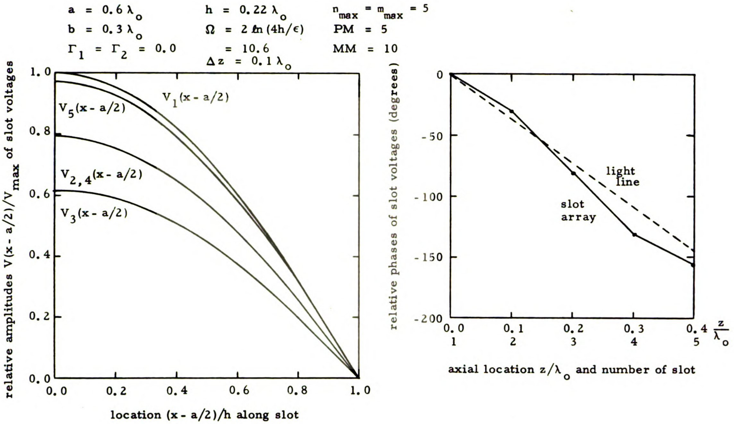

a. Voltage amplitude distribution in the slot elements.

b. Phases of slot voltages.

Figure 3.2. Voltage distributions in the elements of a 5-element waveguide-backed slot array.

($\Gamma_1 = \Gamma_2 = 0$), and the width of the slots is specified by the parameter $\Omega = 2\ln(4h/\varepsilon) = 10.6$. It is interesting to note that the numerically computed voltage amplitude distributions in the slot elements closely approximate sinusoidal variations along the slot axes; this suggests that an extension of the King-Sandler dipole array theory(11) might be applicable to this problem. Maxima of the amplitude distributions in the slot elements also display a standing wave character. Slot number 1 has maximum induced voltage, slot 3 has minimum voltage, slots 2 and 4 have identical distributions of intermediate amplitude, and slot 5 has an induced voltage of amplitude nearly equal to that in slot 1.

Figure (3.2b) indicates an essentially uniform progressive, delay or lag in the phases of (successive) slot voltages along the array aperture. The light line on the figure indicates the shift (lag) which would occur along the array if the wave in its aperture were a traveling wave propagating at the speed of light. This light line gives an indication whether the actual wave excited along the array aperture is a fast or slow wave; a slope greater than that of light line indicates a larger phase constant, it corresponds to a traveling-wave aperture field with a phase velocity slower than the speed of light while a lesser slope indicates the existence of a fast-wave field. It can be identified from Figure (3.2b), therefore, that a wave traveling very nearly at (or, on the average, slightly slower than) the speed of light is excited. Since endfire radiation is expected when the phase velocity of the aperture field is less than or equal to the speed of light, this array is capable of maintaining such a radiation field. This is confirmed by the radiation pattern presented later in Figure (3.6).

Figure (3.3) shows relative amplitude and phase distributions of slot voltages in the aperture of the same 5-element slot array considered in Figure (3.2), except that now the effects of various element spacings, Δz, are considered. From Figure (3.3a), the standing wave nature of the slot voltages (aperture field distribution) is apparent. For example, when $\frac{\Delta z}{\lambda_o} = 0.05$ the array aperture length is $0.20\ \lambda_o$ and the distribution indicates approximately a quarter-wavelength standing wave pattern. Similar conclusions are reached for the array with $\frac{\Delta z}{\lambda_o} = 0.1$ and $\frac{\Delta z}{\lambda_o} = 0.2$.

From Figure (3.3b), it is apparent that spacings of $\frac{\Delta z}{\lambda_o} = 0.05$ and $\frac{\Delta z}{\lambda_o} = 0.1$ yield slow wave aperture fields along the array, and thus an end fire radiation, while $\frac{\Delta z}{\lambda_o} = 0.2$ gives rise to a fast wave and consequent off-endfire radiation. Thus a spacing of $\frac{\Delta z}{\lambda_o} = 0.1$ is identified as an optimum element separation; smaller spacings will create difficulties in the construction of such an array.

Figure (3.4) again indicates amplitude and phase distributions of slot voltages against axial location of the slots with element half-length, h, as a parameter. Again, a standing-wave aperture field pattern, which is indicative of large reflection near the terminal end of the array is demonstrated by Figure (3.4a). Figure (3.4b) indicates a slow wave aperture field along the array for $\frac{h}{\lambda_o} = 0.24, 0.22$ and a wave at nearly the speed of light for $\frac{h}{\lambda_o} = 0.20$. For an element half-length of $\frac{h}{\lambda_o} = 0.26$, a fast wave is indicated. The optimum value for half-length $\frac{h}{\lambda_o}$ appears to be roughly 0.22. Shorter slot lengths or lengths greater than resonance lead to fast wave fields, while lengths close to resonance result in a strong standing wave pattern along the array aperture.

$a = 0.6\,\lambda_o$ $h = 0.22\,\lambda_o$ $n_{max} = m_{max} = 5$

$b = 0.3\,\lambda_o$ $\Omega = 2\,\ln(4h/\epsilon)$ $PM = 5$

$\Gamma_1 = \Gamma_2 = 0.0$ $= 10.6$ $MM = 10$

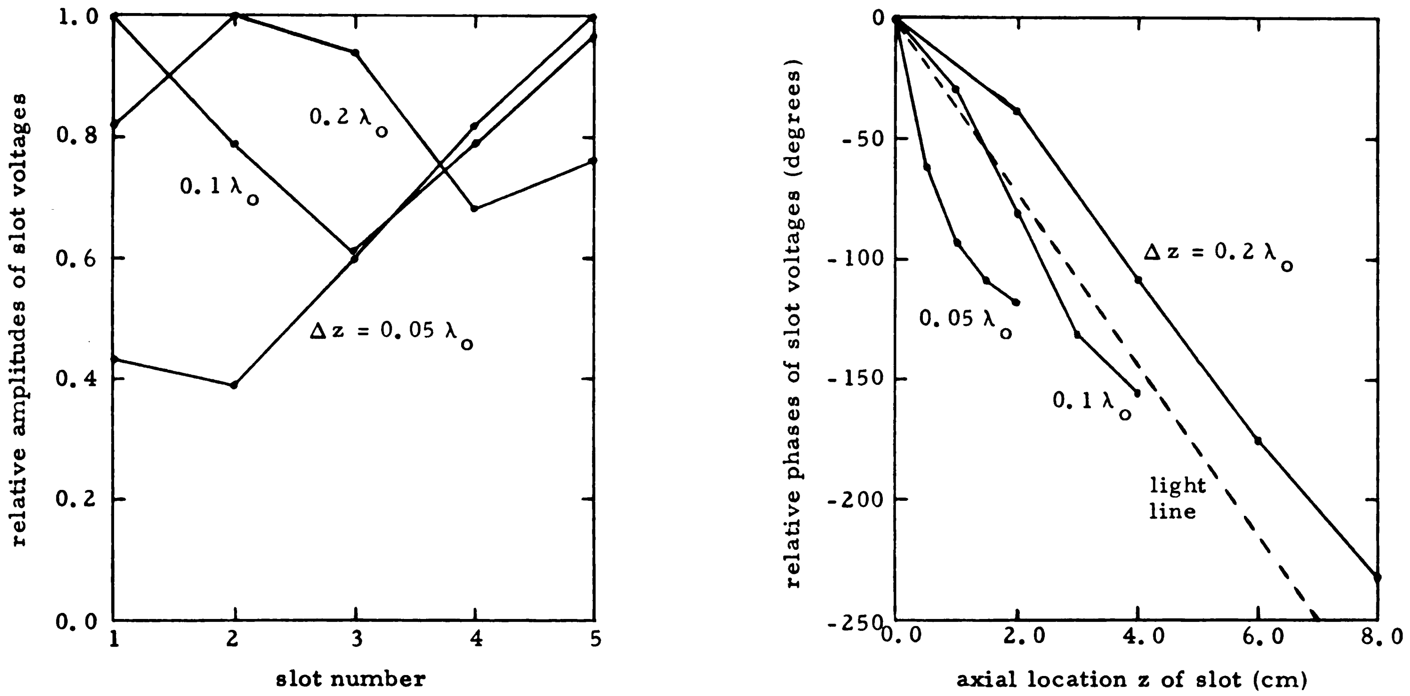

a. Amplitude of slot voltages. b. Phases of slot voltages.

Figure 3.3. Amplitudes and phases of slot voltages in the elements of a 5-element array for various slot spacings.

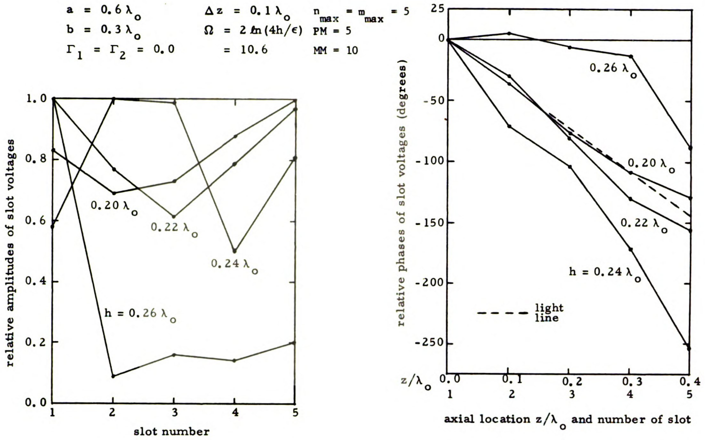

a. Amplitudes of slot voltages.

b. Phases of slot voltages.

Figure 3.4. Amplitudes and phases of slot voltages in the elements of a 5-element array for various slot lengths.

It can, therefore, be concluded that for array parameters of $\frac{\Delta z}{\lambda_o} = 0.1$ and $\frac{h}{\lambda_o} = 0.20$ a slow wave aperture field will be excited along the array.

Figure (3.5) shows the relative slot voltage distribution (in amplitude and phase) vs axial slot location, $\frac{\Delta z}{\lambda_o}$, along the array aperture with the backing waveguide dimension "a" (its width) as a parameter. Figure (3.5a) indicates the amplitude distribution of slot voltages against $\frac{\Delta z}{\lambda_o}$, guide widths of $\frac{a}{\lambda_o} = 0.505$, 0.55, 0.6 and 0.7. The value $\frac{a}{\lambda_o} = 0.50$ is the cut-off dimension for the incident TE_{10} mode wave, at which point its phase velocity becomes infinite, so a fast-wave aperture field is expected for $\frac{a}{\lambda_o} = 0.505$ (cut-off was avoided to prevent numerical difficulties from occurring in the computer program). As the phase plots of Figure (3.5b) indicate, a slow wave field can be excited along the array aperture with $\frac{a}{\lambda_o} = 0.70$ and 0.60 while a fast wave exists with $\frac{a}{\lambda_o} = 0.505$. $\frac{a}{\lambda_o} = 0.55$ results in excitation of a wave along the array that travels perhaps slightly faster than the speed of light. End fire radiation can thus be expected with the backing waveguide dimensions set at $\frac{a}{\lambda_o} = 0.70$ or 0.60 with $\frac{b}{\lambda_o} = 0.30$. Off-endfire radiation is expected for $\frac{a}{\lambda_o} = 0.505$ or 0.55 and $\frac{b}{\lambda_o} = 0.30$.

The above conclusions are confirmed by Figure (3.6) which indicates the radiation field in the E-plane ($\phi = -\frac{\pi}{2}$) of a 5-element slot array with $\frac{a}{\lambda_o}$ as a parameter. The upper half of the figure concerns an array having $\frac{h}{\lambda_o} = 0.22$ backed by waveguides width $\frac{a}{\lambda_o} = 0.505$ and 0.60. It is observed that even though the radiation patterns are rather broad (due to small number of

$b = 0.3\lambda_o$ $h = 0.22\lambda_o$ $n_{max} = m_{max} = 5$
$\Gamma_1 = \Gamma_2 = 0.0$ $\Omega = 2 \ln(4h/\epsilon)$ $PM = 5$
$\Delta z = 0.1\lambda_o$ $= 10.6$ $MM = 10$

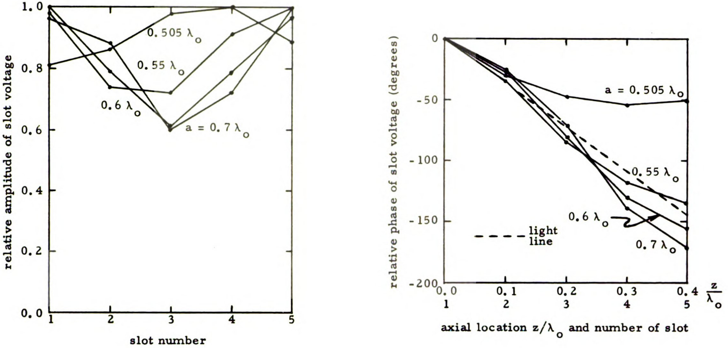

a. Amplitudes of slot voltages.

b. Phases of slot voltages.

Figure 3.5. Amplitudes and phases of the slot voltages in the elements of a 5-element array for various backing-waveguide widths.

$b = 0.3\,\lambda_o$

$\Gamma_1 = \Gamma_2 = 0.0$

$\Delta z = 0.1\,\lambda_o$

$\Omega = 2\,\ell n\,(4h/\epsilon) = 10.6$

$h/\epsilon = 50.0$

$n_{max} = m_{max} = 5$

PM = 5

MM = 10

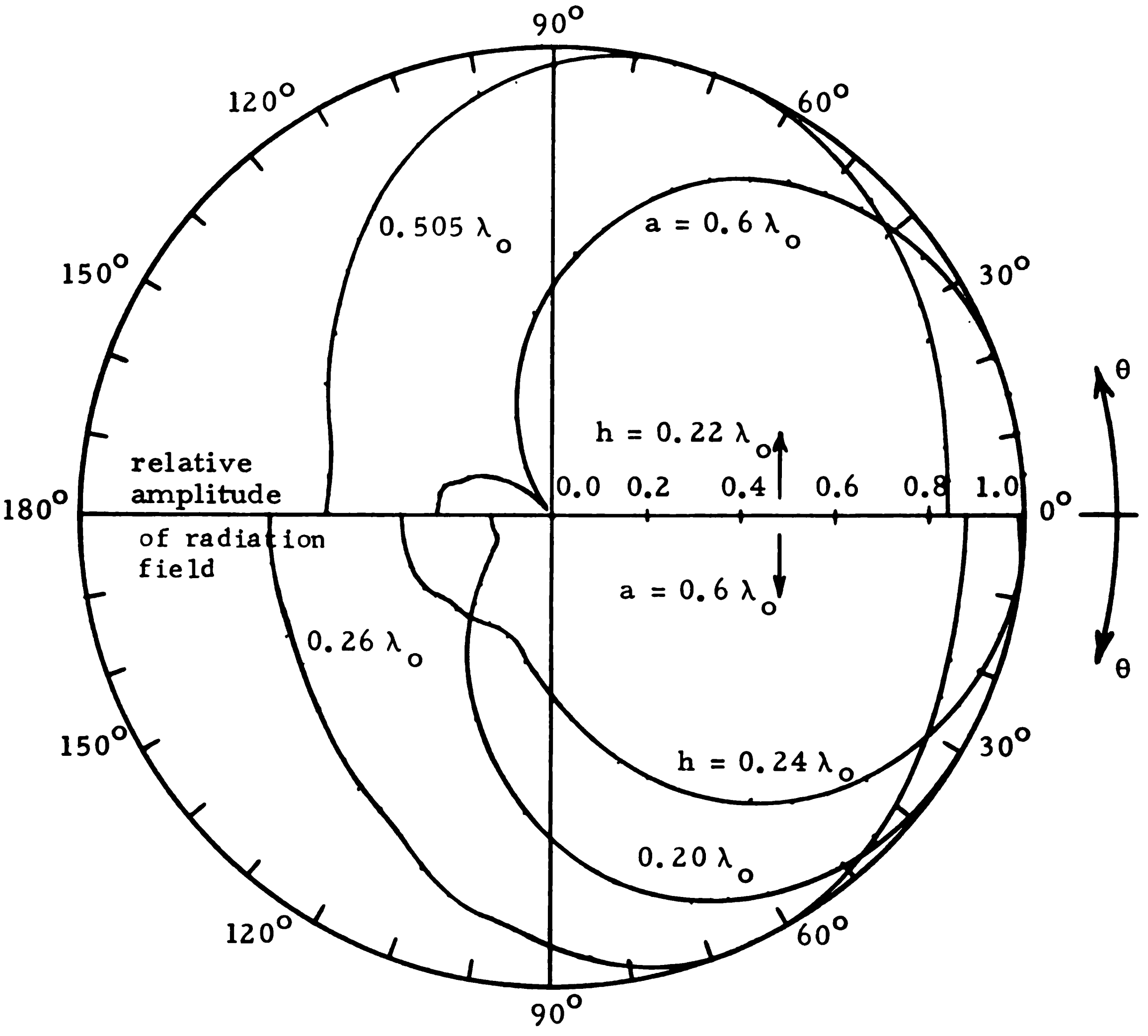

Figure 3.6. **Dependence of E-plane ($\phi = -\pi/2$) radiation field patterns of a 5-element slot array upon width of its backing waveguide and slot length.**

array elements and consequent short aperture electrical length) a beam-scanning capability is achieved by changing $\frac{a}{\lambda_o}$ from 0.6 to 0.505. The lower half of Figure (3.6) shows the dependence of E-plane radiation field patterns upon parameter $\frac{h}{\lambda_o}$ with $\frac{a}{\lambda_o} = 0.60$. Endfire radiation is achieved for $\frac{h}{\lambda_o} = 0.20$ and 0.24, while for $\frac{h}{\lambda_o} = 0.26$ the main beam is in the off-endfire direction of $\theta \approx 65^o$. This is to be expected since Figure (3.4b) predicted a slow wave along the array for $\frac{h}{\lambda_o} = 0.20$, 0.22, and 0.24 but a fast wave for $\frac{h}{\lambda_o} = 0.26$.

With optimum array dimensions $\frac{h}{\lambda_o}$ and $\frac{\Delta z}{\lambda_o}$ now determined as 0.22 and 0.1, respectively, by studies on the 5-element array, an investigation of a 10-element waveguide backed slot array was initiated. Again, the possibility of achieving a beam scanning capability by controlling the backing waveguide dimension $\frac{a}{\lambda_o}$ was considered. Figures (3.7a) and (3.7b) indicate the amplitude and phase distributions of slot voltages (field maintained in array aperture) against the axial slot location for backing waveguide widths of $\frac{a}{\lambda_o} = 0.505$, 0.55, 0.60, and 0.70. The large reflection at the terminal end of the array persists as expected for an array of finite length and the aperture field distribution shows a significant standing wave component. Figure (3.7b) indicates the excitation of a slow wave when $\frac{a}{\lambda_o} = 0.70$ and possibly for $\frac{a}{\lambda_o} = 0.60$. A fast wave is excited along the array with $\frac{a}{\lambda_o} = 0.505$, and 0.55.

Figure (3.8) confirms these predictions by indicating an end fire radiation pattern for $\frac{a}{\lambda_o} = 0.70$ and near end fire radiation for $\frac{a}{\lambda_o} = 0.60$. However, for $\frac{a}{\lambda_o} = 0.55$, the maximum of the radiation field shifts to approximately 45 degrees off-

$b = 0.3\lambda_o$ $\quad h = 0.22\lambda_o$ $\quad n_{max} = m_{max} = 5$

$\Gamma_1 = \Gamma_2 = 0.0$ $\quad \Omega = 2\ln(4h/\epsilon)$ $\quad PM = 5$

$\Delta z = 0.1\lambda_o$ $\quad = 10.6$ $\quad MM = 8$

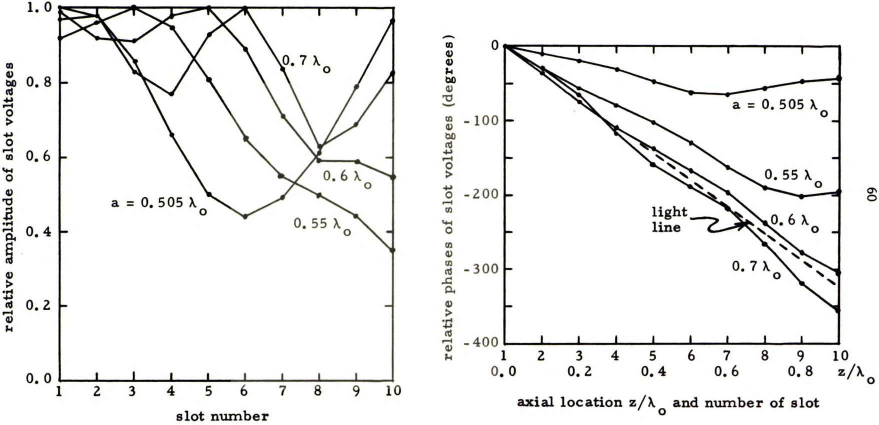

a. Amplitudes of slot voltages.

b. Phases of slot voltages.

Figure 3.7. Amplitudes and phases of slot voltages in the elements of a 10-element array for various backing waveguide widths.

$b = 0.3\,\lambda_o$ $\qquad h = 0.22\,\lambda_o$ $\qquad n_{max} = m_{max} = 5$

$\Gamma_1 = \Gamma_2 = 0.0$ $\qquad \Omega = 2\,\ln(4h/\epsilon)$ $\qquad PM = 5$

$\Delta z = 0.1\,\lambda_o$ $\qquad = 10.6$ $\qquad MM = 8$

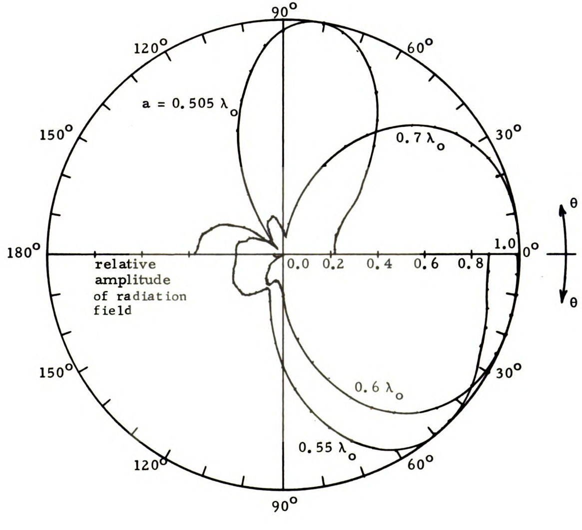

Figure 3.8. Dependence of E-plane ($\phi = -\pi/2$) radiation field patterns of a 10-element slot array upon width of its backing waveguide.

end fire while for $\frac{a}{\lambda_o} = 0.505$, an almost broadside radiation pattern is achieved. The beam scanning capability with respect to $\frac{h}{\lambda_o}$ variation was not investigated for the 10-element array since the half-length h can only be changed electrically (by operating at different frequencies) and results in a simultaneous change in the element spacing $\frac{\Delta z}{\lambda_o}$.

The input impedance Z_{in} to the backing waveguide is computed at the arbitrarily chosen input terminal plane $z = 0$; the standing wave ratio (SWR) in the driving waveguide is subsequently calculated in terms of the normalized input impedance $z_{in} = Z_{in}/Z_{10}^h$. Table (3.1) indicates backing waveguide SWR for a 5-element array with various slot lengths and spacings. It is observed that to minimize SWR optimum slot spacing is $\frac{\Delta z}{\lambda_o} = 0.1$ while the optimum slot half-length is $\frac{h}{\lambda_o} = 0.22$. These dimensions are identical to those determined earlier for optimum excitation of a slow-wave in the aperture.

It is interesting to note that even for very closely spaced slots $(\frac{\Delta z}{\lambda_o} = 0.05)$ the SWR rises only to 6.90, which indicates a reasonably good match is maintained between the backing waveguide and other waveguide circuitory that is employed to excite the array. The SWR increases rapidly to a value of 17.0 for $\frac{h}{\lambda_o} = 0.26$, a slot half-length much in excess of resonant length; earlier results also indicated a rapid decay in the aperture field distribution for this case. It appears that the wave in the array aperture has become evanescent and the slots simply constitute a strong reactive discontinuity which produces a TE_{10} reflected wave of high amplitude. Such slot lengths are, therefore, to be avoided in the

h/λ_o	0.2	0.22	0.24	0.26
SWR	1.79	1.20	3.70	17.0

a. Variable h/λ_o for $\Delta z = 0.1\lambda_o$

$\Delta z/\lambda_o$	0.05	0.10	0.20
SWR	6.90	1.20	2.02

b. Variable $\Delta z/\lambda_o$ for $h = 0.22\lambda_o$

Table 3.1. Backing waveguide SWR (5-slot array) for various slot lengths and spacings ($a = 0.6\lambda_o$, $b = 0.3\lambda_o$, $\Gamma_1 = \Gamma_2 = 0$, $\Omega = 2\,\ln(4h/\epsilon) = 10.6$).

design of waveguide-backed slot arrays. Table (3.2) indicates driving waveguide SWR for a 10-element slot array with various backing waveguide widths, $\frac{a}{\lambda_o}$. This 10-element array utilizes the optimum array dimensions, $\frac{\Delta z}{\lambda_o} = 0.1$ and $\frac{h}{\lambda_o} = 0.22$, obtained by studies on the 5-element array. It is observed that to minimize SWR the optimum backing waveguide width is $\frac{a}{\lambda_o} = 0.70$. This agrees with the results indicated in Figure (3.8) for E-plane radiation field pattern for this 10-element array.

A number of additional numerical results are compared with similar experimental results in Chapter 5.

a/λ_o	0.505	0.55	0.6	0.7
SWR	7.7	1.85	1.77	1.71

Table 3.2. Driving waveguide SWR (10-slot array) for various backing waveguide widths ($b = 0.3\lambda_o$, $h = 0.22\lambda_o$, $\Gamma_1 = \Gamma_2 = 0$, $\Omega = 2\,\ell n\,(4h/\epsilon) = 10.6$).

CHAPTER 4

SLOT ARRAY EXCITED BY IMPRESSED CURRENT: APPROXIMATE ANALYTICAL SOLUTION

4.1 Introductory Remarks:

An approximate analytical solution to the system of integral equations (2.37) is presented in this chapter. Only the impressed current (coaxial current generator) mode of array excitation is considered here; the other mode of array excitation (by an incident TE_{10} mode wave) was considered in Chapter 3.

It should be noted here that a slot array, cut in an infinite ground screen situated in unbounded space and excited by current generators located at centers of the slots, constitutes a complementary problem (by Booker's extension of Babinets' principle (18)) to that of a dipole array excited by voltage generators at centers of the dipoles. This is the special case of the present problem when the waveguide backing is removed (mathematically G^i is replaced by G^o). Since the dipole array problem has been successfully treated using the King-Sandler (12) dipole array theory; an extension of this theory is applied to obtain an approximate analytical solution for the waveguide backed slot array. Section 4.2 outlines the application of the King-Sandler (two term) dipole array theory to the present problem, resulting in an algebraic matrix equation for the coefficients of distribution functions which describe the slot voltages in the array aperture.

Section 4.3 deals with the evaluation of various functions encountered in the matrix equation. All the integrals encountered in evaluation of these functions are evaluated either in closed form or by approximate numerical methods. Section 4.4 develops expressions for the radiation fields in terms of the approximate aperture field distributions. A computer program was developed to implement all of the numerical operations on a high speed digital computer (CDC 6500 system). Numerical results are presented and discussed in Section 4.5.

4.2 Extension of King-Sandler Dipole Array Theory to the Waveguide-Backed Slot Array:

Since it is assumed that no dominant-mode incident wave exists while the impressed currents are non-zero, then $E_o = 0$ and $I_k \neq 0$ such that equations (2.37) can be rewritten as:

$$\sum_{i=1}^{N} \int_{a/2-h_i}^{a/2+h_i} \int_{z_i-\epsilon}^{z_i+\epsilon} V_i(x')K_{ki}(x,x',z')dx'dz' = C_k \cos k_o(x - a/2)$$

$$- j \frac{\zeta_o}{2} I_k \sin k_o|x - a/2| \qquad \ldots \text{ for } k = 1,2,3,\ldots,N, \qquad (4.1)$$

where

$$K_{ki}(x,x',z') = \frac{G(x,z_k,x',z')}{\pi\sqrt{\epsilon^2 - (z'-z_i)^2}} \qquad (4.2a)$$

and

$$G(x,z_k,x',z') = G^i(x,z_k,x',z') + G^o(x,z_k,x',z'). \qquad (4.2b)$$

In view of its definition in expressions (2.29) and (2.35), the function $A_k(x)$ (the left-hand-side of integral equations (4.1)) can be written as

$$A_k(x) = \sum_{i=1}^{N} \int_{a/2-h_i}^{a/2+h_i} V_i(x') \int_{z_i-\varepsilon}^{z_i+\varepsilon} K_{ki}(x,x',z')dx'dz' \tag{4.3a}$$

or

$$A_k(x) = \sum_{i=1}^{N} \int_{a/2-h_i}^{a/2+h_i} V_i(x')\bar{K}_{ki}(x,x')dx' \tag{4.3b}$$

where

$$\bar{K}_{ki}(x,x') = \int_{z_i-\varepsilon}^{z_i+\varepsilon} K_{ki}(x,x',z')dz' \quad . \tag{4.3c}$$

4.2.1 Properties of the Kernel and Resulting Approximations:

The King-Sandler dipole array theory is based on the particular peaking and non-peaking properties of the kernel which appears in the system of integral equations for the dipole array. It is imperative, therefore, that an investigation of the real and imaginary components of kernel $\bar{K}_{ki}$, $\mathrm{Re}(\bar{K}_{ki})$ and $\mathrm{Im}(\bar{K}_{ki})$, be carried out before attempting an extension of the King-Sandler array theory to this problem. The case of primary interest is that where $i = k$, that is when the source point and field point are located in the same slot. Equations (4.2) and (4.3) suggest that the variation of $\bar{K}_{kk}(x,x')$ with x' be studied with x fixed. Rewriting the expressions for $K_{kk}(x,x',z')$:

$$K_{kk}(x,x',z') = \frac{G^i(x,x',z_k,z') + G^o(x,x',z_k,z')}{\pi\sqrt{\varepsilon^2 - (z_k - z')^2}}$$

$$G^o(x,z_k,x',z') = \frac{e^{-jk_oR_{kk}}}{2\pi R_{kk}}$$

$$R_{kk} = \sqrt{(x - x')^2 + (z_k - z')^2}$$

and

$$G^{i}(x,z_k,x',z') = \frac{1}{ab}\sum_{n=1}^{\infty}\sum_{m=0}^{\infty}\frac{\epsilon_m}{\gamma_{nm}[1-(\Gamma_1)_{nm}(\Gamma_2)_{nm}]}\,\mathrm{Sin}(\frac{n\pi x}{a})\mathrm{Sin}(\frac{n\pi x'}{a})$$

$$\cdot\ f_{nm}(z_k,z')$$

$$f_{nm}(z_k,z') = e^{-\gamma_{nm}|z_k-z'|} - (\Gamma_1)_{nm}e^{-\gamma_{nm}(z_k+z')}$$

$$-(\Gamma_2)_{nm}e^{\gamma_{nm}(z_k+z')} - (\Gamma_1)_{nm}(\Gamma_2)_{nm}e^{\gamma_{nm}|z_k-z'|}\,. \qquad (4.4)$$

Since an array of thin slots cut in an infinite ground plane is complementary to an array of thin strip dipoles (and ultimately to an array of equivalent cylindrical dipoles)(1), (19) it is sufficient to investigate the behavior of $G^{i}(x,z_k,x',z')$ with respect to x' and z'. The $G^{o}(x,z_k,x',z')$ Greens' function is complementary to that encountered for the strip dipole array, for which an equivalent array of cylindrical dipoles with appropriate equivalent radii can be found; the kernel for the latter system has been investigated in detail by King and Wu(21).

$G^{i}(x,z_k,x',z')$ as given by equation (4.4) is a function of variables x' and z', The z'-dependence can, however, be analytically integrated out since

$$\int_{z_k-\epsilon}^{z_k+\epsilon}\frac{G^{i}(x,z_k,x',z')dz'}{\pi\sqrt{\epsilon^2-(z_k-z')^2}} = \frac{1}{ab}\sum_{n=1}^{\infty}\sum_{m=0}^{\infty}(\frac{\epsilon_m}{\gamma_{nm}})\mathrm{Sin}(\frac{n\pi x}{a})$$

$$\cdot\ \mathrm{Sin}(\frac{n\pi x'}{a})\int_{z_k-\epsilon}^{z_k+\epsilon}\frac{e^{-\gamma_{nm}|z_k-z'|}}{\pi\sqrt{\epsilon^2-(z_k-z')^2}}\,dz'$$

$$\ldots \text{ for } (\Gamma_1)_{nm} = (\Gamma_2)_{nm} = 0. \qquad (4.5)$$

For the purpose of numerically investigating the properties of K_{kk}, the backing waveguide is assumed to be matched at both ends such that $(\Gamma_1)_{nm} = (\Gamma_2)_{nm} = 0$. The behavior for non-zero reflection coefficients is qualitatively similar. As shown in Appendix II

$$\int_{z_k-\epsilon}^{z_k+\epsilon} \frac{e^{-\gamma_{nm}|z_k - z'|}}{\pi\sqrt{\epsilon^2 - (z_k - z')^2}} dz'$$

$$= \begin{cases} [I_o(\alpha_{nm}\epsilon) - L_o(\alpha_{nm}\epsilon)] \quad \ldots \text{ for } \quad \gamma_{nm} = \alpha_{nm} + j0 \\ [J_o(\beta_{nm}\epsilon) - jH_o(\beta_{nm}\epsilon)] \quad \ldots \text{ for } \quad \gamma_{nm} = 0 + j\beta_{nm} \end{cases} \tag{4.6}$$

where

$I_o(\alpha_{nm}\epsilon)$ = Modified Bessel function of zeroth order and real argument $\alpha_{nm}\epsilon$,

$L_o(\alpha_{nm}\epsilon)$ = Modified Struve function of zeroth order and real argument $\alpha_{nm}\epsilon$,

$J_o(\beta_{nm}\epsilon)$ = Bessel function of zeroth order and real argument $\beta_{nm}\epsilon$, and

$H_o(\beta_{nm}\epsilon)$ = Struve function of zeroth order and real argument $\beta_{nm}\epsilon$.

With expression (4.5), the kernel $\overline{K}_{kk}(x,x')$ can be written as

$$\overline{K}_{kk}(x,x') = \int_{z_k-\epsilon}^{z_k+\epsilon} K_{kk}(x\ ,x',z')dx' = \overline{K}^{i}_{kk}(x,x') + \int_{z_k-\epsilon}^{z_k+\epsilon} K^{o}_{kk}(x,x',z')dz'$$

where the superscripts "i" and "o" refer to the inside or the outside components of the kernel, and

$$\bar{K}^{i}_{kk}(x,x') = \frac{1}{ab}\sum_{n=1}^{\infty}\sum_{m=0}^{\infty}\left(\frac{\epsilon_m}{\gamma_{nm}}\right)\sin\left(\frac{n\pi x}{a}\right)\sin\left(\frac{n\pi x'}{a}\right)$$

$$\cdot\begin{cases}[I_o(\alpha_{nm}\epsilon) - L_o(\alpha_{nm}\epsilon)] \;\cdots\; \text{for} \quad \gamma_{nm} = \alpha_{nm} + j0 \\ [J_o(\beta_{nm}\epsilon) - jH_o(\beta_{nm}\epsilon)] \;\cdots\; \text{for} \quad \gamma_{nm} = 0 + j\beta_{nm}\end{cases} \tag{4.7a}$$

and

$$K^{o}_{kk}(x,x',z') = \frac{G^{o}(x,z_k,x'z')}{\pi\sqrt{\epsilon^2 - (z_k - z')^2}} \; . \tag{4.7b}$$

Using the complementarity principle, the radius of an equivalent dipole is found to be $\frac{\epsilon}{2}$, and, therefore, $\bar{K}^{o}_{kk}(x,x')$ can be approximated as

$$\int_{z_k-\epsilon}^{z_k+\epsilon} K^{o}_{kk}(x,x',z')dz' = \bar{K}^{o}_{kk}(x,x') \approx \frac{2}{\sqrt{3}\,\pi\epsilon}\,\frac{e^{-jk_o\sqrt{(x-x')^2+(\epsilon/2)^2}}}{2\pi\sqrt{(x-x')^2+(\epsilon/2)^2}} \; . \tag{4.7c}$$

Equations (4.7) lead to the following approximate expression for $\bar{K}_{kk}(x,x')$ for the purpose of studying its behavior with respect to x':

$$\bar{K}_{kk}(x,x') \approx \bar{K}^{i}_{kk}(x,x') + \bar{K}^{o}_{kk}(x,x') \; .$$

Figure (4.1) shows the behavior of $|\bar{K}^{o}_{kk}(x,x')|$ and $|\bar{K}^{i}_{kk}(x,x')|$ against $k_o|x - x'|$. It can be seen that as $x' \to x$, both $|\bar{K}^{o}_{kk}|$ and $|\bar{K}^{i}_{kk}|$ have significant peaks. It is also noted that $|\bar{K}^{i}_{kk}|$ follows $|\bar{K}^{o}_{kk}|$ closely if $\epsilon = \lambda_o/200$ with $n_{max} = m_{max} = 100$. Other points on the figure show effects of variation of ϵ from $\lambda_o/400$ to $\lambda_o/60$. There is no significant change in the shape of the curve. Figure (4.2) shows $\mathrm{Re}(\bar{K}^{o}_{kk}(x,x'))$, $\mathrm{Im}(\bar{K}^{o}_{kk}(x,x'))$,

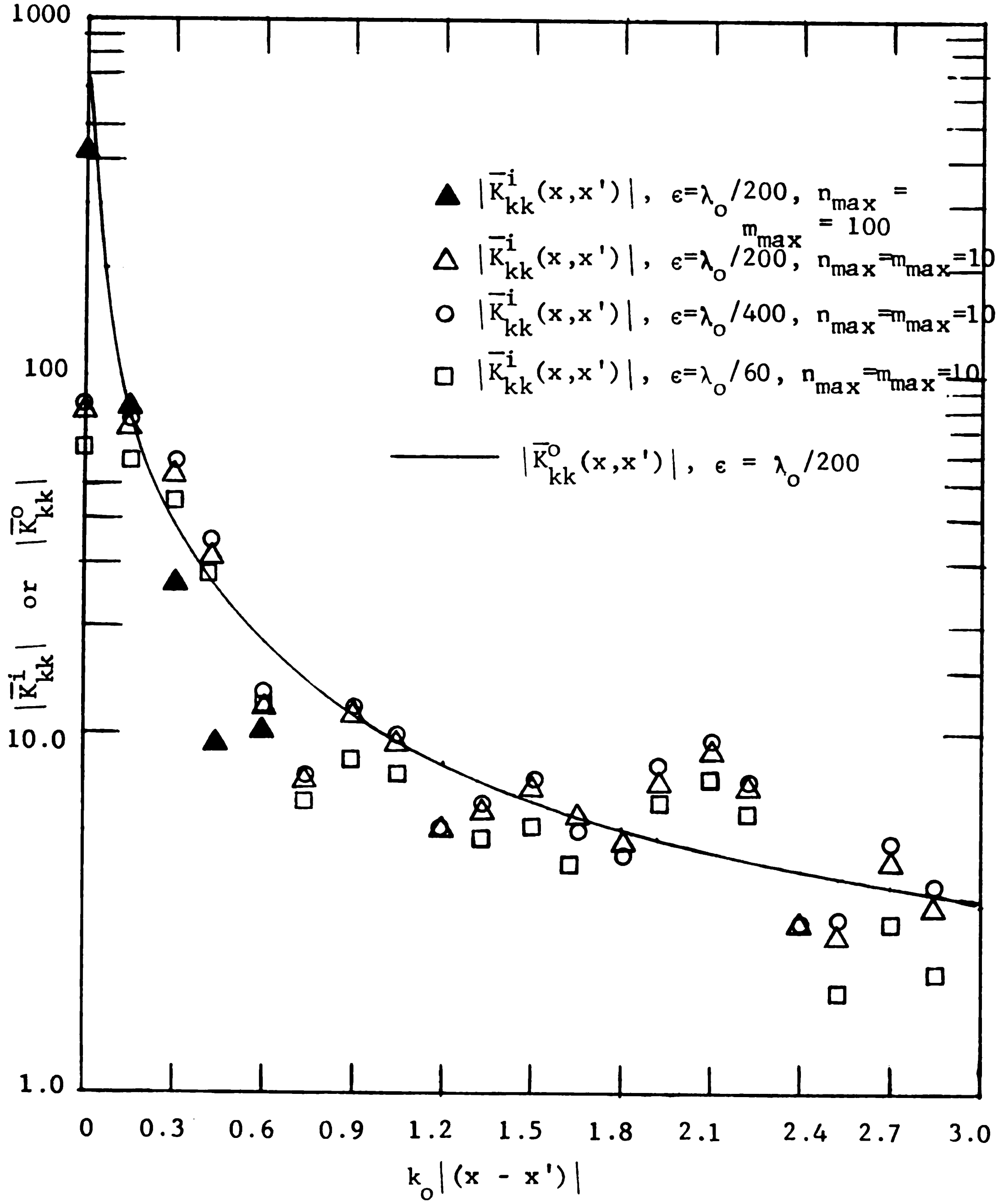

Figure 4.1. Magnitude of $\bar{K}_{kk}$ vs $k_o|(x-x')|$.

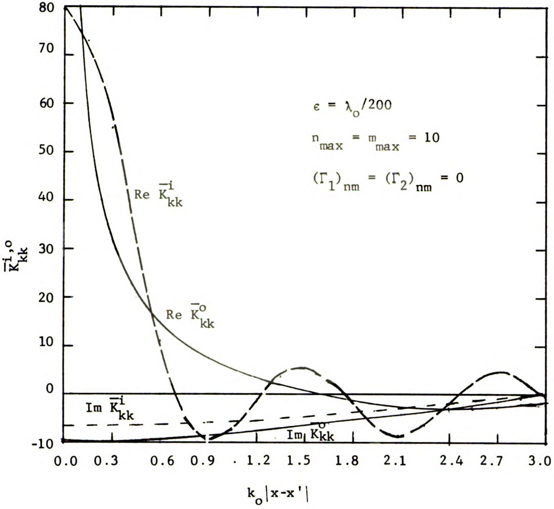

Figure 4.2. $\overline{K}^{i,o}_{ki}(x,x')$ vs $k_o|x-x'|$.

$\mathrm{Re}(\overline{K}^{i}_{kk}(x,x'))$ and $\mathrm{Im}(\overline{K}^{i}_{kk}(x,x'))$ vs $k_o|x - x'|$. Again, as $x \to x'$, the real parts of both $\overline{K}^{o}_{kk}$ and $\overline{K}^{i}_{kk}$ have significant peaks while the imaginary parts of both $\overline{K}^{o}_{kk}$ and $\overline{K}^{i}_{kk}$ remain relatively constant.

This behavior of $\overline{K}_{kk}(x,x')$ leads to the following expressions for $\mathrm{Re}[A_k(x)]$ and $\mathrm{Im}[A_k(x)]$. According to the definition for $A_k(x)$, its real and imaginary parts are

$$\mathrm{Re}[A_k(x)] = A_{kR}(x) = \sum_{i=1}^{N} \int_{a/2-h_i}^{a/2+h_i} V_i(x')\overline{K}_{kiR}(x,x')dx'$$

and

$$\mathrm{Im}[A_k(x)] = A_{kI}(x) = \sum_{i=1}^{N} \int_{a/2-h_i}^{a/2+h_i} V_i(x')\overline{K}_{kiI}(x,x')dx'$$

where

$$\overline{K}_{ki}(x,x') = \overline{K}_{kiR}(x,x') + j\overline{K}_{kiI}(x,x').$$

Since the kernel $\overline{K}_{kkR}(x,x')$ is quite small except at or near $x' = x$, where it rises to a large value, while $\overline{K}_{kiR}(x,x')$ is always relatively small for $i \neq k$, then it is clear that slot voltage $V_k(x')$ near $x' = x$ is primarily significant in determining the value of $A_{kR}(x)$ at x. In other words

$$\begin{aligned} A_{kR}(x) &= \sum_{i=1}^{N} \int_{a/2-h_i}^{a/2+h_i} V_i(x')\overline{K}_{kiR}(x,x')dx' \\ &\approx \sum_{i=1}^{N} \Big[(1-\delta_{ik}) \int_{a/2-h_i}^{a/2+h_i} V_i(x')\overline{K}_{kiR}(x,x')dx' + \delta_{ik}\Psi_{kkR}V_k(x)\Big] \qquad (4.8a) \end{aligned}$$

where

$$\delta_{ik} = \begin{cases} 0 & \ldots \text{ if } i \neq k \\ 1 & \ldots \text{ if } i = k \end{cases}$$

and Ψ_{kkR} is a proportionality constant.

Due to the non-peaking nature of $\bar{K}_{kiR}$ for $i \neq k$, the remaining integrals in equation (4.8a) are relatively small in amplitude with functional forms which can be approximated analytically. Through extensive numerical computations, King and his co-workers (12) have demonstrated that the functional forms of each of these integrals is approximately proportional to $\cos k_o(x - a/2)$. $A_{kR}(x)$ can, consequently, be approximated as

$$A_{kR}(x) \approx \sum_{i=1}^{N} (1 - \delta_{ik})\Psi_{kiR}\cos k_o(x - a/2) + \delta_{ki}\Psi_{kkR}V_k(x) \qquad (4.8b)$$

where the Ψ_{ki} are constants.

Integrals involved in $A_{kI}(x)$ can be approximated due to the non-peaking property of kernel $\bar{K}_{kiI}$ for all values of i and k. Again, King and his co-workers (12) have demonstrated that a simple analytical approximation for $\bar{K}_{kiI}$ is valid for antennas with half lengths satisfying $k_oh_i \leq \frac{5\pi}{4}$. Subject to this approximation for $\bar{K}_{kiI}$, it follows that each of the integrals in the expression for $A_{kI}(x)$ is approximately proportional to $\cos k_o(x - a/2)$. Consequently, an approximation for $A_{kI}(x)$ which is valid for $k_oh_k \leq \frac{5\pi}{4}$ is given by

$$A_{kI}(x) \approx A_{kI}(a/2)\cos \tfrac{1}{2}k_o(x - a/2) \qquad (4.8c)$$

where $A_{kI}(a/2)$ is, of course, a constant.

Expression (4.8b) is essentially the proportionality exploited by King-Sandler dipole array theory. As indicated earlier, the contribution to $A_{kR}(x)$ in equation (4.8b) from terms with $i \neq k$ is small compared to the term for $i = k$. Thus to a good approximation

$$A_{kR}(x) \approx \Psi_{kk} V_k(x) \ . \tag{4.8d}$$

However, $V_k(x = a/2 + h_k) = 0$ while $A_{kR}(x = a/2 + h_k)$ is small but non-zero. It is therefore apparent that a more accurate proportionality is

$$V_k(x) \propto [A_{kR}(x) - A_{kR}(a/2 + h_k)],$$

such that $V_k(a/2 + h_k) = 0$. Evidently, a better approximation than equation (4.8b) is

$$A_{kR}(x) - A_{kR}(a/2 + h_k) \approx \sum_{i=1}^{N} (1 - \delta_{ik})\Psi_{dkiR} F_{ox}^{k}(x) + \delta_{ik}\Psi_{dkkR} V_k(x) \tag{4.9a}$$

where $F_{ox}^{k}(x) = \cos k_o(x - a/2) - \cos k_o(h_k)$. Similarly, a good approximation for the difference form of $A_{kI}(x)$ is

$$A_{kI}(x) - A_{kI}(a/2 + h_k) \approx A_{kI}(a/2)[\cos \tfrac{1}{2}k_o(x - a/2) - \cos k_o(h_k)]. \tag{4.9b}$$

4.2.2 Alternative System of Difference Integral Equations for the $V_i(x)$:

It is now necessary to formulate an alternative system of integral equations for the $V_i(x)$ in terms of the difference $A_k(x) - A_k(a/2 + h_k)$.

From equation (2.33) it is found that

$$A_k(a/2 + h_k) = C_k \cos k_o h_k - j \frac{\zeta_o}{2} I_k \sin k_o h_k \ . \tag{4.10}$$

Subtracting equation (4.10) from equation (2.33) gives

$$\begin{aligned} A_k(x) - A_k(a/2 + h_k) &= C_k[\cos k_o(x - a/2) - \cos(k_o h_k)] \\ &\quad - j \frac{\zeta_o}{2} I_k[\sin k_o|x - a/2| - \sin k_o h_k]. \end{aligned} \tag{4.11}$$

Solving equation (4.10) for C_k leads to

$$C_k = \frac{1}{\cos(k_o h_k)} [A_k(a/2 + h_k) + j \frac{\zeta_o}{2} I_k \sin(k_o h_k)],$$

or

$$C_k = \frac{j\zeta_o}{\cos(k_o h_k)} [U_k + \frac{I_k}{2} \sin(k_o h_k)] \tag{4.12}$$

where U_k has been defined as

$$U_k = \frac{1}{j\zeta_o} A_k(a/2 + h_k)$$

$$= \frac{1}{j\zeta_o} \sum_{i=1}^{N} \int_{a/2-h_i}^{a/2+h_i} V_i(x')\bar{K}_{ki}(a/2 + h_k,x')dx' .$$

Substituting expression (4.12) for C_k in equation (4.11):

$$A_k(x) - A_k(a/2 + h_k) = \frac{j\zeta_o}{\cos(k_o h_k)} \{\frac{I_k}{2} \sin k_o(h_k - |x - a/2|) +$$

$$U_k[\cos k_o(x - a/2) - \cos k_o h_k]\}$$

or

$$A_k(x) - A_k(a/2 + h_k) = \frac{j\zeta_o}{\cos(k_o h_k)} [\frac{I_k}{2} M^k_{ox}(x) + U_k F^k_{ox}(x)] \tag{4.13a}$$

where by definition

$$\left.\begin{aligned} M^k_{ox}(x) &= \sin k_o(h_k - |x - a/2|) \\ F^k_{ox}(x) &= \cos k_o(x - a/2) - \cos k_o h_k \end{aligned}\right\} . \tag{4.13b}$$

Definition (4.3) for $A_k(x)$ yields the integral representation

$$A_k(x) - A_k(a/2 + h_k) = \sum_{i=1}^{N} \int_{a/2-h_i}^{a/2+h_i} V_i(x')\bar{K}_{dki}(x,x')dx', \tag{4.14a}$$

where $\bar{K}_{dki}(x,x') = \bar{K}_{ki}(x,x') - K_{ki}(a/2 + h_k,x')$.

Equations (4.13) and (4.14) lead to an alternative system of integral equations for the $V_i(x)$ in terms of the difference $A_k(x) - A_k(a/2 + h_k)$, as:

$$\sum_{i=1}^{N} \int_{a/2-h_i}^{a/2+h_i} V_i(x')\bar{K}_{dki}(x,x')dx' = \frac{j\zeta_o}{\cos(k_o h_k)} [\frac{I_k}{2} M^k_{ox}(x) + U_k F^k_{ox}(x)]. \quad (4.15)$$

4.2.3 Analytical Approximations for Slot Voltage Distributions:

The next step is to make use of the approximations contained in equations (4.9) in order to deduce a simple analytical approximation for the slot voltages $V_i(x)$. With equations (4.9), it is clear that the integral in equation (4.15) can be approximated as follows:

$$\sum_{i=1}^{N} \int_{a/2-h_i}^{a/2+h_i} V_i(x')\bar{K}_{dki}(x,x')dx' \approx [\Psi_{dkkR} V_k(x) + Q\, F^k_{ox}(x) + W\, H^k_{ox}(x)] \quad (4.16)$$

where Q and W are constant coefficients and $H^k_{ox}(x)$ is defined as

$$H^k_{ox}(x) = \cos \tfrac{1}{2}k_o(x - a/2) - \cos k_o h_k. \quad (4.13c)$$

Substituting approximation (4.16) into integral equations (4.15) and solving the resulting equation for $V_k(x)$ it is found that

$$V_k(x) \approx \frac{j\zeta_o}{\Psi_{dkkR}\cos(k_o h_k)} [\frac{I_k}{2} M^k_{ox}(x) + (U_k + \frac{jQ \cos(k_o h_k)}{\zeta_o})F^k_{ox}(x)$$

$$+ \frac{jW \cos(k_o h_k)}{\zeta_o} H^k_{ox}(x)].$$

The above expression for $V_k(x')$ suggests the following zeroth-order approximation

$$V_k(x) \approx V_{kV}(x) + V_{kU}(x) + V_{kD}(x) \quad (4.17)$$

with

$$\left.\begin{aligned} V_{kV}(x) &= V_{kV}M^{k}_{ox}(x) \\ V_{kU}(x) &= V_{kU}F^{k}_{ox}(x) \\ V_{kD}(x) &= V_{kD}H^{k}_{ox}(x) \end{aligned}\right\} , \qquad (4.18)$$

where V_{kV}, V_{kU}, and V_{kD} are constant coefficients to be evaluated. King and his co-workers (12, 20) refer to the array theory using equation (4.17) as an approximation to $V_k(x)$ as the "three-term theory". It is also well known that the "two term" approximation to $V_k(x)$ obtained by dropping $V_{kD}(x)$ leads to results of good accuracy for arrays with element lengths satisfying $k_o h_k \leq \pi$. The latter two-term voltage approximation will be utilized in the investigation of the waveguide-backed slot array from this point on.

4.2.4 Reduction of the System of Integral Equations to a System of Algebraic Equations:

A differential equation for the difference $A_k(x) - A_k(a/2+h_k)$ is obtained by adding $-k_o^2 A_k(a/2 + h_k)$ to both sides of equation (2.30) (with $E_o = 0$) as

$$\left(\frac{\partial^2}{\partial x^2} + k_o^2\right)[A_k(x) - A_k(a/2 + h_k)] = -j\zeta_o k_o I_k \delta(x - a/2) - k_o^2 A_k(a/2+h_k) . \qquad (4.19)$$

If $\overline{K}_{dki}(x,x')$ is split into real and imaginary components as

$$\overline{K}_{dki}(x,x') = \overline{K}_{dkiR}(x,x') + j\overline{K}_{dkiI}(x,x') ,$$

then

$$[A_k(x) - A_k(a/2 + h_k)] = \sum_{i=1}^{N} \int_{a/2-h_i}^{a/2+h_i} V_i(x')\bar{K}_{dki}(x,x')dx'$$

$$= \sum_{i=1}^{N} \int_{a/2-h_i}^{a/2+h_i} [V_{iV}M^i_{ox}(x') + V_{iU}F^i_{ox}(x')]\cdot[\bar{K}_{dkiR}(x,x')$$

$$+ j\bar{K}_{dkiI}(x,x')]dx \ . \qquad (4.20)$$

Based upon the peaking property of $\bar{K}_{dkkR}$ and the non-peaking nature of $\bar{K}_{dkiR}$ $(i \neq k)$ and $\bar{K}_{dkiI}$, the various integrals can be approximated in terms of simple trigonometric functions as demonstrated by King et al. (12), (20). The results of these approximations are as follows:

$$\sum_{i=1}^{N} \int_{a/2-h_i}^{a/2+h_i} V_{iV}M^i_{ox}(x')\bar{K}_{dki}(x,x')dx' \approx V_{kV}\Psi_{dkkR}M^k_{ox}(x)$$

$$+ jV_{kV}\Psi_{dkkI}F^k_{ox}(x) + \sum_{i=1}^{N}(1 - \delta_{ik})V_{iV}\Psi_{dVki}F^i_{ox}(x) \qquad (4.21a)$$

$$\sum_{i=1}^{N} \int_{a/2-h_i}^{a/2+h_i} V_{iU}F^i_{ox}(x')\bar{K}_{dki}(x,x')dx' \approx \sum_{i=1}^{N} V_{iU}\Psi_{Uki}F^i_{ox}(x) \ . \qquad (4.21b)$$

The various approximately constant Ψ functions in equations (4.21) are defined as follows:

$$\Psi_{dkkR} = \begin{cases} \Psi_{dkkR}(a/2) & \ldots \text{ for } h_k \leq \lambda_o/4 \\ \Psi_{dkkR}(a/2 + h_k - \lambda_o/4) & \ldots \text{ for } h_k > \lambda_o/4 \end{cases}$$

$$\Psi_{dkkR}(x) = \frac{1}{M^k_{ox}(x)} \int_{a/2-h_k}^{a/2+h_k} M^k_{ox}(x')\bar{K}_{dkkR}(x,x')dx'$$

$$\Psi_{dkkI} = \frac{1}{F^k_{ox}(a/2)} \int_{a/2-h_k}^{a/2+h_k} M^k_{ox}(x')\bar{K}_{dkkI}(a/2,x')dx' \tag{4.22}$$

$$\Psi_{dVki} = \frac{1}{F^i_{ox}(a/2)} \int_{a/2-h_i}^{a/2+h_i} M^i_{ox}(x')\bar{K}_{dki}(a/2,x')dx' \quad \ldots \text{ for } i \neq k$$

$$\Psi_{dUki} = \frac{1}{F^i_{ox}(a/2)} \int_{a/2-h_i}^{a/2+h_i} F^i_{ox}(x')\bar{K}_{dki}(a/2,x')dx' \quad .$$

Substituting approximations (4.21) into equation (4.19):

$$\left(\frac{\partial^2}{\partial x^2} + k_o^2\right)\Big\{ \sum_{i=1}^{N} V_{iV}[\Psi_{dkiR}M^i_{ox}(x)\delta_{ik} + j\Psi_{dkiI}F^i_{ox}(x)\delta_{ik}$$

$$+ (1 - \delta_{ik})\Psi_{dVki}F^i_{ox}(x)] + \sum_{i=1}^{N} V_{iU}\Psi_{dUki}F^i_{ox}(x)\Big\}$$

$$= -jk_o\zeta_o I_k\delta(x - a/2) - k_o^2 A_k(a/2 + h_k). \tag{4.23}$$

Noting that the differentiations on M^k_{ox} and F^k_{ox} can be carried out as

$$\left(\frac{\partial^2}{\partial x^2} + k_o^2\right)M_{ox}^k(x) = -2k_o\delta(x - a/2)\cos(k_oh_k)$$

$$\left(\frac{\partial^2}{\partial x^2} + k_o^2\right)F_{ox}^k(x) = -k_o^2 \cos(k_oh_k)$$

and that $A_k(a/2 + h_k)$ can be evaluated in the form

$$\begin{aligned} A_k(a/2 + h_k) &= \sum_{i=1}^{N} \int_{a/2-h_i}^{a/2+h_i} V_i(x')\bar{K}_{ki}(a/2 + h_k,x')dx' \\ &= \sum_{i=1}^{N} [V_{iV}\Psi_{Vki} + V_{iU}\Psi_{Uki}] \end{aligned} \tag{4.24}$$

where

$$\left.\begin{aligned} \Psi_{Vki} &= \int_{a/2-h_i}^{a/2+h_i} M_{ox}^i(x')\bar{K}_{ki}(a/2 + h_k,x')dx' \\ \Psi_{Uki} &= \int_{a/2-h_i}^{a/2+h_i} F_{ox}^i(x')\bar{K}_{ki}(a/2 + h_k,x')dx' \end{aligned}\right\} , \tag{4.25}$$

equation (4.23) becomes

$$\begin{aligned} &\sum_{i=1}^{N} \{V_{iV}[2k_o\delta_{ik}\Psi_{dkiR}\delta(x - a/2)\cos(k_oh_i) + jk_o^2\delta_{ik}\Psi_{dkiI} \cos(k_oh_i) \\ &+ k_o^2(1 - \delta_{ik})\Psi_{dVki} \cos(k_oh_i)] + V_{iU}[k_o^2\Psi_{dUki} \cos(k_oh_i)]\} \\ &= jk_o\zeta_oI_k\delta(x - a/2) + k_o^2 \sum_{i=1}^{N} [V_{iV}\Psi_{Vki} + V_{iU}\Psi_{Uki}] . \end{aligned} \tag{4.26}$$

Equating the coefficients of $\delta(x - a/2)$ on both sides of equation (4.26) leads to

$$V_{kV}\Psi_{dkkR} \cos(k_oh_k) = \frac{j\zeta_oI_k}{2}$$

or

$$V_{kV} = \frac{j\zeta_oI_k}{2\Psi_{dkkR} \cos(k_oh_k)} , \text{ for } k = 1,\ldots,N, \tag{4.27}$$

while equality of the remaining terms in (4.26) yields

$$\sum_{i=1}^{N}\{V_{iV}[(1-\delta_{ik})\Psi_{dVki}\cos(k_o h_i) + j\delta_{ik}\Psi_{dkiI}\cos(k_o h_i)] + V_{iU}\Psi_{dUki}\cos(k_o h_i)] = \sum_{i=1}^{N}[V_{iV}\Psi_{Vki} + V_{iU}\Psi_{Uki}].$$

Rearranging the above equation finally leads to the desired matrix equation for the V_{iU} as

$$\sum_{i=1}^{N} V_{iU}[\Psi_{dUki}\cos(k_o h_i) - \Psi_{Uki}] = \sum_{i=1}^{N} V_{iV}\{\Psi_{Vki} - [\Psi_{dVki}(1-\delta_{ik}) + j\Psi_{dkiI}\delta_{ik}]\cos(k_o h_i)\} \quad \ldots \text{ for } k = 1,2,3,\ldots,N \qquad (4.28)$$

or in matrix form

$$[\Phi_U][V_U] = [\Phi_V][V_V], \qquad (4.29)$$

where

$$\left.\begin{aligned} \Phi_{Vki} &= \Psi_{Vki} - [\Psi_{dVki}(1-\delta_{ik}) + j\Psi_{dIki}\delta_{ik}]\cos k_o h_i \\ \text{and} \\ \Phi_{Uki} &= \Psi_{dUki}\cos k_o h_i - \Psi_{Uki} \end{aligned}\right\} . \qquad (4.30)$$

$[\Phi_U]$ and $[\Phi_V]$ are $(N \times N)$ square matrices whereas $[V_V]$ and $[V_U]$ are column matrices of order $(N \times 1)$. The elements V_{iV} of $[V_V]$ are known from equations (4.27) while the elements V_{iU} of $[V_U]$ are to be determined by inversion of equation (4.29). Once all the Ψ-functions as defined in expressions (4.22) and (4.25) are evaluated, the $[\Phi_U]$ and $[\Phi_V]$ matrices can be computed and equation (4.29) can be solved numerically for the unknown elements of $[V_U]$. Formally, the V_{iU} are given by

$$[V_U] = [\Phi_U]^{-1}[\Phi_V][V_V] . \qquad (4.31)$$

With equations (4.27) and (4.31), the approximate expressions for the slot voltage distributions can be written as:

$$V_k(x) \approx \frac{j\zeta_o I_k}{2\Psi_{dkkR}\cos(k_o h_k)} \sin k_o(h_k - |x-a/2|)$$

$$+ \{[\Phi_U]^{-1}[\Phi_V][V_V]\}_k[\cos k_o(x-a/2) - \cos k_o h_k]. \qquad (4.32)$$

The driving-point admittance Y_k of the kth slot is defined as

$$Y_k = \frac{I_k}{V_k(a/2)} . \qquad (4.33)$$

The corresponding input impedance to the slot is $Z_k = 1/Y_k$.

4.3 Evaluation of Various Ψ-Functions:

An inspection of equations (4.2), (4.3), (4.22), and (4.25) reveals that there are, basically, two types of integrals involved in the evaluation of the various Ψ-functions, one with $G^i(x,z_k,x',z')$ in the integrand and the other with $G^o(x,z_k,x',z')$ in the integrand. The integrals involving G^i will be evaluated analytically while those involving G^o will be evaluated numerically, using the same x and z partitioning scheme as described in Chapter 3 (Section 3.3.1).

4.3.1 Evaluation of Ψ_{dkkR} and Ψ_{dkkI} (for $h_k \leq \lambda_o/4$):

Equations (4.22) indicate that

$$\Psi_{dkk} = \Psi_{dkkR} + j\Psi_{dkkI} \qquad (4.34)$$

or

$$\Psi_{dkk} = [\frac{1}{M^k_{ox}(a/2)} \mathrm{Re}(I_{dkk}) + j\,\frac{1}{F^k_{ox}(a/2)} \mathrm{Im}(I_{dkk})] , \qquad (4.35)$$

where

$$I_{dkk} = \int_{a/2-h_k}^{a/2+h_k} \int_{z_k-\epsilon}^{z_k+\epsilon} \frac{\sin k_o(h_k - |x'-a/2|)}{\pi\sqrt{\epsilon^2-(z_k-z')^2}} \{G^i(a/2,z_k,x',z')$$

$$+ G^o(a/2,z_k,x',z') - G^i(a/2 + h_k,z_k,x',z')$$

$$- G^o(a/2 + h_k,z_k,x',z')\}dx'dz' \tag{4.36}$$

Equation (4.36) indicates that I_{dkk} involves two types of integrals; one with G^o in the integrand, denoted by I^o_{dkk}, and the other with G^i in the integrand, denoted by I^i_{dkk}. Using the fact that $\sin k_o(h_k - |x' - a/2|)$ in the integrand in I^o_{dkk} is an even function of x' about $x' = a/2$ and using the same partitioning scheme as described by equations (3.5) and (3.12) (see Fig. 3.1), I^o_{dkk} can be written as

$$I^o_{dkk} \approx \sum_{m=1}^{M_k} \sum_{p=1}^{p} \int_{(\Delta z')_{kp}} \int_{(\Delta x')_{km}} \frac{\sin k_o(h_k - x' + a/2)}{\pi\sqrt{\epsilon^2 - (z_k-z')^2}} \{G^o(a/2,z_k,x',z')$$

$$+ G^o(a/2,z_k,a-x',z') - G^o(a/2 + h_k,z_k,x',z') -$$

$$- G^o(a/2 + h_k, z_k,a-x',z')\}dx'dz' \tag{4.37}$$

where

$$\int_{(\Delta x)_{km}} \rightarrow \int_{x_{km}-\Delta x_k/2}^{x_{km}+\Delta x_k/2}, \text{ and } \int_{(\Delta z)_{kp}} = \int_{z_{kp}-\Delta z/2}^{z_{kp}+\Delta z/2} .$$

Integral I^o_{dkk} can finally be expressed as

$$I^o_{dkk} \approx \sum_{m=1}^{M_k} \sum_{p=1}^{p} [T_{mp}(k) - U_{mp}(k)] \tag{4.38}$$

where

$$T_{mp}(k) = \begin{cases} \left(\frac{\Delta x_k \cdot \Delta z}{\pi}\right) \frac{\sin k_o(h_k - x_{km} + a/2)}{\sqrt{\epsilon^2 - (z_k - z_{kp})^2}} [G^o(a/2, z_k, x_{km}, z_{kp}) \\ \quad + G^o(a/2, z_k, a - x_{km}, z_{kp})] \quad \text{... excluding } p = 1,\ p = P, \\ \qquad\qquad (p = \frac{P+1}{2} \text{ and } m = 1) \\ [0.5 + \frac{1}{\pi} \text{arc } \sin(\frac{\Delta z}{\epsilon} - 1)] \sin k_o(h_k - x_{km} + a/2)[G^o(a/2, z_k, \\ x_{km}, z_{kp}) + G^o(a/2, z_k, a - x_{km}, z_{kp})]\Delta x_k \quad \text{... for } p = 1 \text{ and} \\ \qquad\qquad p = P \text{ only.} \\ \left(\frac{2 \sin k_o h_k}{\pi^2 \epsilon}\right)[-jk_o \frac{\Delta x_k}{2} \frac{\Delta z}{2} + \frac{\Delta z}{2} \ell n(\frac{2\,\Delta x_k}{\Delta z} + \sqrt{1 + 4(\frac{\Delta x_k}{\Delta z})^2}) \\ \quad + \Delta x_k\, \ell n(\frac{\Delta z}{2\,\Delta x_k} + \sqrt{1 + 0.25(\frac{\Delta z}{\Delta x_k})^2})] \quad \text{... for } p = \frac{P+1}{2} \\ \qquad\qquad \text{and } m = 1. \end{cases} \tag{4.39a}$$

$$U_{mp}(k) = \begin{cases} \left(\frac{\Delta x_k \Delta z}{\pi}\right) \frac{\sin k_o(h_k - x_{km} + a/2)}{\sqrt{\epsilon^2 - (z_k - z_{kp})^2}} [G^o(a/2 + h_k, z_k, x_{km}, z_{kp}) \\ \quad + G^o(a/2 + h_k, z_k, z - x_{km}, z_{kp})] \quad \text{... excluding } p = 1,\ p = P, \\ \qquad\qquad (p = \frac{P+1}{2} \text{ and } m = M_k) \\ [0.5 + \frac{1}{\pi} \text{arc } \sin(\frac{\Delta z}{\epsilon} - 1)] \sin k_o(h_k - x_{km} + a/2)[G^o(a/2 + h_k, z_k, \\ x_{km}, z_{kp}) + G^o(a/2 + h_k, z_k, a - x_{km}, z_{kp})]\Delta x_k \quad \text{... for } p = 1 \\ \qquad\qquad \text{and } p = P \text{ only} \\ \frac{\sin(k_o \frac{\Delta x_k}{2})}{\pi^2 \epsilon} [\pi\, \Delta x_k \Delta z\, G^o(a/2 + h_k, z_k, a - x_{km}, z_{kp}) + \frac{\Delta z}{2} \ell n(\frac{2\Delta x_k}{\Delta z} \\ \quad + \sqrt{1 + 4(\frac{\Delta x_k}{\Delta z})^2}) + \Delta x_k \ell n(\frac{\Delta z}{2\Delta x_k} + \sqrt{1 + 0.25(\frac{\Delta z}{\Delta x_k})^2}) - jk_o \frac{\Delta x_k \Delta z}{2}] \\ \qquad\qquad \text{... for } p = \frac{P+1}{2} \text{ and } m = M_k. \end{cases} \tag{4.29b}$$

These results are obtained using the same approximation techniques described in Section 3.3.1 of Chapter 3.

Integrals I^{i}_{dkk} can be evaluated analytically in closed form, and are given as

$$I^{i}_{dkk} = \sum_{n=1}^{\infty} \sum_{m=0}^{\infty} [\sin(\frac{n\pi}{2}) - \sin(\frac{n\pi}{2} + k_x h_k)] D_{nm} L_n(k) Y_{nm}(k) \tag{4.40}$$

where $k_x = (\frac{n\pi}{a})$ while

$$D_{nm} = \frac{\epsilon_m}{\pi ab\, \gamma_{nm}[1 - (\Gamma_1)_{nm}(\Gamma_2)_{nm}]} , \tag{4.41a}$$

$$\begin{aligned} L_n(k) &= \int_{a/2-h_k}^{a/2+h_k} \sin k_o(h_k - |x' - a/2|) \sin k_x x' dx' \\ &= \frac{2k_o \sin(\frac{n\pi}{2})}{[k_o^2 - (\frac{n\pi}{a})^2]} (\cos k_x h_k - \cos k_o h_k) , \end{aligned} \tag{4.41b}$$

and (in terms of $f_{nm}(z,z')$ defined in Chapter 2)

$$Y_{nm}(k) = \int_{z_k-\epsilon}^{z_k+\epsilon} \frac{f_{nm}(z_k,z')dz'}{\sqrt{\epsilon^2 - (z_k - z')^2}}$$

$$Y_{nm}(k) = \begin{cases} \pi\{[I_o(\alpha_{nm}\epsilon) - L_o(\alpha_{nm}\epsilon)] - (\Gamma_1)_{nm} e^{-2\alpha_{nm} z_k} I_o(\alpha_{nm}\epsilon) \\ \quad - (\Gamma_2)_{nm} e^{2\alpha_{nm} z_k} I_o(\alpha_{nm}\epsilon) + (\Gamma_1)_{nm}(\Gamma_2)_{nm}[I_o(\alpha_{nm}\epsilon) \\ \quad + L_o(\alpha_{nm}\epsilon)]\} \quad \ldots \text{ if } \gamma_{nm} = \alpha_{nm} + j0 \\ \pi\{[J_o(\beta_{nm}\epsilon) - jH_o(\beta_{nm}\epsilon)] - (\Gamma_1)_{nm} e^{-2j\beta_{nm} z_k} J_o(\beta_{nm}\epsilon) \\ \quad - (\Gamma_2)_{nm} e^{2j\beta_{nm} z_k} J_o(\beta_{nm}\epsilon) + (\Gamma_1)_{nm}(\Gamma_2)_{nm}[J_o(\beta_{nm}\epsilon) \\ \quad + jH_o(\beta_{nm}\epsilon)]\} \quad \ldots \text{ if } \gamma_{nm} = 0 + j\beta_{nm} . \end{cases} \tag{4.41c}$$

(J_o, H_o) = Bessel and Struve functions, respectively of zeroth order and real argument;

(I_o, L_o) = Modified Bessel and Struve functions, respectively of zeroth order and real argument.

Appendix II demonstrates the details of the z'-integration involved in obtaining equation (4.41c).

Equations (4.38) through (4.41), when substituted in expression (4.35), determine Ψ_{dkk} and, from expression (4.34), Ψ_{dkkR} and Ψ_{dkkI}.

4.3.2 Evaluation of Ψ_{dVki}:

Equations (4.22) defines expression for Ψ_{dVki} as

$$\Psi_{dVki} = \frac{1}{F^i_{ox}(a/2)} \int_{a/2-h_i}^{a/2+h_i} M^i_{ox}(x')\bar{K}_{dki}(a/2,x')dx' .$$

This definition can be rewritten as

$$\Psi_{dVki} = (1 - \cos k_o h_i)^{-1} I_{dVki} = (1 - \cos k_o h)^{-1} (I^o_{dVki} + I^i_{dVki}) \qquad (4.42)$$

where

$$I^o_{dVki} = \int_{a/2-h_i}^{a/2+h_i} \int_{z_i-\epsilon}^{z_i+\epsilon} \frac{\sin k_o(h_i - |x' - a/2|)}{\pi\sqrt{\epsilon^2 - (z_i - z')^2}} \{G^o(a/2,z_k,x',z')$$

$$- G^o(a/2 + h_k,z_k,x',z')\}dx'dz' \qquad (4.43a)$$

and

$$I^i_{dVki} = \int_{a/2-h_i}^{a/2+h_i} \int_{z_i-\epsilon}^{z_i+\epsilon} \frac{\sin k_o(h_i - |x' - a/2|)}{\pi\sqrt{\epsilon^2 - (z_i - z')^2}} \{G^i(a/2,z_k,x',z')$$

$$- G^i(a/2 + h_k,z_k,x',z')\}dx'dz'. \qquad (4.43b)$$

Again, I^o_{dVki} involves the function $M^i_{ox}(x')$ in its integrand which is even about $x' = a/2$. Also, since $i \neq k$, z' can be taken to be approximately z_i for the purpose of performing the x'-integration, that is, G^o is a slowly varying function of z' (good approximation for narrow slots, $k_o\epsilon \ll 1$). It is therefore possible to write equation (4.43a) as

$$I^o_{dVki} \approx \int_{z_i-\epsilon}^{z_i+\epsilon} \frac{dz'}{\pi\sqrt{\epsilon^2 - (z_i - z')^2}} \int_{a/2}^{a/2+h_i} \sin k_o(h_i - x' + a/2)$$

$$[G^o(a/2,z_k,x',z_i) + G^o(a/2,z_k,a-x',z_i) - G^o(a/2 + h_k,z_k,x',z_i)$$

$$- G^o(a/2 + h_k,z_k,a-x',z_i)]dx' .$$

The z'-integration evaluates to unity as follows

$$\int_{z_i-\epsilon}^{z_i+\epsilon} \frac{dz'}{\pi\sqrt{\epsilon^2 - (z_i - z')^2}} = \frac{1}{\pi} \text{arc sin} \left.\frac{(z'-z_i)}{\epsilon}\right|_{-\epsilon}^{+\epsilon} = 1,$$

and I^o_{dVki} becomes:

$$I^o_{dVki} \approx \int_{a/2}^{a/2+h_i} \sin k_o(h_i - x' + a/2)[G^o(a/2,z_k,x',z')$$

$$+ G^o(a/2,z_k,a-x',z_i) - G^o(a/2 + h_k,z_k,x',z_i)$$

$$- G^o(a/2 + h_k,z_k,a-x',z_i)]dx' .$$

Using the same x-partitioning scheme described in equations (3.5), I^o_{dVki} can be calculated numerically as

$$I^o_{dVki} = \sum_{m=1}^{M_i} \sin k_o(h_i - x_{im} + a/2)Q_m(k,i)\Delta x_i$$

where

$$Q_m(k,i) = G^o(a/2,z_k,x_{im},z_i) + G^o(a/2,z_k,a-x_{im},z_i)$$

$$- G^o(a/2 + h_k,z_k,x_{im},z_i) - G^o(a/2 + h_k,z_k,a-x_{im},z_i). \qquad (4.44a)$$

In evaluating I^i_{dVki}, the fact that for $i \neq k$, $z' \approx z_i$ insofar as the z'-dependence of G^i is concerned (i.e., $f_{nm}(z_k,z') \approx f_{nm}(z_k,z_i)$), leads to the following evaluation of I^i_{dVki}:

$$I^i_{dVki} \approx \sum_{n=1}^{\infty} \sum_{m=0}^{\infty} \pi[\sin(\tfrac{n\pi}{2}) - \sin(\tfrac{n\pi}{2} + k_x h_k)] D_{nm} f_{nm}(z_k,z_i) L_n(i) \qquad (4.44b)$$

where k_x and D_{nm} were defined earlier while

$$f_{nm}(z_k,z_i) = e^{-\gamma_{nm}|z_k-z_i|} - (\Gamma_1)_{nm} e^{-\gamma_{nm}(z_k+z_i)}$$

$$- (\Gamma_2)_{nm} e^{\gamma_{nm}(z_k+z_i)} + (\Gamma_1)_{nm}(\Gamma_2)_{nm} e^{\gamma_{nm}|z_k-z_i|} \qquad (4.44c)$$

and

$$L_n(i) = \frac{2k_o \sin(\frac{n\pi}{2})}{[k_o^2 - (\frac{n\pi}{2})^2]} (\cos k_x h_i - \cos k_o h_i) . \qquad (4.44d)$$

Equations (4.44) together with equations (4.43) and (4.42) completely determine Ψ_{dVki}.

4.3.3 <u>Evaluation of</u> Ψ_{duki}:

According to definition (4.22), Ψ_{duki} is

$$\Psi_{duki} = (1 - \cos k_o h_i)^{-1} \int_{a/2-h_i}^{a/2+h_i} [\cos k_o(x'-a/2) - \cos k_o h_i]$$

$$\bar{K}_{dki}(a/2,x')dx'.$$

This equation can be expressed in the form

$$\Psi_{duki} = (1 - \cos k_o h_i)^{-1}[I^o_{duki} + I^i_{duki}] \qquad (4.45)$$

where

$$I^o_{duki} = \int_{a/2-h_i}^{a/2+h_i} \int_{z_i-\epsilon}^{z_i+\epsilon} [\cos k_o(x'-a/2) - \cos(k_o h_i)][G^o(a/2,z_k,x',z') - G^o(a/2 + h_k,z_k,x',z')]dx'dz', \qquad (4.46)$$

and

$$I^i_{duki} = \int_{a/2-h_i}^{a/2+h_i} \int_{z_i-\epsilon}^{z_i+\epsilon} [\cos k_o(x'-a/2) - \cos k_o h_i]\{G^i(a/2,z_k,x',z') - G^i(a/2 + h_k,z_k,x',z')\}dx'dz'. \qquad (4.47)$$

Since the shifted cosine function in the integrand of I^o_{dUki} is an even function of x' about $x' = a/2$, then, using the same numerical techniques discussed in evaluating I^o_{dVki} and I^o_{dkk}, equation (4.46) can be approximated as

$$I^o_{duki} \approx (\Delta x_i) \sum_{m=1}^{M_i} [\cos k_o(x_{im}-a/2) - \cos k_o h_i]Q_m(k,i) \quad \ldots \text{ for } i \neq k, \qquad (4.48a)$$

$$I^o_{duki} \approx \sum_{m=1}^{M_i} \sum_{p=1}^{P} [T'_{mp}(k) - U'_{mp}(k)] \quad \ldots \text{ for } i = k, \qquad (4.48b)$$

where $Q_m(k,i)$ is defined in equation (4.44a) while $T'_{mp}(k)$ and $U'_{mp}(k)$ are given by:

$$T'_{mp}(k) = \begin{cases} \frac{(\Delta x_k)(\Delta z)}{\pi} \frac{[\cos k_o(x_{km}-a/2)-\cos k_oh_k]}{\sqrt{\epsilon^2 - (z_k-z_{kp})^2}} [G^o(a/2,z_k,x_{km},z_{kp}) \\ \quad + G^o(a/2,z_k,a-x_{km},z_{kp})] \ \ldots \text{ excluding } p = 1,\ p = P, \\ \qquad\qquad (p = \frac{P+1}{2} \text{ and } m = 1) \\ [0.5 + \frac{1}{\pi} \text{arc sin}(\frac{\Delta z}{\epsilon} - 1)][\cos k_o(x_{km}-a/2)-\cos k_oh_k] \\ [G^o(a/2,z_k,x_{km},z_{kp}) + G^o(a/2,z_k,a-x_{km},z_{kp})]\Delta x_k \\ \qquad\qquad \ldots \text{ for } p = 1 \text{ and } p = P, \text{ only,} \\ \frac{2}{\pi^2\epsilon}(1 - \cos k_oh_k)[\frac{-jk_o\Delta x_k\Delta z}{2} + \frac{\Delta z}{2}\ln(\frac{2\Delta x_k}{\Delta z} + \sqrt{1 + 4(\frac{\Delta x_k}{\Delta z})^2}) \\ \quad + \Delta x_k\ln(\frac{\Delta z}{2\Delta x_k} + \sqrt{1 + 0.25(\frac{\Delta z}{\Delta x_k})^2})] \\ \qquad\qquad \ldots \text{ for } p = \frac{P+1}{2} \text{ and } m = 1 \text{ only} \end{cases} \tag{4.48c}$$

and

$$U'_{mp}(k) = \begin{cases} \frac{(\Delta x_k)(\Delta z)}{\pi} \frac{[\cos k_o(x_{km}-a/2)-\cos k_oh_k]}{\sqrt{\epsilon^2 - (z_k-z_{kp})^2}} [G^o(a/2+h_k,z_k,x_{km},z_{kp}) \\ + G^o(a/2+h_k,z_k,a-x_{km},z_{kp})] \ \ldots \text{ excluding } p = 1,\ p = P, \\ \qquad\qquad (p = \frac{P+1}{2} \text{ and } m = M_k) \\ [0.5 + \frac{1}{\pi} \text{arc sin}(\frac{\Delta z}{\epsilon} - 1)][\cos k_o(x_{km}-a/2)-\cos k_oh_k] \\ [G^o(a/2+h_k,z_k,x_{km},z_{kp}) + G^o(a/2+h_k,z_k,a-x_{km},z_{kp})] \\ \qquad\qquad \ldots \text{ for } p = 1,\ p = P \text{ only} \\ \frac{1}{\pi^2\epsilon}[\cos k_o(h_k-\frac{\Delta x_k}{2})-\cos k_oh_k][\pi G^o(a/2+h_k,z_k,a-x_{km},z_{kp})\Delta x_k\Delta z \\ + \frac{\Delta z}{2}\ln(\frac{2\Delta x_k}{\Delta z})+\sqrt{1 + 4(\frac{\Delta x_k}{\Delta z})^2}) + \Delta x_k\ln(\frac{\Delta z}{2\Delta x_k} + \sqrt{1+0.25(\frac{\Delta z}{\Delta x_k})^2}) \\ -jk_o \frac{\Delta x_k\ \Delta z}{2}] \ \ldots \text{ for } p = \frac{P+1}{2} \text{ and } m = M_k. \end{cases} \tag{4.48d}$$

Again, noting that for $i \neq k$, $f_{nm}(z_k,z') \approx f_{nm}(z_k,z_i)$ in the integrand of expression (4.47), the closed form evaluation of I^i_{dUki} is

$$I^i_{dUki} = \begin{cases} \displaystyle\sum_{n=1}^{\infty}\sum_{m=0}^{\infty} \frac{2\pi k_o[k_o \sin(k_x h_i)\cos(k_o h_i) - k_x \sin(k_o h_i)\cos(k_x h_i)]}{k_x(k_o^2 - k_x^2)} D_{nm} \sin(\tfrac{n\pi}{2}) \\ \qquad f_{nm}(z_k,z_i)[\sin k_x(a/2 + h_k) - \sin(\tfrac{n\pi}{2})] \\ \qquad\qquad \ldots \text{ for } i \neq k \qquad (4.49a) \\ \displaystyle\sum_{n=1}^{\infty}\sum_{m=0}^{\infty} \frac{2k_o[k_o \sin(k_x h_k)\cos(k_o h_k) - k_x \sin(k_o h_k)\cos(k_x h_k)]}{k_x(k_o^2 - k_x^2)} \sin(\tfrac{n\pi}{2}) \\ \qquad D_{nm} Y_{nm}(k)[\sin k_x(a/2 + h_k) - \sin(\tfrac{n\pi}{2})] \ldots \text{ for } i = k \qquad (4.49b) \end{cases}$$

where $Y_{nm}(k)$ was defined in equation (4.41e).

Equations (4.49) and (4.48) along with equation (4.45) completely specify Ψ_{dUki}.

4.3.4 <u>Evaluation of</u> Ψ_{Vki}.

Equation (4.25) defines Ψ_{Vki} to be

$$\Psi_{Vki} = \int_{a/2-h_i}^{a/2+h_i} \sin k_o(h_i - |x'-a/2|)\bar{K}_{ki}(a/2 + h_k, x')dx'.$$

This definition can be expressed alternatively in the form

$$\Psi_{Vki} = \Psi^o_{Vki} + \Psi^i_{Vki} \qquad (4.50)$$

where

$$\Psi^o_{vKi} = \int_{a/2-h_i}^{a/2+h_i} \int_{z_i-\varepsilon}^{z_i+\varepsilon} \frac{\sin k_o(h_i - |x'-a/2|)}{\pi\sqrt{\varepsilon^2 - (z_i - z')^2}} G^o(a/2+h_k, z_k, x', z')dx'dz'$$

and

$$\Psi^{i}_{Vki} = \int_{a/2-h_i}^{a/2+h_i} \int_{z_i-\epsilon}^{z_i+\epsilon} \frac{\sin k_o(h_i-|x'-a/2|)}{\pi\sqrt{\epsilon^2-(z_i-z')^2}} G^{i}(a/2+h_k,z_k,x',z')dx'dz' .$$

Comparing these expressions for Ψ^{o}_{Vki} and Ψ^{i}_{Vki} with expressions (4.43a) and (4.43b), respectively, it is clear that the evaluation for Ψ^{o}_{Vki} and Ψ^{i}_{Vki} are given by certain terms from equations (4.44). Therefore, by inspection of the earlier results for $i \neq k$

$$\Psi^{o}_{Vki} = \Delta x_i \sum_{m=1}^{M_k} \{\sin k_o(h_i-x_{im}+a/2)[G^{o}(a/2+h_k,z_k,x_{im},z_i) + G^{o}(a/2+h_k,z_k,a-x_{im},z_i)]\} \quad \ldots \text{ for } i \neq k \tag{4.51a}$$

and

$$\Psi^{i}_{Vki} = \sum_{n=1}^{\infty} \sum_{m=0}^{\infty} \pi \sin k_x(a/2+h_k)D_{nm}f_{nm}(z_k,z_i)L_n(i) \quad \ldots \text{ for } i \neq k. \tag{4.51b}$$

For $i = k$, a comparison with expression (4.36) yields the following evaluation for Ψ^{o}_{Vkk} and Ψ^{i}_{Vkk}

$$\Psi^{o}_{Vkk} = \sum_{m=1}^{M_k} \sum_{p=1}^{P} U_{mp}(k) \quad \ldots \text{ for } i = k, \tag{4.52a}$$

and

$$\Psi^{i}_{Vkk} = \sum_{n=1}^{\infty} \sum_{m=0}^{\infty} \sin k_x(a/2+h_k)D_{nm}L_n(k)Y_{nm}(k) \quad \ldots \text{ for } i = k, \tag{4.52b}$$

where expressions for $U_{mp}(k)$, D_{nm}, $L_n(k)$, and $Y_{nm}(k)$ are given by expressions (4.39b) and (4.41), respectively.

4.3.5 Evaluation of Ψ_{Uki}.

Equations (4.25) define Ψ_{Uki} as

$$\Psi_{Uki} = \int_{a/2-h_i}^{a/2+h_i} [\cos k_o(x'-a/2) - \cos k_o h_i]\bar{K}_{ki}(a/2+h_k,x')dx' .$$

An equivalent expression for Ψ_{Uki} is

$$\Psi_{Uki} = \Psi^{i}_{Uki} + \Psi^{o}_{Uki} \qquad (4.53)$$

where

$$\Psi^{i}_{Uki} = \int_{a/2-h_i}^{a/2+h_i} \int_{z_i-\epsilon}^{z_i+\epsilon} \frac{[\cos k_o(x'-a/2) - \cos k_o h_i]}{\pi\sqrt{\epsilon^2 - (z_i-z')^2}}\, G^{i}(a/2+h_k, z_k, x', z')\,dx'dz'$$

and

$$\Psi^{o}_{Uki} = \int_{a/2-h_i}^{a/2+h_i} \int_{z_i-\epsilon}^{z_i+\epsilon} \frac{[\cos k_o(x'-a/2) - \cos k_o h_i]}{\pi\sqrt{\epsilon^2 - (z_i-z')^2}}\, G^{o}(a/2+h_k, z_k, x', z')\,dx'dz'.$$

Comparing the above expressions for Ψ^{o}_{Vki} and Ψ^{i}_{Vki} with expressions (4.46) and (4.47), respectively, it is clear that certain terms from equations (4.48) and (4.49) constitute the evaluations for Ψ^{o}_{Uki} and Ψ^{i}_{Uki}, respectively. Therefore, by inspection of the earlier results

$$\Psi^{o}_{Uki} = \begin{cases} (\Delta x_i) \sum_{m=1}^{M_i} [\cos k_o(x_{im}-a/2) - \cos k_o h_i][G^{o}(a/2+h_k, z_k, x_{im}, z_i) \\ \qquad + G^{o}(a/2+h_k, z_k, a-x_{im}, z_i)] \;\ldots\; \text{for} \quad i \neq k & (4.54a) \\ \sum_{m=1}^{M_k} \sum_{p=1}^{P} U'_{mp}(k) \quad \ldots \; \text{for} \quad i = k & (4.54b) \end{cases}$$

and

$$\Psi^{i}_{Uki} = \begin{cases} \sum_{n=1}^{\infty} \sum_{m=0}^{\infty} \frac{2\pi k_o[k_x \sin(k_o h_i)\cos(k_x h_i) - k_o \cos(k_o h_i)\sin(k_x h_i)]}{k_x(k_o^2 - k_x^2)} \\ \sin(\frac{n\pi}{2} + k_x h_k)\sin(\frac{n\pi}{2}) D_{nm} f_{nm}(z_k, z_i) \;\ldots\; \text{for} \quad i \neq k & (4.55a) \\ \sum_{n=1}^{\infty} \sum_{m=0}^{\infty} \frac{2k_o[k_x \sin(k_o h_k)\cos(k_x h_k) - k_o \cos(k_o h_k)\sin(k_x h_k)]}{k_x(k_o^2 - k_x^2)} \\ \sin(\frac{n\pi}{2} + k_x h_k)\sin(\frac{n\pi}{2}) D_{nm} Y_{nm}(k) \quad \ldots \; \text{for} \quad i = k. & (4.55b) \end{cases}$$

With equations (4.35) through (4.52), all the Ψ-functions are now completely evaluated. Equation (4.27), then, yields V_{kV}, $k = 1,2,3,\ldots,N$, while expressions (4.30) for the elements of $[\Phi_U]$ and $[\Phi_V]$ can be calculated in terms of the known Ψ-functions. A computer program was developed to numerically calculate the elements of $[V_V]$, $[\Phi_V]$ and $[\Phi_U]$ and subsequently solve numerically the matrix equation (4.92) to generate the elements of $[V_U]$. Knowing $[V_V]$ and $[V_U]$, the slot voltages $V_k(x)$, $k = 1,2,3,\ldots,N$, can be found using equation (4.17). In the next section, the radiation fields maintained by these slot voltage distributions are determined.

4.4 Radiation Field Maintained by the Slot Array:

It was shown in section (2.4) that the radiation fields maintained by the slot array in two principle planes, namely, E-plane ($\varphi = -\pi/2$) and H-plane ($\varphi = 0$) are given by

$$\vec{E}^r_E(\vec{r}) \approx -\hat{\theta}\,\frac{jk_o e^{-jk_or}}{2\pi r} \sum_{i=1}^{N} e^{jk_oz_i\cos\theta} \int_{a/2-h_i}^{a/2+h_i} V_i(x')dx'$$

... E-plane radiation field (2.42)

and

$$\vec{E}^r_H(\vec{r}) \approx \hat{\phi}\,\frac{jk_o e^{-jk_or}}{2\pi r}\cos\theta \sum_{i=1}^{N} e^{jk_oz_i\cos\theta} \int_{a/2-h_i}^{a/2+h_i} V_i(x')e^{jk_ox'\sin\theta}dx'$$

... H-plane radiation field. (2.43)

Substituting the approximate analytical expression for $V_i(x')$ from equation (4.17) recognizing that coefficients V_{iV} and V_{iU} have now been determined, the x'-integrals in the above radiation field equations takes the form

$$\int_{a/2-h_i}^{a/2+h_i} \{V_{iV}\sin k_o(h_i - |x'-a/2|) + V_{iU}[\cos k_o(x'-a/2) - \cos k_o h_i]\}dx' \quad \ldots \text{ E-plane radiation field} \qquad (4.56a)$$

and

$$\int_{a/2-h_i}^{a/2+h_i} \{V_{iV}\sin k_o(h_i - |x'-a/2|) + V_{iU}[\cos k_o(x'-a/2) - \cos k_o h_i]\}e^{jk_o x'\sin\theta}dx' \quad \ldots \text{ for H-plane radiation field} \qquad (4.56b)$$

Noting that

$$\left.\begin{aligned}
&\int_{a/2-h_i}^{a/2+h_i} \sin k_o(h_i - |x'-a/2|)dx' = \frac{-2}{k_o}(\cos k_o h_i - 1), \\
&\int_{a/2-h_i}^{a/2+h_i} \cos k_o(x'-a/2)dx' = \frac{2}{k_o}\sin k_o h_i, \text{ and} \\
&\int_{a/2-h_i}^{a/2+h_i} \cos k_o h_i dx' = 2h_i \cos k_o h_i
\end{aligned}\right\} \qquad (4.56c)$$

then equations (4.56a) and (2.45) yield a final-expression for $\vec{E}^r_E(\vec{r})$ as

$$\vec{E}^r_E(\vec{r}) \approx -\hat{\theta}\,\frac{je^{-jk_o r}}{\pi r}\sum_{i=1}^{N} e^{jk_o z_i\cos\theta}[V_{iV}(1 - \cos k_o h_i) + V_{iU}(\sin k_o h_i - k_o h_i\cos k_o h_i)] \quad \ldots \text{ for } \vec{E}\text{-plane radiation field.} \qquad (4.57)$$

Noting further that

$$\int_{a/2-h_i}^{a/2+h_i} \sin k_o(h_i - |x'-a/2|)e^{jk_o x'\sin\theta}\,dx' = (\frac{-2}{k_o})\frac{e^{jk_o \frac{a}{2}\sin\theta}}{\cos^2\theta}$$

$$[\cos k_o h_i - \cos(k_o h_i \sin\theta)] \tag{4.58}$$

and

$$\int_{a/2-h_i}^{a/2+h_i} [\cos k_o(x'-a/2) - \cos k_o h_i]e^{jk_o x'\sin\theta}\,dx'$$

$$= \frac{-2\,e^{jk_o \frac{a}{2}\sin\theta}}{k_o}\{\frac{1}{\cos^2\theta}[\cos(k_o h_i)\sin\theta\,\sin(k_o h_i \sin\theta)$$

$$-\sin k_o h_i \cos(k_o h_i \sin\theta)] - \frac{\sin(k_o h_i \sin\theta)}{\sin\theta}\}, \tag{4.59}$$

euqations (4.56b) and (2.44) yield for $\vec{E}^r_H(\vec{r})$

$$\vec{E}^r_H(\vec{r}) \approx -\hat{\phi}\,\frac{je^{-jk_o r}}{\pi r}\,\frac{e^{jk_o \frac{a}{2}\sin\theta}}{\cos\theta}\sum_{i=1}^{N} e^{jk_o z_i \cos\theta}\{V_{iV}[\cos k_o h_i -$$

$$\cos(k_o h_i \sin\theta)] + V_{iU}[\cos(k_o h_i)\sin\theta\,\sin(k_o h_i \sin\theta) -$$

$$\sin k_o h_i \cos(k_o h_i \sin\theta) + \cos(k_o h_i)\sin(k_o h_i \sin\theta)(\cos^2\theta/\sin\theta)\}]$$

$$\ldots \text{ excluding } \theta = 0,\ \pi \text{ and } \frac{\pi}{2}\,. \tag{4.60}$$

Equation (4.60) becomes singular for $\theta = 0$, π and $\frac{\pi}{2}$. For these values of θ, the x'-integrals must be revaluated. Therefore, for $\theta = 0$, equation (2.43) assumes the form

$$\vec{E}^r_H(\vec{r}) \approx \hat{\phi}\,\frac{jk_o e^{-jk_o r}}{2\pi r}\sum_{i=1}^{N} e^{jk_o z_i}\int_{a/2-h_i}^{a/2+h_i}\{V_{iV}\sin k_o(h_i - |x'-a/2|)$$

$$+ V_{iU}[\cos k_o(x'-a/2) - \cos(k_o h_i)]\}dx' \ \ldots \text{ for } \theta = 0.$$

Using the results of expressions (4.56c), the above equation becomes

$$\vec{E}_H^r(\vec{r}) \approx -\hat{\phi}\,\frac{je^{-jk_or}}{\pi r}\sum_{i=1}^{N} e^{jk_oz_i}[V_{iV}(\cos k_oh_i - 1) + V_{iU}(k_oh_i\cos k_oh_i - \sin k_oh_i)] \quad \ldots \text{ for } \theta = 0. \tag{4.61}$$

For $\theta = \pi/2$, equation (2.43) gives

$$\vec{E}_H^r(\vec{r}) = 0 \quad \ldots \text{ for } \theta = \pi/2. \tag{4.62}$$

For $\theta = \pi$, equation (2.43) yields

$$\vec{E}_H^r(\vec{r}) \approx \hat{\theta}\,\frac{jk_oe^{-jk_or}}{2\pi r}\sum_{i=1}^{N} e^{-jk_oz_i}\int_{a/2-h_i}^{a/2+h_i}\{V_{iV}\sin k_o(h_i - |x'-a/2|) + V_{iU}[\cos k_o(x'-a/2) - \cos k_oh_i]\}dx'. \tag{4.63}$$

Using expressions (4.56c), the final form of $\vec{E}_H^r(\vec{r})$, for $\theta = \pi$ becomes

$$\vec{E}_H^r(\vec{r}) = -\hat{\phi}\,\frac{je^{-jk_or}}{\pi r}\sum_{i=1}^{N} e^{-jk_oz_i}[V_{Vi}(1 - \cos k_oh_i) + V_{Ui}(\sin k_oh_i - k_oh_i\cos k_oh_i)] \quad \ldots \text{ for } \theta = \pi. \tag{4.64}$$

Equations (4.57), (4.60), (4.61), (4.62) and (4.64) completely determine the radiation field maintained in the principle planes of the slot array.

4.5 Numerical Results:

In order to solve for the slot voltage distributions, the driving point admittance of the array and its radiation field, a computer program was developed and implemented on a CDC 6500 system.

As indicated by matrix equation (4.29) the order of the matrix involved is $(N \times N)$. For a 10-element array, then, a matrix of order of (10×10) results. This is to be compared with the matrix of minimum order of (100×100) that must be inverted to obtain adequate accuracy in a direct numerical solution (Section 3.6). Based on the results of section 3.6, ten x-partitions ($M_k = 10$) and five z-partitions ($P = 5$) were found to yield adequate accuracy in the numerical solution of the various Ψ-integrals while the double Fourier series truncated at $n_{max} = m_{max} = 10$ is found to provide sufficiently accurate results.

4.5.1 Investigation of Several Special Cases:

In order to check the accuracy of the extended King-Sandler theory for a waveguide backed slot array and to test the computer program, several special cases were considered and the numerical results compared to those of previously published research.

Figure (4.3) indicates the admittance $Y_o = G_o + jB_o$ of a single cavity-backed slot as a function of the cavity depth. These theoretical results of the new, extended King-Sandler array theory are compared to Galejs' theoretical (based upon a variational approach) and experimental results (8). Various dimensions are listed on the upper right hand corner of the figure. It is observed that for shallow cavities, the G_o (and B_o) values do not compare well, however, for $b/\lambda_o = 0.2$ and 0.5, both G_o and B_o compare

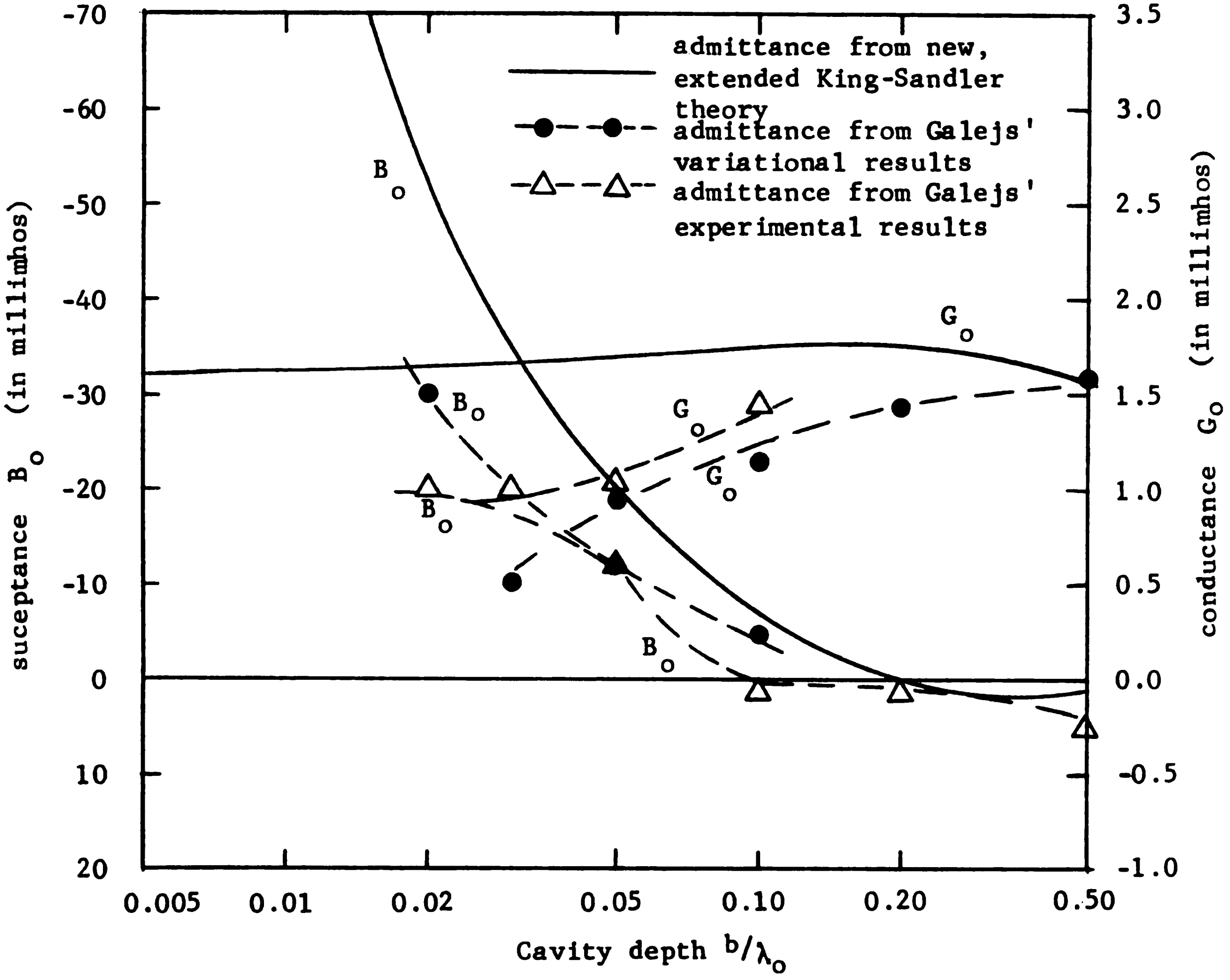

$a = 0.59\ \lambda_o$

$c = 0.116\ \lambda_o$

$\Gamma_1 = \Gamma_2 = -1.0$

$h_1 = 0.275\ \lambda_o$

$\epsilon = 2 \times 10^{-4}\ \lambda_o$

$\Omega = 2\ \ell n(4\ h_1/\epsilon) = 17.2$

$Z_1 = 2 \times 10^{-4} \lambda_o = \epsilon_o$

Figure 4.3. Admittance of a single cavity-backed slot as a function of cavity depth.

fairly well with Galejs' results. A decreasing cavity depth makes B_o approach an inductive short circuit ($B_o \rightarrow -\infty$). Resonance which is defined by $B_o = 0$, occurs at a cavity depth $b/\lambda_o = 0.3$. These deviations are to be expected since, for shallow cavities, the voltage distribution in the slot cannot be accurately predicted (8) using the simple sine $(M^k_{ox}(x))$ and shifted cosine $(F^k_{ox}(x))$ distribution functions.

The inaccuracy of the voltage distributions in a slot backed by a shallow cavity is confirmed in Figure (4.4), which shows the relative amplitude distribution of slot voltage for a single cavity backed slot with various cavity depths as a parameter. It can be observed that the new theoretical results based upon the modified and extended King-Sandler theory compare quite favorably with those predicted by Galejs' variational solution for $b/\lambda_o = 0.27$ and 0.5. However, for shallow cavities ($b/\lambda_o = 0.005$ and 0.05) the new array theory does not accurately predict the voltage distributions. The inability to accurately describe the voltage distribution in a narrow slot backed by a shallow cavity in terms of simple trigonometric functions was also observed by Galejs (8). It is evident that the new array theory is limited to slot arrays with backing waveguide having depths of $b \geq 0.25\ \lambda_o$.

Figure (4.5) demonstrates another special case consisting of a two element parasitic slot array. Front-to-back ratio of this array is plotted as a function of the element-spacing, $\Delta z/\lambda_o$, in the figure. It is observed that with a parasite element length of $h_2/\lambda_o = 0.25$ this element behaves like a reflector, while for $h_2/\lambda_o = 0.20$ the parasite behaves like a director for $0.05 \leq \Delta z/\lambda_o \leq 0.25$, and as a

$a = 0.6\ \lambda_o$ $\qquad \epsilon = Z_1 = 0.001\ \lambda_o$

$c = 0.05\ \lambda_o$ $\qquad h_1 = 0.3\ \lambda_o$

$\Gamma_1 = \Gamma_2 = -1.0$ $\qquad \Omega = 2\ \ell n(4h_1/\epsilon) = 14.2$

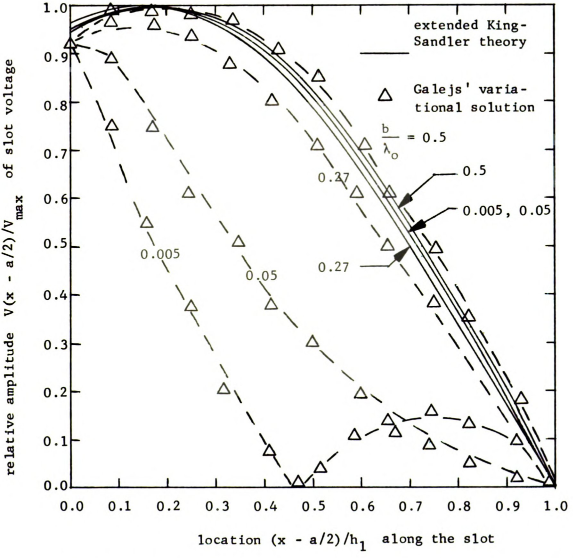

Figure 4.4. Slot voltage distribution in a single cavity-backed slot for various cavity depths (comparison with Galejs' variational solution).

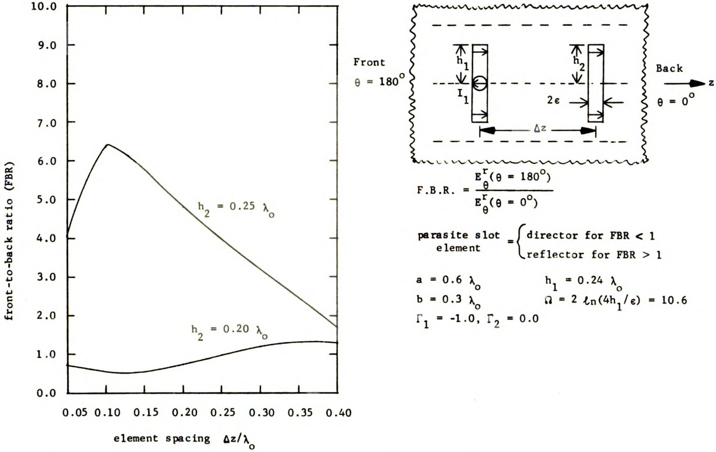

$$\text{F.B.R.} = \frac{E^r_\theta(\theta = 180^o)}{E^r_\theta(\theta = 0^o)}$$

$$\text{parasite slot element} = \begin{cases} \text{director for FBR} < 1 \\ \text{reflector for FBR} > 1 \end{cases}$$

$a = 0.6\ \lambda_o$ $\qquad h_1 = 0.24\ \lambda_o$

$b = 0.3\ \lambda_o$ $\qquad \Omega = 2\ \ell n(4h_1/\epsilon) = 10.6$

$\Gamma_1 = -1.0,\ \Gamma_2 = 0.0$

Figure 4.5. Dependence of the front-to-back ratios of the radiation field patterns for a two-element parasitic slot array upon the slot spacing.

reflector with $0.25 < \Delta z/\lambda_o \leq 0.40$. This indicates that with a driven element of near-resonant length $h_1/\lambda_o = 0.24$, the director length should be shorter than its resonant length with $\Delta z/\lambda_o \leq 0.25$ while the reflector length should be greater than its resonant length.

It was pointed out in section 4.2 that a slot array cut in an infinite ground screen situated in otherwise unbounded space is complementary to an array of strip dipoles and ultimately to an array of cylindrical dipoles. Consequently, the results for a single slot cut in an infinite ground plane and surrounded by free space on both sides $(G^i = G^o)$ should give the same results as those for the complementary cylindrical dipole radiating in free-space. Table 4.1 shows such a comparison for a slot with half length $h = 0.125\ \lambda_o$ and $\Omega = 10.6$. Numerical results for the cylindrical dipole were taken from the book by King, Mack, and Sandler (12). It is observed that the complementarity between a slot antenna and an equivalent cylindrical dipole is well established by numerical results of the slot theory developed here.

Figure (4.6) demonstrates a comparison between results for a ten-element (8-director) Yagi-Uda array of cylindrical dipoles and a complementary ten-element slot array studied using the new slot array theory with the backing waveguide removed. Figure (4.6) shows the relative amplitude and phase distributions of slot fields (complementary dipole antenna currents) in the elements of a 8-director Yagi-Uda array. The results for a Yagi-Uda array of cylindrical dipoles are taken from King, Mack and Sandler (12) (abbreviated as "KMS results" in the diagrams). An excellent agreement between result for the complementary Yagi-Uda slot array and the complementary

quantity	slot antenna (new theory)	complementary dipole (published results)
Ψ_{dR}	6.8646	6.9307
Ψ_{dI}	-0.1924	-0.1934
$\Psi_V(h)$	0.8202 - j0.5166	0.8222 - j0.5189
$\Psi_u(h)$	0.4542 - j0.2670	0.4583 - j0.2682
Ψ_{du}	7.1853 - j0.09915	7.2607 - j0.0963
Z_{in} (ohms)	3.2022 + j91.488	3.1804+j92.5250 (after conversion)

Table 4.1. Comparison of various Ψ-functions and input impedences for a slot antenna (new theory) and its complementary dipole (published results).

$G^i = G^o$

$(\Delta z)_{dir} = 0.30\ \lambda_o \quad h_1 = 0.25\ \lambda_o \quad \Omega = 2\ln(4h_2/\epsilon) = 10.6$

$(\Delta z)_{ref} = 0.25\ \lambda_o \quad h_2 = 0.245\ \lambda_o \quad h_3 - h_{10} = 0.20\ \lambda_o$

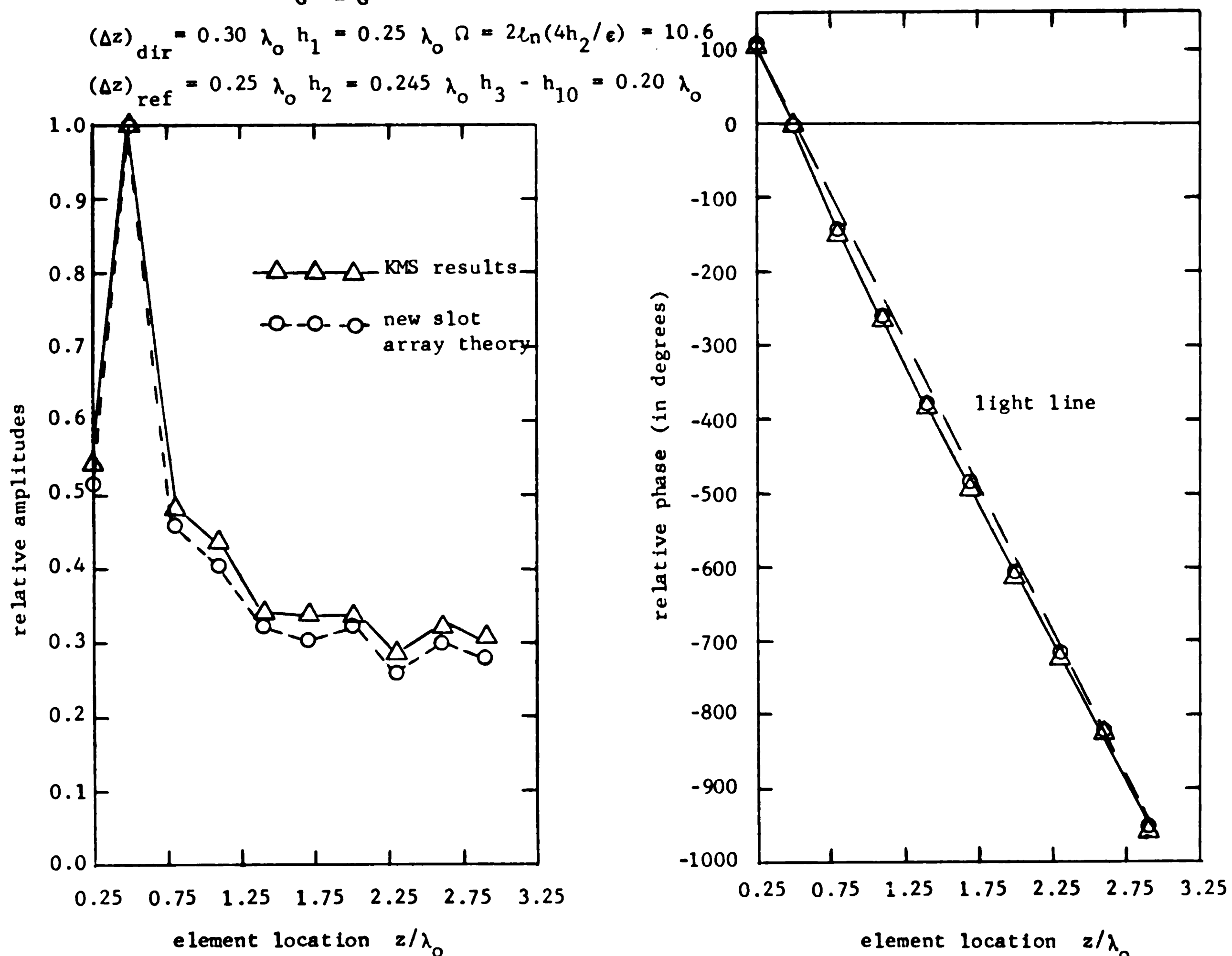

a. Amplitudes of element voltages and currents.

b. Phases of element voltages and currents.

Figure 4.6. Comparison of amplitudes and phases of slot voltages with those of currents in a complementary dipole array.

dipole array is obtained; this confirms the accuracy of both the analytical formulation of the new slot array theory and the computer program developed to implement it. Figure (4.7) indicates the associated E-plane radiation patterns, and again a good agreement between results for the two complementary arrays is obtained.

4.5.2 Five and Ten-Element, Waveguide-Backed, Yagi-Uda Slot Arrays:

A five-element, waveguide-backed Yagi-Uda slot array (one reflector and three directors) was investigated initially to ascertain the optimum values for the various array parameters (with minimum expenditure of computer time). Figure (4.8) shows the relative amplitude and phase distributions of voltages in the elements of the 5-element Yagi-Uda slot array. Various dimensions are identified at the top left-hand corner of the figure. The impressed currents $I_k = 0$ for $k = 1,3, 4$ and 5 while for $k = 2$, $I_k = (1 + j0)$ amperes. The half-length for director elements, $h_3 - h_5$ is fixed at $0.20\ \lambda_o$ while $h_1 = 0.25\ \lambda_o$ (reflector) and $h_2 = 0.24\ \lambda_o$ (driven element). The spacings between reflector and driven element as well as between the driven and director and all adjacent director elements is $\Delta z = 0.25\ \lambda_o$. The backing waveguide is matched at the output terminals ($\Gamma_2 = 0$) while it is short circuited a quarterwave length in front of the reflector element ($\Gamma_1 = -1.0$). The width of the slots is specified by the parameter $\Omega = 2\ell n(4h_2/\epsilon) = 10.6$.

The voltage amplitude distributions (Figure (4.8a)) in the slot elements of near resonant length closely approximate sinusoidal variations along the slot axes, which is expected since the slot voltage is described by shifted cosine and sinusoidal functions. Maxima of the amplitude distributions at the centers of slot elements

$G^i = G^o$ $h_1 = 0.255\ \lambda_o$ $\Omega = 2\ell n(4h_2/\varepsilon) = 10.6$

$h_2 = 0.245\ \lambda_o$ $h_3 - h_{10} = 0.20\ \lambda_o$

$(\Delta z)_{dir} = 0.3\ \lambda_o$ $(\Delta z)_{ref} = 0.25\ \lambda_o$

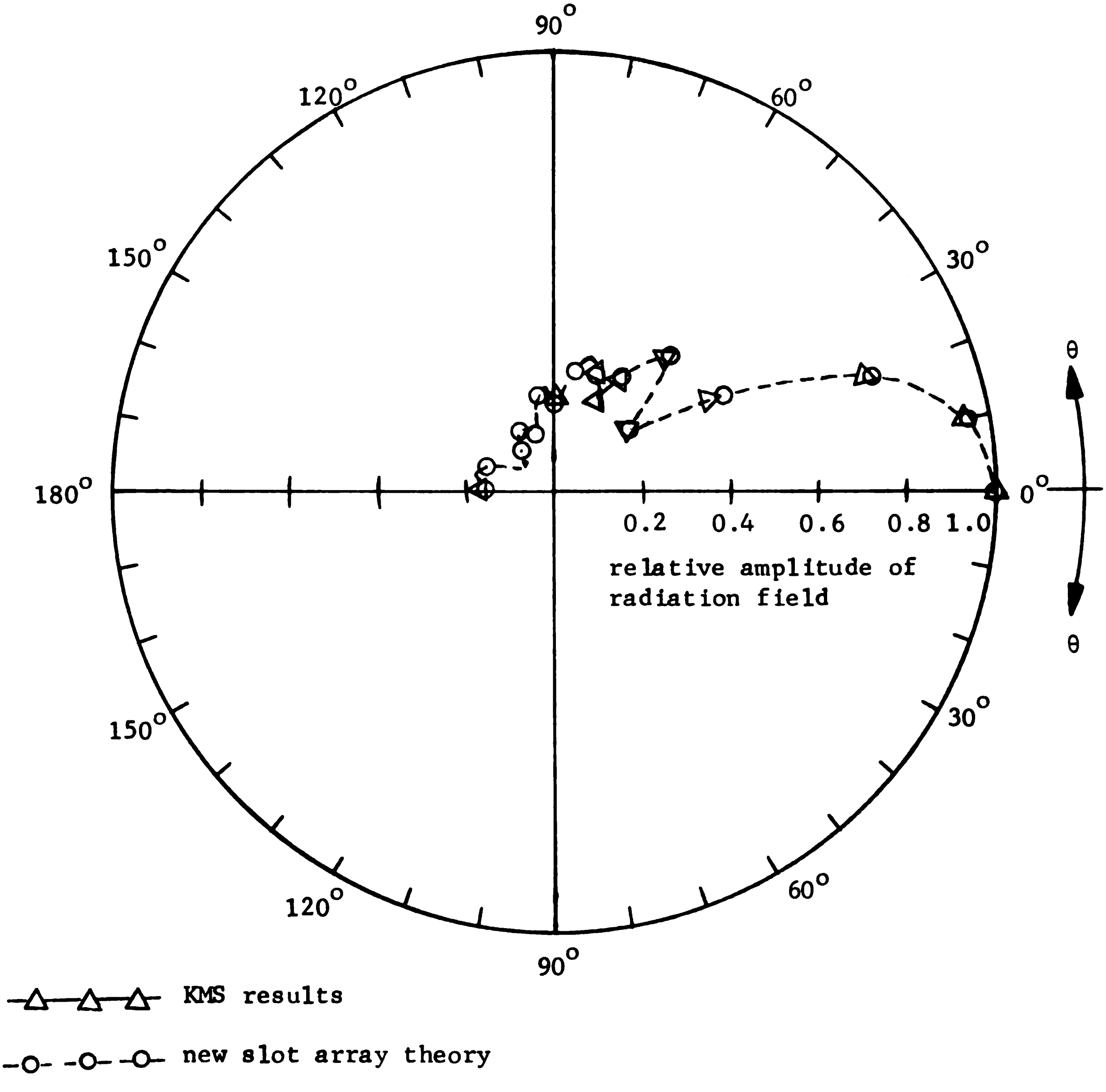

Figure 4.7. Comparison of E-plane radiation patterns for a 8-director Yagi-Uda slot array with those of a complementary dipole array.

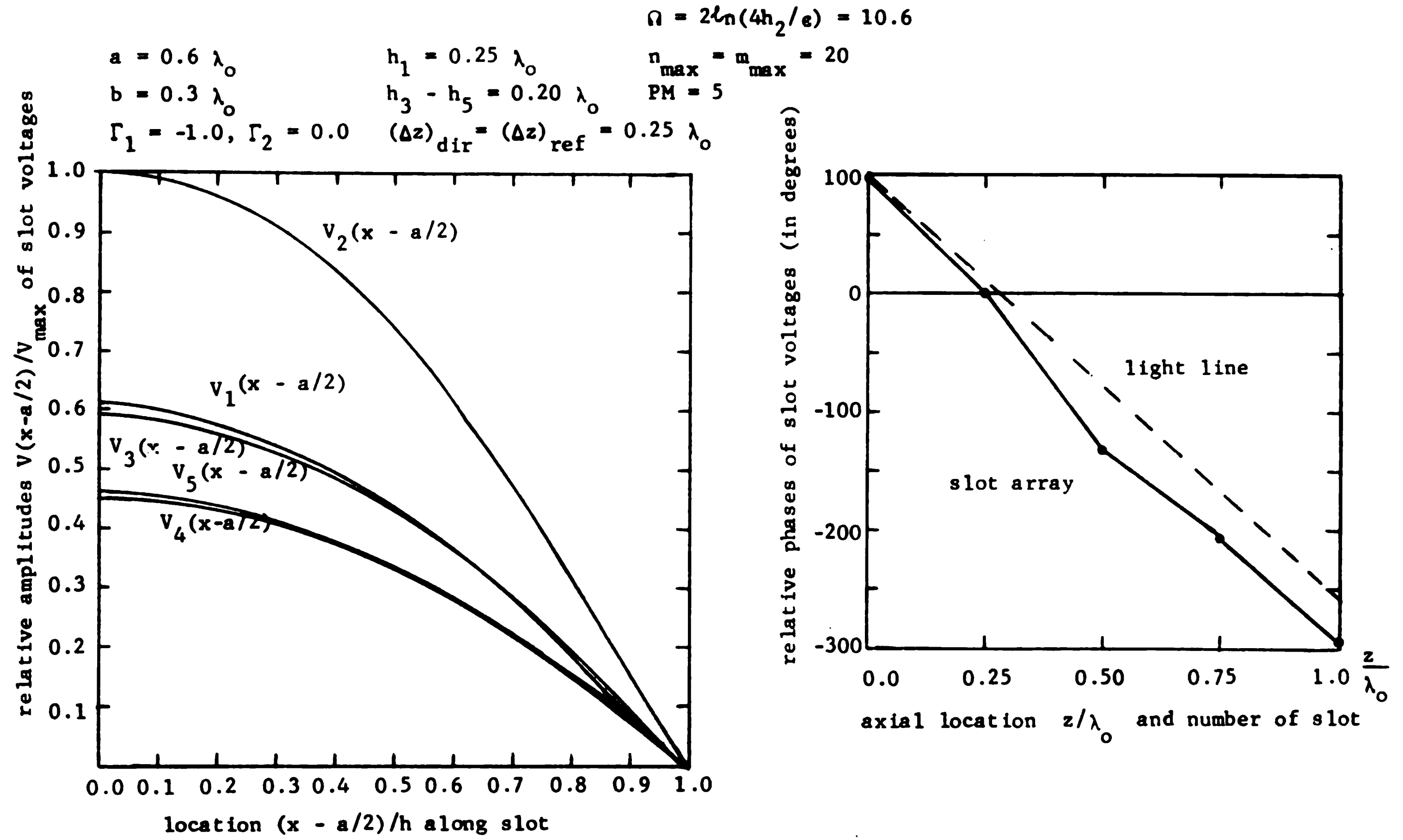

a. Voltage amplitude distributions in the slot elements.

b. Phases of slot voltages.

Figure 4.8. Voltage distributions in the elements of a 5-element Yagi-Uda slot array.

also display a standing-wave character. Slot number 2 has maximum induced voltage at its center, slots 1 and 3 have almost identical amplitude distributions of intermediate amplitude while slots 4 and 5 have nearly identical distributions of minimum amplitude, slot 5 having a slightly greater induced voltage than slot 4. This is expected, since slot number 2 is the driven element with slots 1 and 3 situated symmetrically relative to slot 2. Slot 5 has a greater induced voltage amplitude than slot 4 since the array is a finite one, and reflection of the wave in the aperture of the array is expected at its terminal end, thus resulting in a standing-wave field distribution in the elements along the array aperture.

Figure (4.8b) indicates an essentially uniform, progressive delay or lag in the phases of (successive) slot voltages along the array aperture. As before, the light line on Figure (4.8b) gives an indication whether the actual wave excited along the array aperture is a fast wave or a slow wave; since a slope greater than that of the light line indicates a larger phase constant, it corresponds to a traveling-wave aperture field with a phase velocity slower than the speed of light while a lesser slope indicates the existence of a fast-wave field. It can be identified from Figure (4.8b), therefore, that a wave traveling slightly slower than the speed of light exists along the array aperture. Thus, endfire radiation is expected from this array configuration, as is confirmed by Figure (4.10).

Figure (4.9) demonstrates relative amplitudes and phases of slot voltages in the aperture of the same 5-element Yagi-Uda slot array considered in Figure (4.8), except that now the effects of various element spacings, Δz, are considered. From Figure (4.9a),

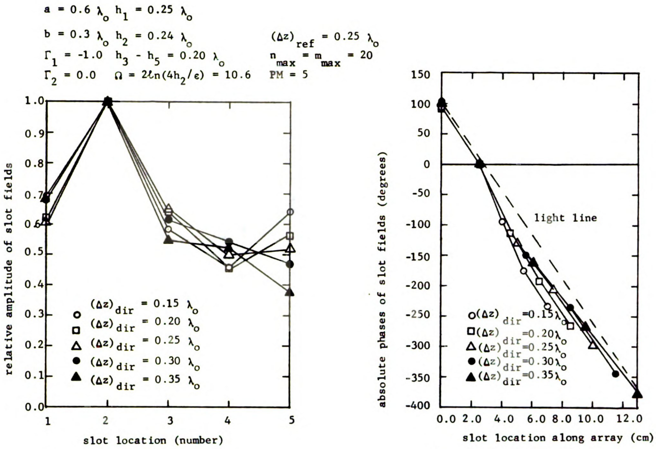

a. **Amplitudes of slot fields**

b. **Phases of slot fields**

Figure 4.9. Amplitudes and phases of the slot fields in the elements of a 5-element Yagi-Uda slot array for various director spacings.

$a = 0.6\ \lambda_o$

$b = 0.3\ \lambda_o$ $h_1 = 0.25\ \lambda_o$

$\Gamma_1 = -1.0$ $h_2 = 0.24\ \lambda_o$ $(\Delta z)_{ref} = 0.25\ \lambda_o$ $n_{max} = m_{max} = 20$

$\Gamma_2 = 1.0$ $h_3 - h_5 = 0.20\ \lambda_o$ $\Omega = 2\ell n(4h_2/\epsilon) = 10.6$ PM = 5

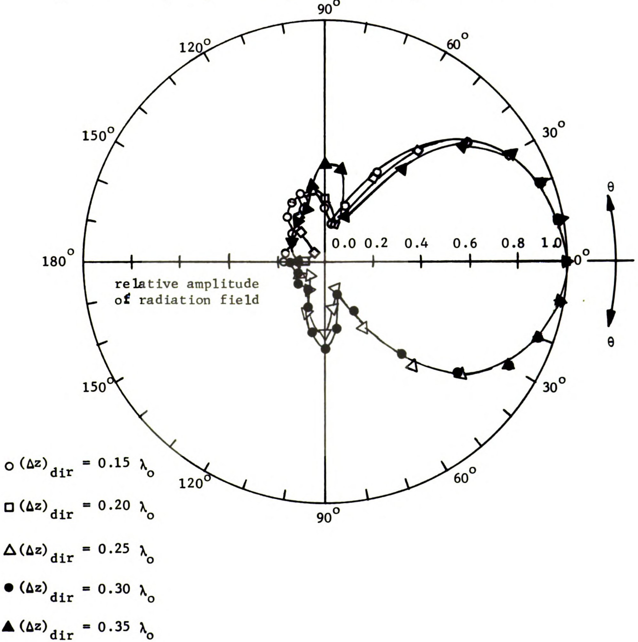

Figure 4.10. Dependence of $\vec{E}$-plane ($\phi = -\pi/2$) radiation field patterns of a 5-element Yagi-Uda slot array upon element spacings.

the essentially decaying, traveling-wave nature of the slot voltages (aperture field distribution) is apparent. Slot 5 again has a greater induced voltage amplitude than slot 4 when the element spacings are small, resulting in a short array aperture, due to reflections at the terminal end of the array. For large element spacings, for example, $(\Delta z)_{dir}/\lambda_o = 0.30$ or 0.35, which results in a large array aperture slot 5 has lower induced voltage amplitude than slot 4, indicating smaller terminal-end reflections.

Figure (4.9b) indicates a progressive phase delay (lag) in the elements along the array, and all values of $(\Delta z)_{dir}$ give rise to a slow wave aperture field. Endfire radiation is, therefore, expected for all values of $(\Delta z)_{dir}$, and in order to identify an optimum director-element separation, the radiation field of the array must be investigated.

Figure (4.10) shows the E-plane radiation field pattern of the same five-element, Yagi-Uda slot array investigated in Figure (4.9). All the radiation fields are end-fire in nature as expected. It is observed from Figure (4.10) that for $(\Delta z)_{dir}/\lambda_o = 0.15$ and 0.20, the side lobe amplitude is quite small with maxima of those lobes occurring at approximately 110 and 100 degrees, respectively. The mainlobe beam width, however, is relatively large due to the fact that the array has only five elements, one reflector and two directors. Major lobe beam width is decreased as the number of elements in the array is increased. For $(\Delta z)_{dir}/\lambda_o = 0.30$ and 0.35, the main lobe profiles are essentially the same as those discussed above, but the side lobes are now more pronounced while their maxima lie in the broadside direction. If $(\Delta z)_{dir}/\lambda_o = 0.25$, the major lobe is identical to that for $(\Delta z)_{dir}/\lambda_o = 0.30$, these are sharper patterns than for $(\Delta z)_{dir}/\lambda_o = 0.15$ and 0.20. The side lobe for the $(\Delta z)_{dir}/\lambda_o = 0.25$ array has its maximum along the broadside direction and its amplitude is smaller than those for $(\Delta z)_{dir}/\lambda_o = 0.30$ and 0.35. The back lobe radiation (at $\theta = 180^o$) is observed to be quite small for $(\Delta z)_{dir}/\lambda_o = 0.20$ and 0.25. Therefore, it appears that an optimal director element separation for this five element array is $(\Delta z)_{dir}/\lambda_o = 0.25$.

Figure (4.11) studies the same five-element array discussed in connection with Figures (4.9) and (4.10) except that in this case the director lengths (h_D) are being varied from 0.18 λ_o to 0.22 λ_o while $(\Delta z)_{dir}/\lambda_o = 0.25$. Figure (4.11a) indicates the relative amplitudes of the slot voltages versus the slot location $(\Delta z/\lambda_o)$ or number. For $h_D/\lambda_o = 0.18$ and 0.20, the relative amplitudes are as expected, i.e., maximum field (voltage) is excited in slot number 2, but for $h_D/\lambda_o = 0.22$, the maximum slot field occurs in element number 4. This is due to the fact that for near-resonant length slots with $h_D/\lambda_o = 0.22$ a standing wave field is set up along with the array aperture. A similar phenomenon is observed in connection with Yagi-Uda dipole arrays (20) as the director lengths approach resonance. However, the array with shorter directors maintain aperture fields having an attenuating traveling wave nature. Figure (4.11b) shows the absolute phases of the slot voltages along the array versus slot location $(\Delta z/\lambda_o)$, and it can be observed that each value of h_D/λ_o results in a slow-wave aperture field and expected end-fire radiation. To find the optimum director length, the E-plane radiation field patterns for various values of h_D/λ_o, as shown in Figure (4.12) must be considered.

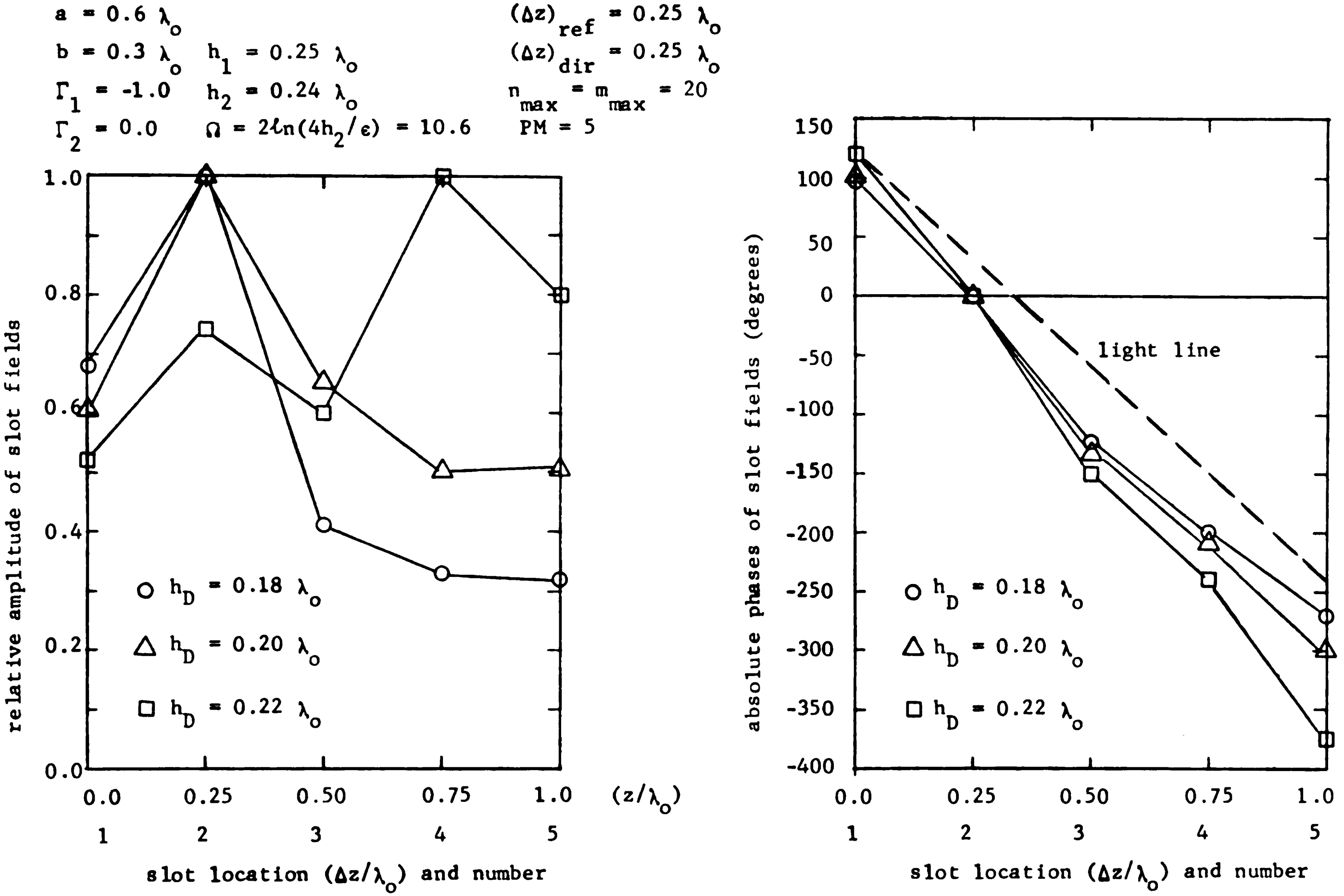

a. Amplitudes of slot fields

b. Phases of slot fields

Figure 4.11. Amplitudes and phases of the slot fields in the elements of a 5-element Yagi-Uda slot array for various director lengths.

$a = 0.6\ \lambda_o$

$b = 0.3\ \lambda_o$ $h_1 = 0.25\ \lambda_o$ $(\Delta z)_{ref} = 0.25\ \lambda_o$

$\Gamma_1 = -1.0$ $h_2 = 0.24\ \lambda_o$ $(\Delta z)_{dir} = 0.25\ \lambda_o$

$\Gamma_2 = 0.0$ $\Omega = 2\ell n(4h_2/\epsilon) = 10.6$ PM = 5

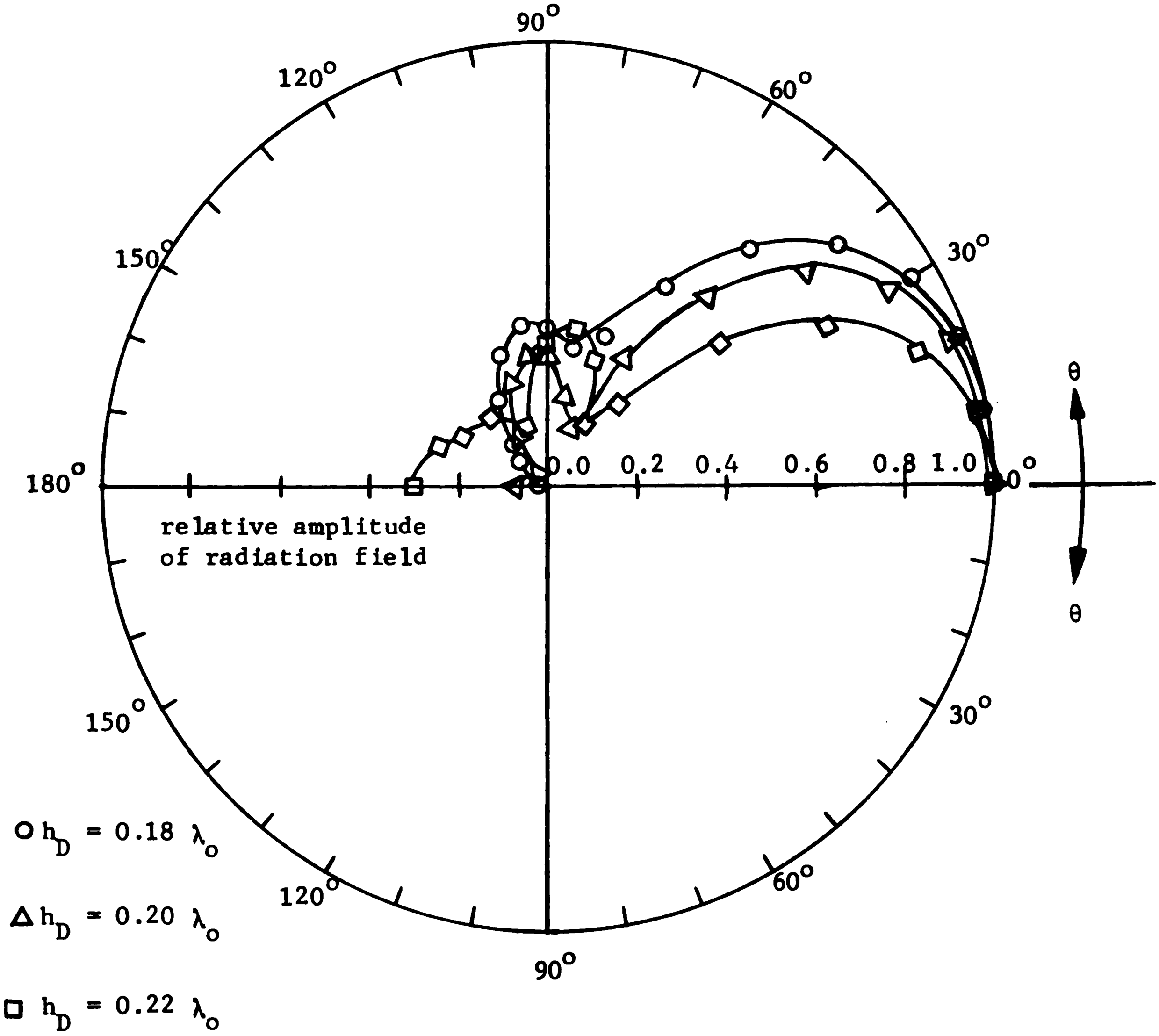

Figure 4.12. E-plane ($\varphi = -\pi/2$) radiation patterns for a 5-element Yagi-Uda slot array for various director lengths.

It is observed from the radiation patterns Figure (4.12) that for $h_D/\lambda_o = 0.20$, the main lobe is reasonably narrow while the back lobe remains quite small in amplitude. For $h_D/\lambda_o = 0.18$, the main lobe becomes quite broad, while for $h_D/\lambda_o = 0.22$ the back lobe radiation is singificantly increased in amplitude. In all cases, however, endfire radiation is obtained, as expected. It appears, then, that $h_D/\lambda_o = 0.20$ is an optimum director length for this 5-element Yagi-Uda slot array with waveguide backing.

With the optimum parameters of $(\Delta z)_{dir}/\lambda_o = 0.25$ and $h_D/\lambda_o = 0.20$, the circuit properties of the waveguide-backed, 5-element, Yagi-Uda slot array are investigated. Figure (4.13a) demonstrates the variation of the input admittance Y_o to the driven element of the array as a function of electrical length h_2/λ_o of the driven element. It is observed that both the input conductance (G_o) and input suceptance (B_o) increase monotonically with increasing h_2/λ_o for $0.15 \leq h_2/\lambda_o \leq 0.35$. The resonant length of the driven element is found to be $h_2 = 0.225 \lambda_o$ for this array. Input admittance to the array depends upon its driven element length in a manner very similar to the dependence of impedance of a single, isolated slot as a function of its length. In the range $h_2/\lambda_o = 0.20$ to 0.25, the array admittance passes through the resonance and presents a relatively low input conductance which can provide a near match to practical transmission lines.

The study of a ten-element, waveguide-backed, Yagi-Uda slot array proceeds in an identical manner to that just discussed for five element array. Figure (4.14) indicates the relative amplitudes and absolute phases of slot voltages in the elements of a 10-element

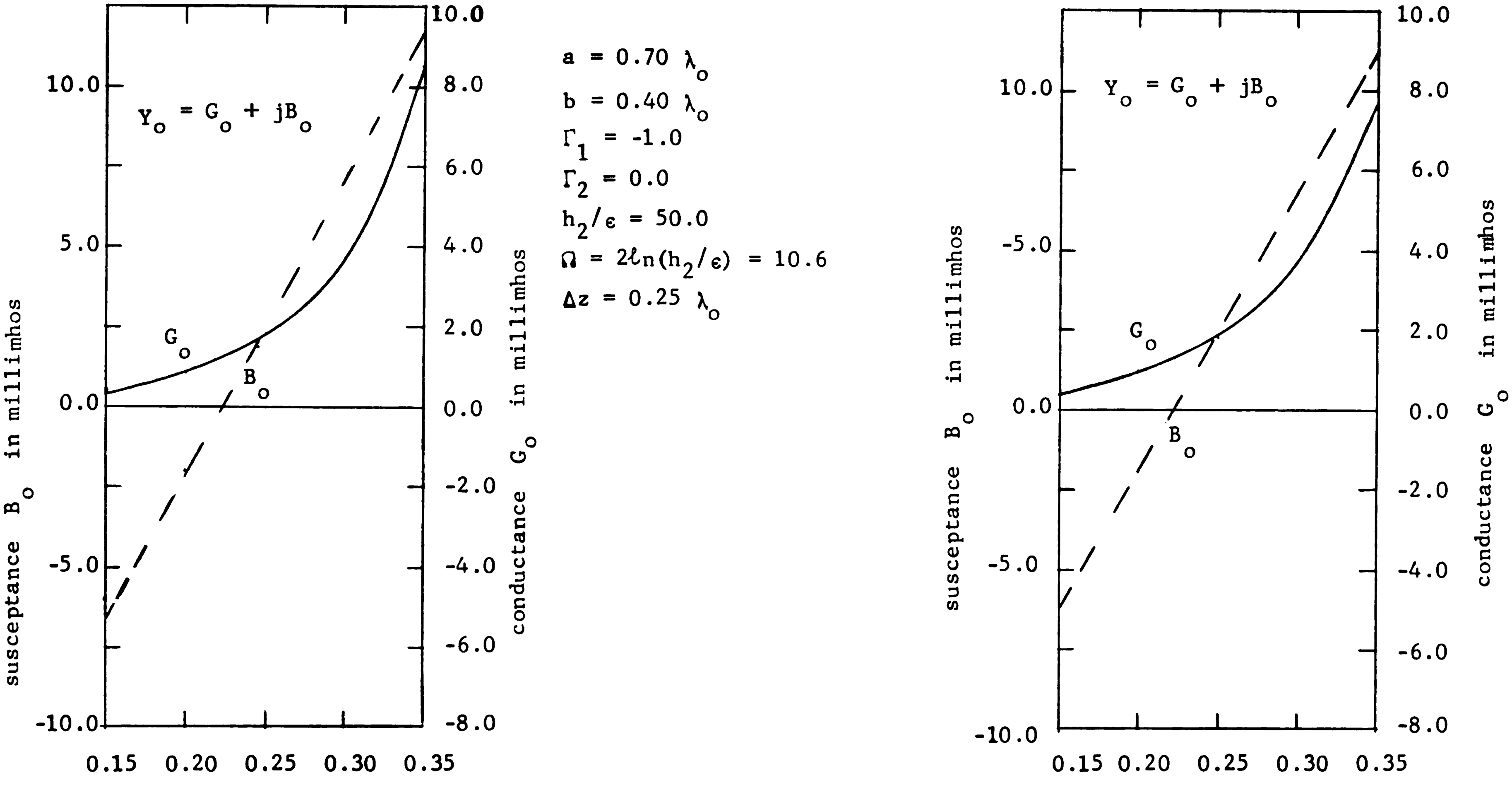

$a = 0.70\ \lambda_o$

$b = 0.40\ \lambda_o$

$\Gamma_1 = -1.0$

$\Gamma_2 = 0.0$

$h_2/\varepsilon = 50.0$

$\Omega = 2\ell n(h_2/\varepsilon) = 10.6$

$\Delta z = 0.25\ \lambda_o$

a. 5-element parasitic array.

b. 10-element parasitic array.

Figure 4.13. Input admittance to the driven element of a Yagi-Uda parasitic slot array as a function of its half length h_2/λ_o.

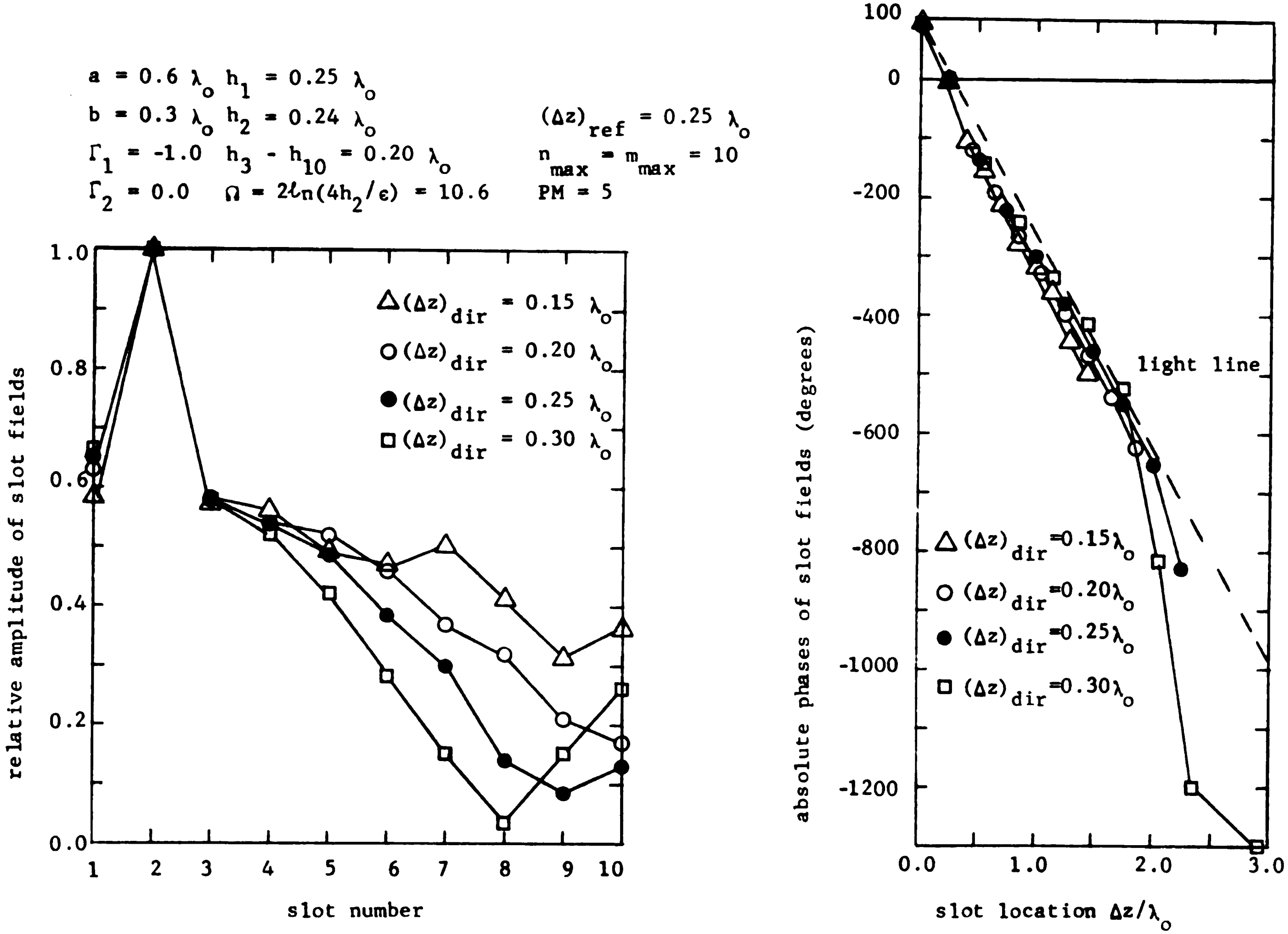

a. Amplitudes of slot fields.

b. Phases of slot fields.

Figure 4.14. Amplitudes and phases of the slot fields (voltages) in the elements of a 10-element Yagi-Uda slot array for various director spacings.

Yagi-Uda slot array as a function of its director spacing, $(\Delta z)_{dir}/\lambda_o$. The array dimensions are listed at the top left-hand corner of the figure. These dimensions are essentially equal to those used for the 5-element array, except that $n_{max} = m_{max} = 10$ instead of 20. This reduction in number of terms retained in the double Fourier series Greens' function G^i was made in order to save computation time without sacrificing too much accuracy.

Figure (4.14a) shows the decaying, traveling-wave nature of the array's aperture field, consisting of the slot fields excited in the array elements. The "end-effect" of a finite array is observed to result in a standing wave component near its terminal end; slot voltage amplitude in element number 10 is larger than that for slot number 9 in all cases. The relative amplitudes of slot fields along the array decay more rapidly for greater values of $(\Delta z)_{dir}/\lambda_o$. This is understandable, since a large value of $(\Delta z)_{dir}/\lambda_o$ corresponds to an array aperture of greater length, and hence greater attenuation of the aperture field as it travels down the array.

Figure (4.14b) demonstrates the absolute phases of slot fields (voltages) versus axial slot location, $(\Delta z)_{dir}/\lambda_o$. It is observed that all values of $(\Delta z)_{dir}/\lambda_o$ will excite a slow wave in the array aperture. Larger values of director spacing result in lower phase velocities but a high rate of aperture field decay, which results in a degraded E-plane radiation pattern for that case as shown in Figure (4.15).

Figure (4.15) compares the E-plane radiation field patterns for various values of $(\Delta z)_{dir}/\lambda_o$ in the 10-element array. It is interesting to compare these plots with those of Figure (4.10). It

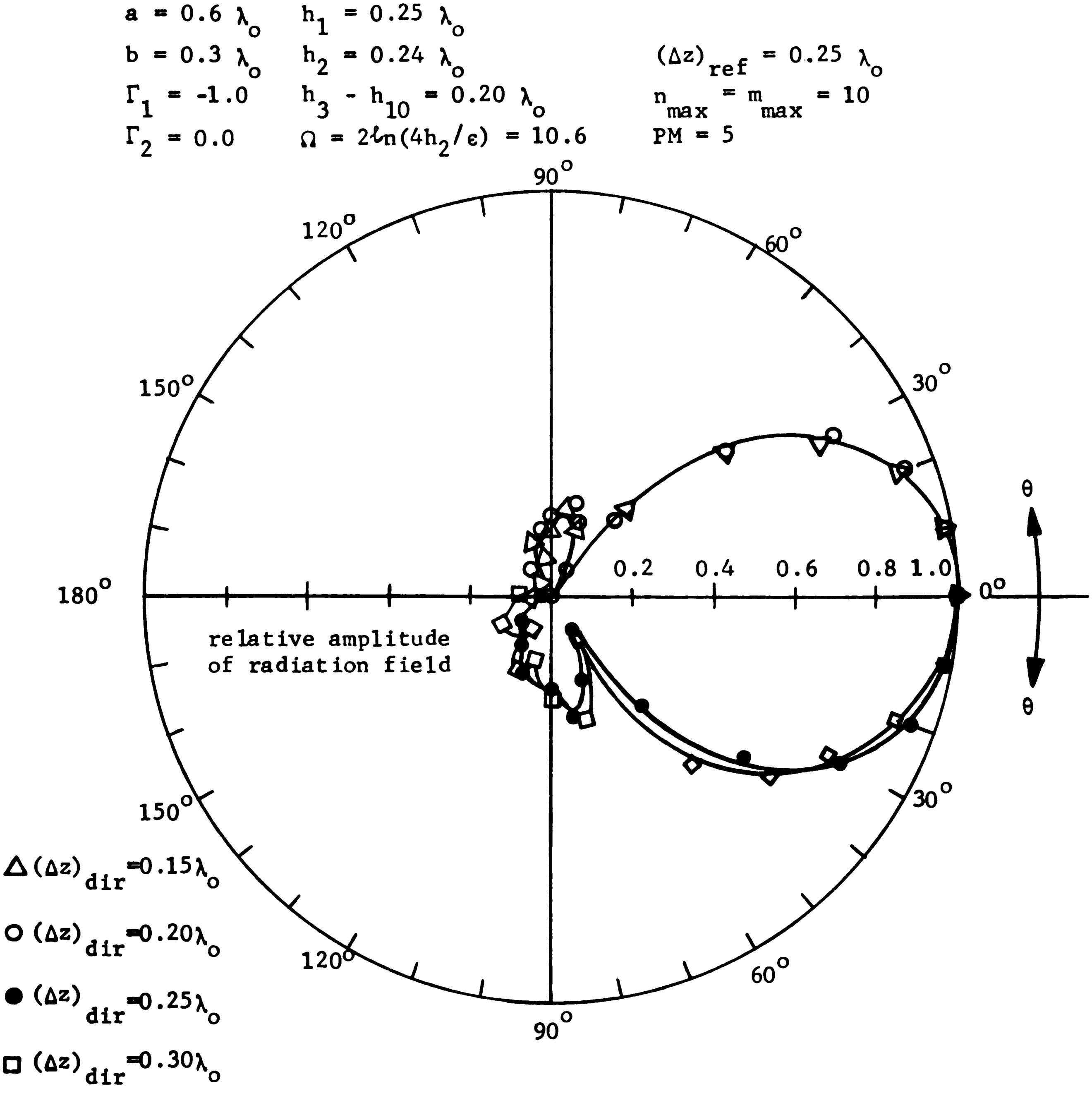

Figure 4.15. E-plane radiation patterns of a 10-element Yagi-Uda slot array for various director spacings.

is immediately obvious that main lobe beam width is much sharper for the 10-element array than for its 5-element counterpart, as one would expect it should be. Radiation field ($\vec{E}$-plane, $\varphi = -\pi/2$) plots for $(\Delta z)_{dir}/\lambda_o = 0.15$ and 0.20 are almost identical as far as their main lobes are concerned, even though for $(\Delta z)_{dir}/\lambda_o = 0.15$ a minimum at $\theta = 60^o$ is sharper than that for $(\Delta z)_{dir}/\lambda_o = 0.20$. The back lobe for $(\Delta z)_{dir}/\lambda_o = 0.20$ is of smaller amplitude than that for $(\Delta z)_{dir}/\lambda_o = 0.15$. As $(\Delta z)_{dir}/\lambda_o$ values are increased to 0.25 and 0.30, the main lobe becomes broader, the minimum at $\theta = 60^o$ becomes less sharp and the back lobes become larger. It appears that a value of $(\Delta z)_{dir}/\lambda_o = 0.20$ will provide an optimal $\vec{E}$-plane radiation pattern, and the mechanical difficulties associated with the construction of closely-spaced slot arrays will also be reduced. Therefore, $(\Delta z)_{dir}/\lambda_o = 0.20$ is the optimum dimension for director spacing in the 10-element array. It is different from that optimal dimension which was obtained for a 5-element array, though not significantly so.

Figure (4.16a) indicates relative amplitudes of slot fields (voltages) against slot location, $\Delta z/\lambda_o$, for various values of director lengths, $h_D/\lambda_o = 0.18$, 0.20 and 0.22. Curves for $h_D/\lambda_o = 0.16$ are identical in shape to that for $h_D/\lambda_o = 0.18$ and therefore this case is not plotted in Figures (4.16) and (4.17). The relative amplitudes for larger values (approaching resonant length) of h_D/λ_o are greater than those for $h_D/\lambda_o = 0.16$ and 0.18. Again, the decaying, traveling-wave nature of the aperture field as described by relative amplitudes of slot fields along the aperture is apparent from Figure (4.16a). For near-resonant-length directors

$a = 0.6\ \lambda_o$ $h_1 = 0.25\ \lambda_o$ $(\Delta z)_{ref} = 0.25\ \lambda_o$
$b = 0.3\ \lambda_o$ $h_2 = 0.24\ \lambda_o$ $(\Delta z)_{dir} = 0.20\ \lambda_o$
$\Gamma_1 = -1.0$ $h_3 - h_{10} = h_D$ $n_{max} = m_{max} = 10$
$\Gamma_2 = 0.0$ $\Omega = 2\ell n(4h_2/\epsilon) = 10.6$ PM = 5

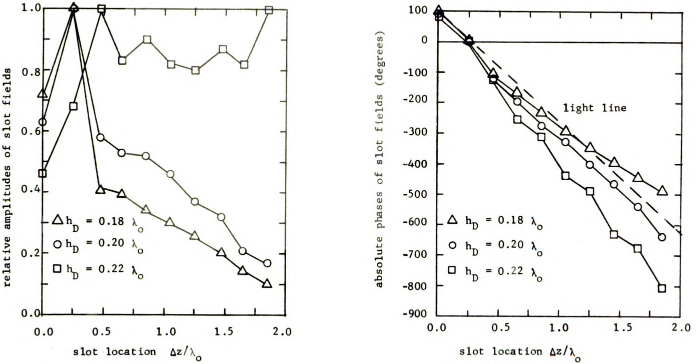

a. Amplitudes of slot fields.

b. Phases of slot fields.

Figure 4.16. Amplitudes and phases of the slot fields (voltages) in the elements of a 10-element Yagi-Uda slot array for various director lengths.

$a = 0.6\ \lambda_o$ $h_1 = 0.25\ \lambda_o$ $(\Delta z)_{ref} = 0.25\ \lambda_o$

$b = 0.3\ \lambda_o$ $h_2 = 0.24\ \lambda_o$ $(\Delta z)_{dir} = 0.20\ \lambda_o$

$\Gamma_1 = -1.0$ $h_3 - h_{10} = h_D$ $n_{max} = m_{max} = 10$

$\Gamma_2 = 0.0$ $\Omega = 2\ell n(4h_2/\varepsilon) = 10.6$ PM = 5

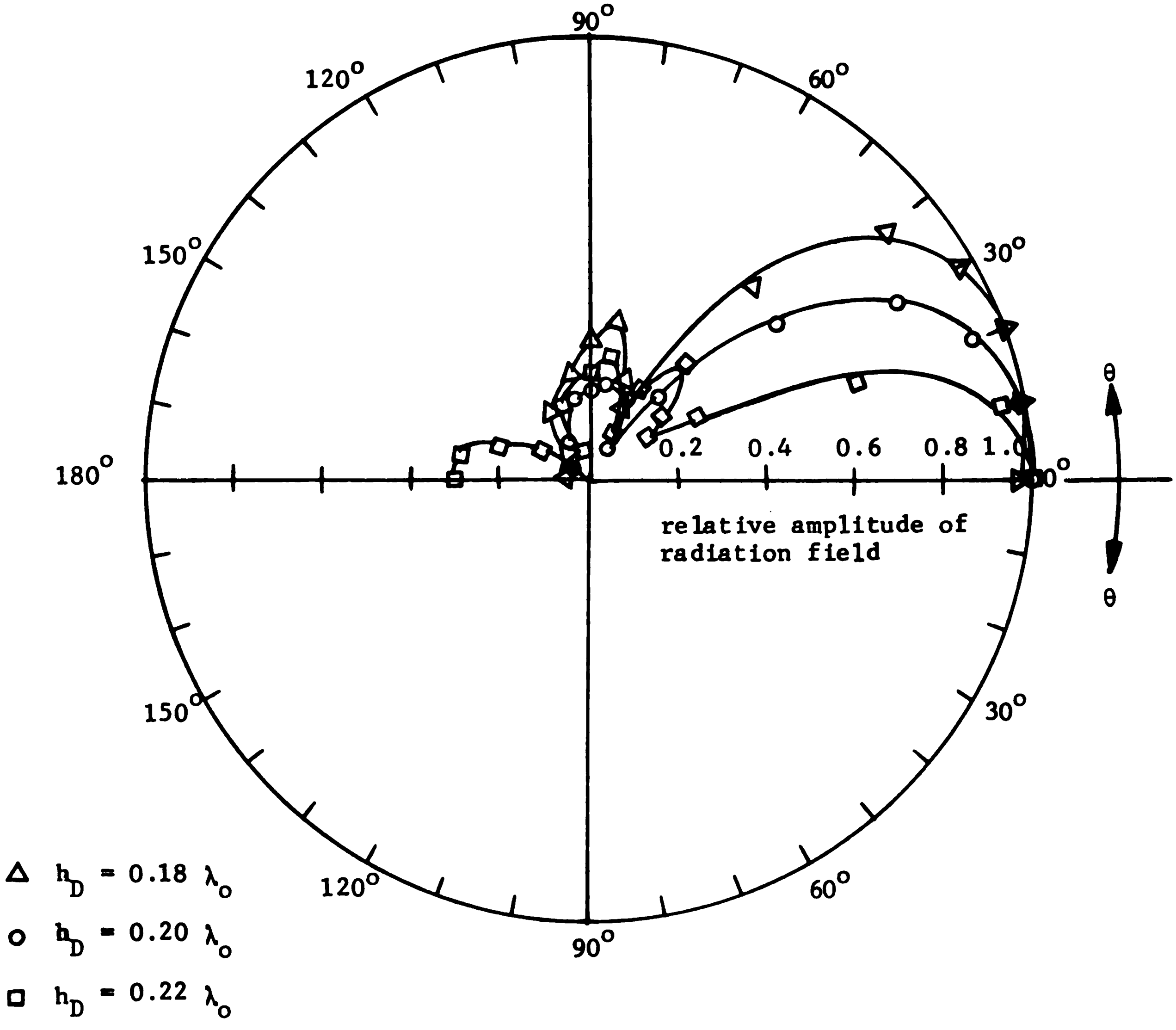

Figure 4.17. E-plane radiation field patterns of a ten-element Yagi-Uda slot array for various director lengths.

with $h_D/\lambda_o = 0.22$, however, the relative amplitude distribution is quite irregular with relatively little decay and a large standing-wave component similar to the situation which was observed for a 5-element Yagi-Uda slot array.

Figure (4.16b) indicates a progressive phase delay along the array aperture. It is observed that for $h_D/\lambda_o = 0.18$, a fast wave is excited along the array aperture and off-end fire radiation would be expected in this case. For $h_D/\lambda_o = 0.20$ and 0.22, slow waves are excited and consequently end-fire radiation is expected for these cases. Due to the significant standing-wave component in the aperture field for directors of $h_D/\lambda_o = 0.22$, a significant back lobe (back radiation) is expected in the array's radiation pattern.

Figure (4.17) shows the E-plane ($\varphi = -\pi/2$) radiation patterns for $h_D/\lambda_o = 0.18$, 0.20 and 0.22. A slightly off-end fire radiation pattern (maximum occurs at $\theta = 20^o$) is indicated for $h_D/\lambda_o = 0.18$. For $h_D/\lambda_o = 0.20$, end-fire radiation is achieved and main lobe beam width is much narrower than that for $h_D/\lambda_o = 0.18$. The side lobe with a maximum at $\theta = 80^o$ is also much lower in amplitude than that for $h_D/\lambda_o = 0.18$. The radiation pattern for $h_D/\lambda_o = 0.22$ has an even narrower main beam, but it has two significant side lobes with maxima at $\theta = 35^o$ and 80^o in addition to a back lobe of significant amplitude. Thus a director length $h_D/\lambda_o = 0.20$ is identified as an optimum parameter for the 10-element, waveguide-backed, Yagi-Uda slot array.

Figure (4.13b) indicates the variation of input admittance, $Y_o = G_o + jB_o$, to the excited element of a 10-element, Yagi-Uda slot array with $(\Delta z)_{dir}/\lambda_o = 0.20$ and $h_D/\lambda_o = 0.20$ as a function of its driven element length. A comparison of this admittance with that for an isolated slot, in an otherwise unbounded space ($\Omega = 10.6$) shows the two admittances are quite similar. However, the resonant length (h_2/λ_o at which $B_o = 0$) has shifted from $\beta_o h = 1.57$ for the single, isolated slot $^{(24)}$ to $\beta_o h_2 = 1.415$ ($h_2/\lambda_o = 0.223$) for the 10-element, waveguide-backed, Yagi-Uda slot array.

4.5.3 Ten-Element, Waveguide-Backed Slot Array:

In this section, a ten-element waveguide-backed slot array similar to that studied in the previous section is investigated with all elements of equal length, element number 1 as feed point, and all remaining elements acting as directors. Such a slot array simulates to some degree, the array investigated in chapter 3 when the slot array was excited by means of an incident TE_{10} mode wave travelling in the backing waveguide. A similar unbounded slot array has been investigated experimentally by Burton and King $^{(1)}$. A large waveguide-backed array with a large number of director elements will be studied further in this section. The beam-scanning capability of this array as achieved by varying the backing waveguide dimension a/λ_o will also be studied, and comparison will be made to the results obtained in chapter 3.

Figures (4.18a) and (4.18b) indicate the relative amplitudes and absolute phases of slot fields in the aperture of a ten-element slot array as a function of location along the aperture for various director spacings $(\Delta z)_{dir}/\lambda_o$. Relevant dimensions for the array are given in the top left-hand corner of the figure. The first element of this array is assumed to be excited by an input current

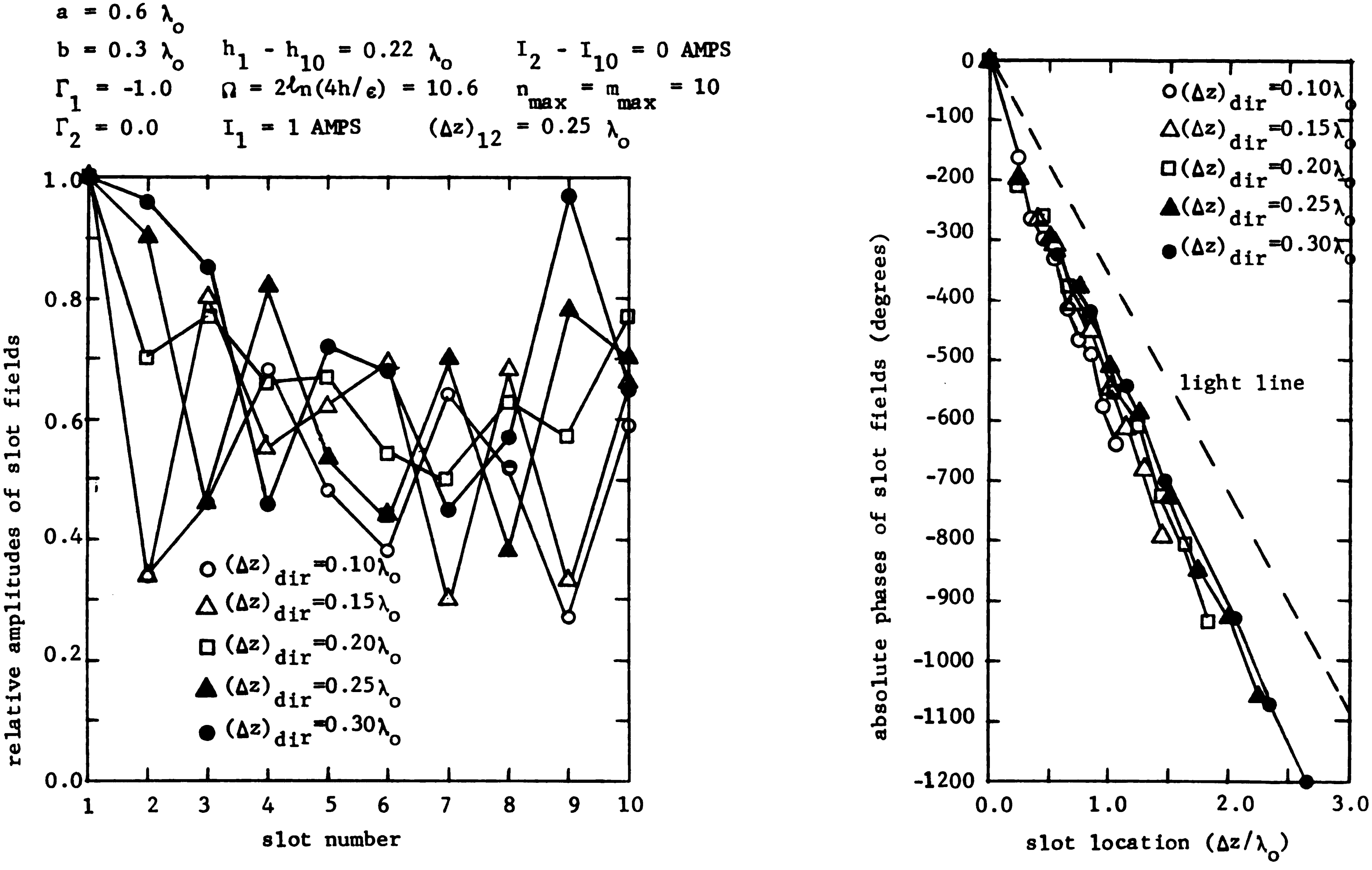

a. Amplitudes of element fields.

b. Phases of element fields.

Figure 4.18. Amplitudes and phases of slot fields in the aperture of a ten-element slot array for various director element spacings.

$I_1 = (1 + j0)$ amps., while all the remaining parasitic elements act as director elements. $(\Delta z)_{12}$ is the distance between first and second elements of the array. Figure (4.18a) indicates a strong standing-wave nature of the aperture field, which is indicative of large reflections near the terminal and of the array. Figure (4.18b) indicates a slow wave aperture field along the array for all values of $(\Delta z)_{dir}/\lambda_o$. In order to determine the optimum value of $(\Delta z)_{dir}/\lambda_o$ for this array, the E-plane $(\varphi = -\pi/2)$ radiation field patterns for various director spacings must be investigated as is carried out in Figure (4.19).

Figure (4.19) shows that for small values of $(\Delta z)_{dir}/\lambda_o$ such as 0.1, 0.15 and 0.20, there exists a large amplitude back lobe in the radiation patterns. For $(\Delta z)_{dir}/\lambda_o = 0.1$, the main beam is quite broad. It is interesting to note that in Chapter 3, for a similar 10-element array excited by a propagating TE_{10}-mode incident wave in the backing waveguide, $(\Delta z)/\lambda_o = 0.1$ was found to be the optimal element spacing. Therefore, even though the array is similar in both cases, the mode of excitation significantly changes the array behavior and its optimum element spacing. For $(\Delta z)_{dir}/\lambda_o = 0.25$ and 0.30, the radiation pattern main lobes are sufficiently narrow while their back lobes are relatively small. It is observed from Figure (4.19) that an optimal choice for director spacings is $(\Delta z)_{dir}/\lambda_o = 0.30$.

Figure (4.20) shows the relative amplitudes and phases of the aperture field in the elements of the same array, except that in this case the backing waveguide width is varied from $a = 0.505\ \lambda_o$ (near cut off) to $0.70\ \lambda_o$. Figure (4.20a) demonstrates large

$a = 0.6\ \lambda_o$ $h_1 - h_{10} = 0.22\ \lambda_o$ $n_{max} = m_{max} = 10$
$b = 0.3\ \lambda_o$ $\Omega = 2\ell n(4h/\epsilon)$ $PM = 5$
$\Gamma_1 = -1.0$ $= 10.6$ $I_1 = 1$ AMP
$\Gamma_2 = 0.0$ $(\Delta z)_{12} = 0.25\ \lambda_o$ $I_2 - I_{10} = 0$ AMP

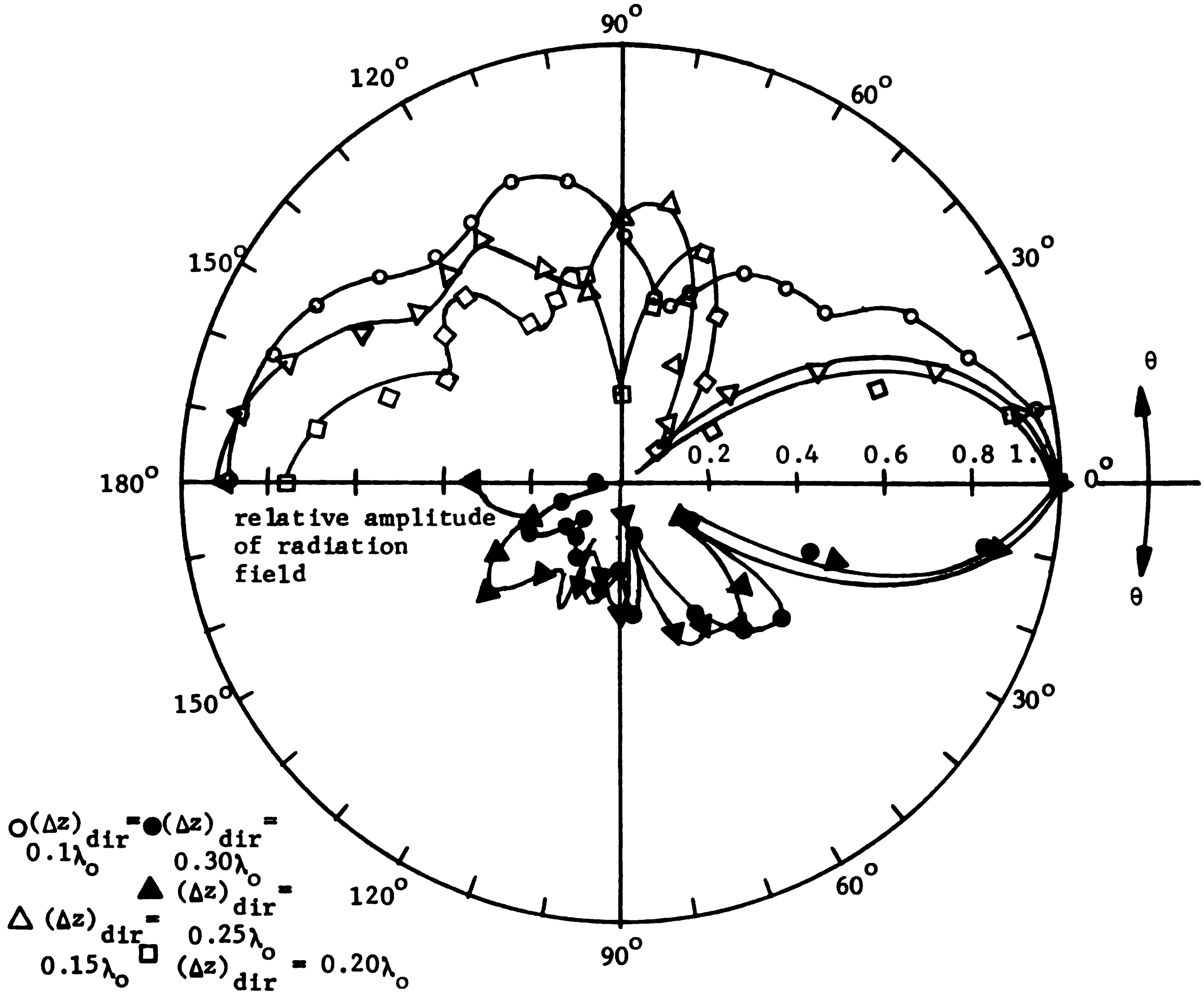

Figure 4.19. E-plane radiation field patterns of a ten-element slot array for various director spacings.

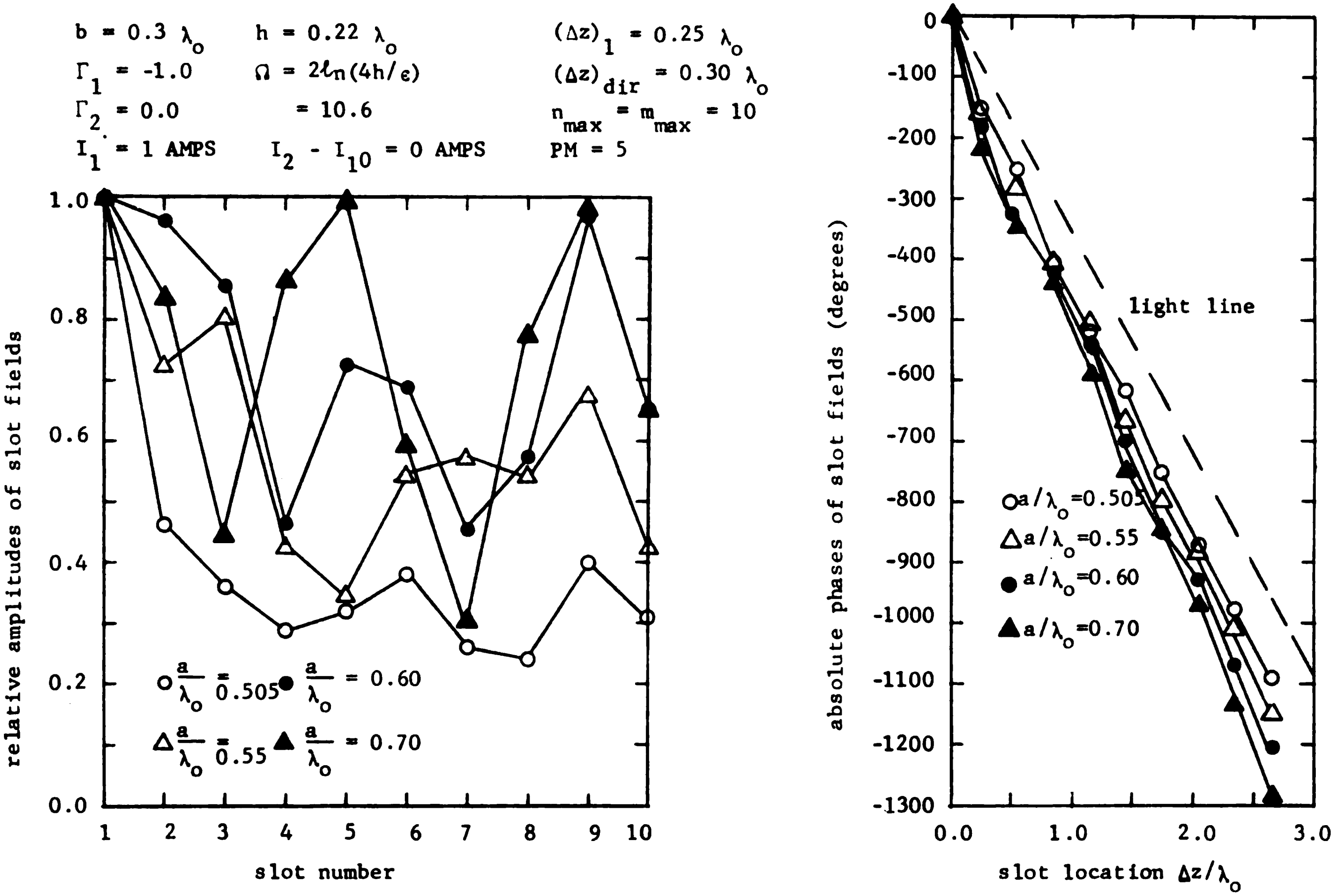

a. Amplitudes of slot fields.

b. Phases of slot fields.

Figure 4.20. Amplitudes and phases of slot voltages in the elements of a 10-element slot array for various backing waveguide widths.

amplitudes of slot fields with a strong standing wave component in the elements of this array for $a = 0.60\ \lambda_o$ and $a = 0.70\ \lambda_o$. This may be because a large dimension "a" results in a smaller decay rate for evanescent modes in the backing waveguide, thus contributing to evanescent mode coupling between elements and greater induced fields. However, for waveguide dimensions of $a/\lambda_o = 0.505$ and $a/\lambda_o = 0.55$, the amplitudes of slot fields along the array are low to moderate with a greatly reduced standing-wave component. Since for $a/\lambda_o = 0.505$ the dominant-mode wave in the backing waveguide is near cut off, the evanescent-mode coupling is reduced. Figure (4.20b) demonstrates a progressive phase delay in the aperture field. All values of a/λ_o appear to result in excitation of a slow wave, thus end-fire radiation is expected for each of these cases.

Figure (4.21), which indicates the radiation field patterns in the E-plane of this array, confirms the above conclusions. For the array with $a/\lambda_o = 0.70$, the back lobe amplitude is quite large. In the case of $a/\lambda_o = 0.505$ and 0.55, the back lobe amplitudes are reduced but remain significantly large. For $a/\lambda_o = 0.60$, both the major lobe beam-width and the side (and back) lobe amplitudes are optimized to reasonable values. Beam width of the major lobe is very insensitive to variations in a/λ_o. Figure (4.21) illustrates that beam scanning cannot be achieved (as was the case when this array was excited by a traveling TE_{10} mode incident wave) by varying a/λ_o. Significant control of back radiation is, however, achieved by variation of a/λ_o or $(\Delta z)_{dir}/\lambda_o$ (Figure (4.19)).

Figure (4.22) indicates the relative amplitudes and phases of the aperture fields in the elements of a twenty-five element,

$b = 0.3\ \lambda_o$ $\quad$ $n_{max} = m_{max} = 10$

$\Gamma_1 = -1.0$ $\quad$ $h = 0.22\ \lambda_o$ $\quad$ PM = 5

$\Gamma_2 = 0.0$ $\quad$ $\Omega = 2\ell n(4h/\varepsilon) = 10.6$ $\quad$ $(\Delta z)_1 = 0.25\ \lambda_o$

$(\Delta z)_{dir} = 0.30\ \lambda_o$ $\quad$ $I_1 = 1$ AMPS $\quad$ $I_2 - I_{10} = 0.0$ AMPS

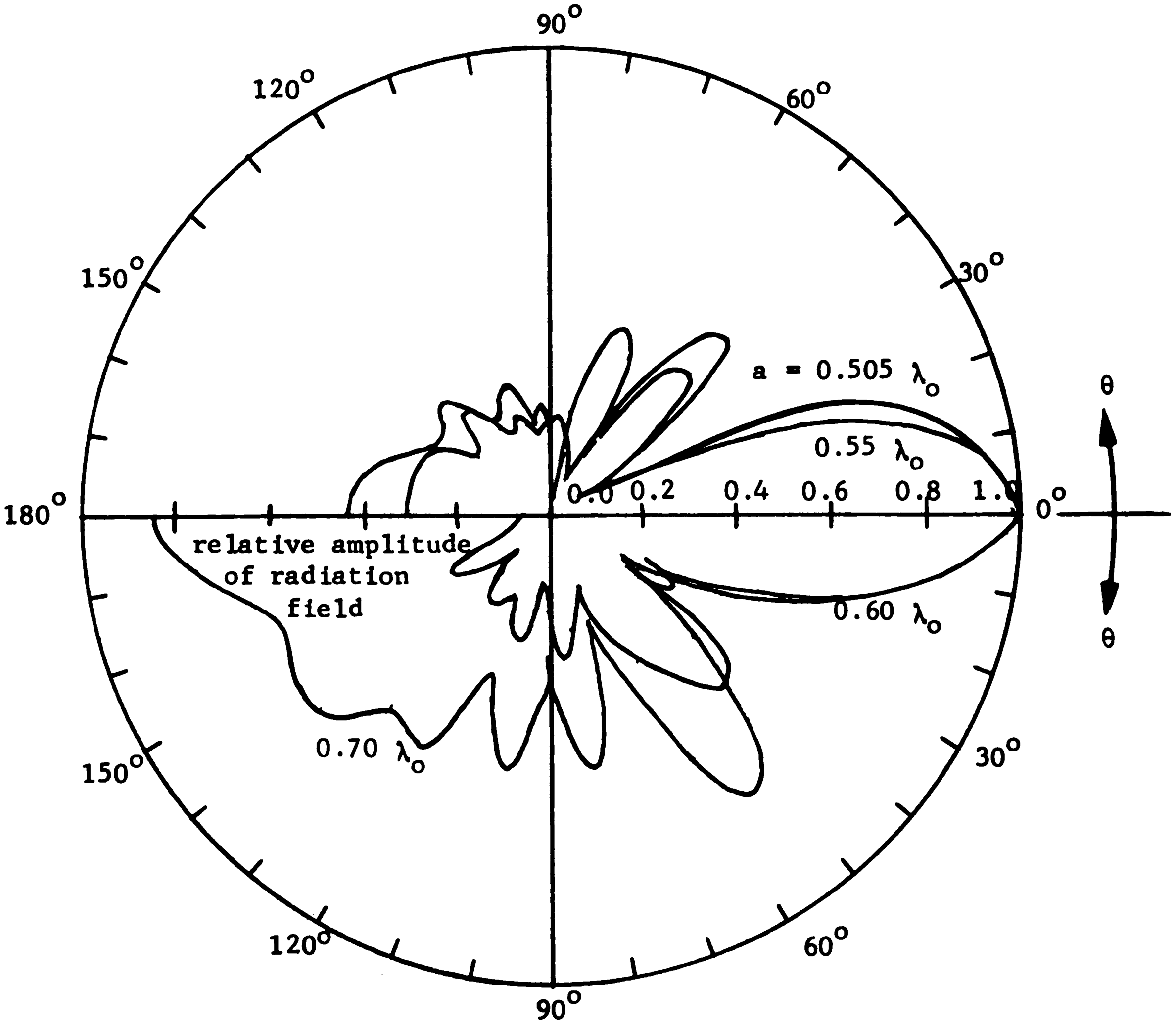

Figure 4.21. Dependence of E-plane ($\varphi = -\pi/2$) radiation field patterns of a 10-element slot array upon width of its backing waveguide.

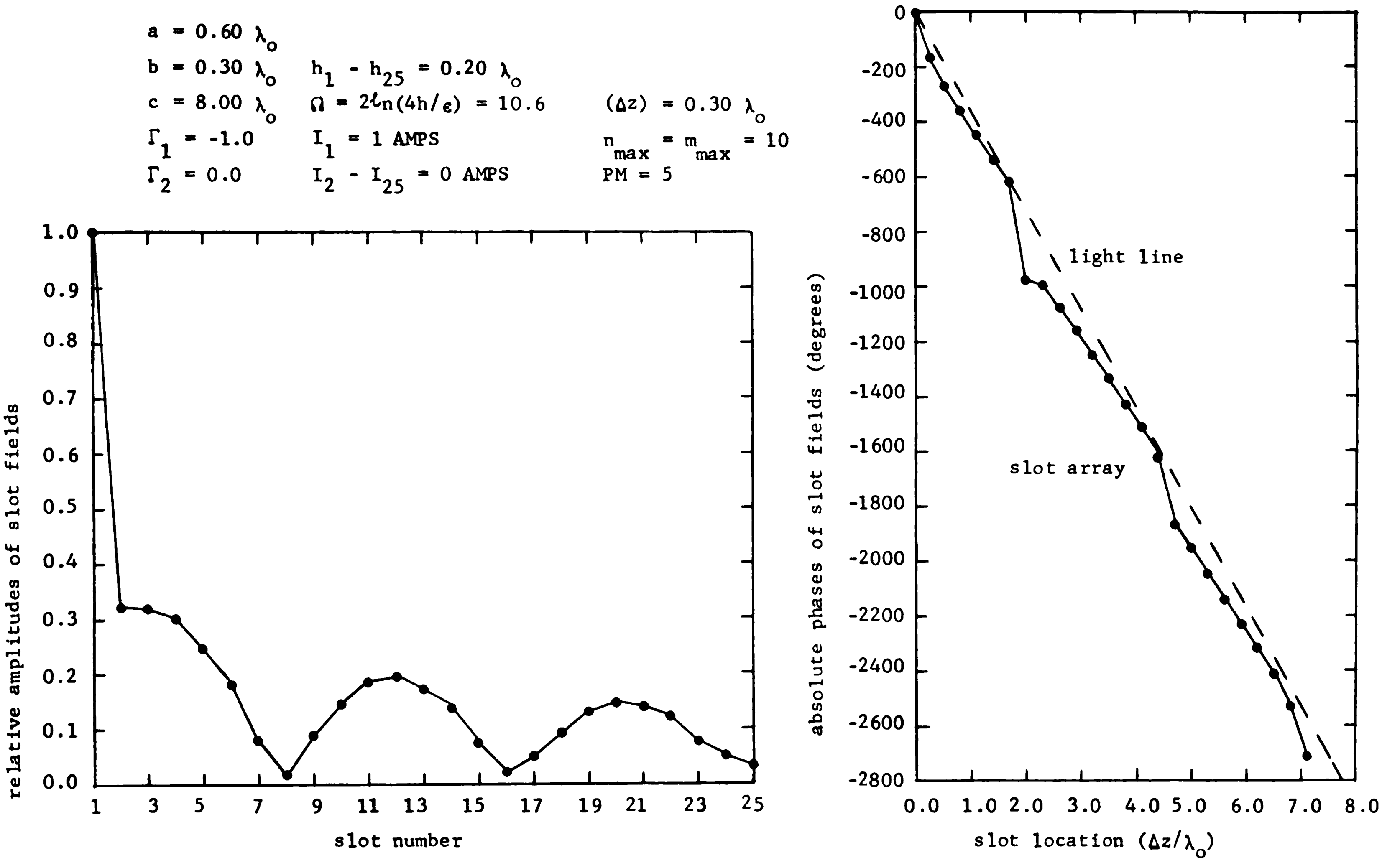

$a = 0.60\ \lambda_o$

$b = 0.30\ \lambda_o$ $h_1 - h_{25} = 0.20\ \lambda_o$

$c = 8.00\ \lambda_o$ $\Omega = 2\ell n(4h/\epsilon) = 10.6$ $(\Delta z) = 0.30\ \lambda_o$

$\Gamma_1 = -1.0$ $I_1 = 1$ AMPS $n_{max} = m_{max} = 10$

$\Gamma_2 = 0.0$ $I_2 - I_{25} = 0$ AMPS PM = 5

a. Amplitudes of element fields.

b. Phases of element fields.

Figure 4.22. Amplitudes and phases of slot fields in the aperture of a twenty-five elements, waveguide-backed, slot array.

waveguide-backed slot array. The array parameters are shown in the top left-hand corner of the figure. All the elements have the same half-length, $h_1 - h_{25} = 0.20\ \lambda_o$. This particular dimension for element half length was chosen to avoid exciting a very strong standing wave component in the aperture field of the array. The width of the backing waveguide is $a/\lambda_o = 0.60$ while the optimal dimension for $\Delta z/\lambda_o$ was chosen to be 0.30. Figure (4.22a) indicates an attenuating aperture field amplitude along the aperture of the array. The standing wave (small amplitude) character of the slot field (voltage) distribution is apparent from Figure (4.22a). This is indicative of significant reflection of the travelling-wave aperture field at the terminal end of the array.

Figure (4.22b) indicates a progressive phase delay in the slot fields along the array aperture. It is observed that the slope of the phase distribution plot for the array is nearly equal to that of the light line, indicating an aperture field with a phase velocity equal to the speed of light. Thus, an end-fire radiation pattern is expected.

Figure (4.23), which indicates the E-plane radiation field pattern for the array, confirms the above conclusion. The main lobe is sharper than that for a ten-element array (Figure (4.19)). The first minimum is 10.5db down and occurs at $\theta = 25^o$. A large side lobe is observed at $\theta = 50^o$. The back-lobe has a (nearly) constant relative amplitude of 0.33. The previous conclusion that a small standing-wave component in the aperture field distribution (relative amplitudes of slot fields) results in a back lobe of small amplitude is thus again verified.

$a = 0.6\ \lambda_o$
$b = 0.3\ \lambda_o$
$c = 8.0\ \lambda_o$
$\Gamma_1 = -1.0$
$\Gamma_2 = 0.0$

$h_1 - h_{25} = 0.20\ \lambda_o$
$\Omega = 2\ell n(4h/\epsilon) = 10.6$
$I_1 = 1$ AMPS
$I_2 - I_{25} = 0$ AMPS

$(\Delta z) = 0.30\ \lambda_o$
$n_{max} = m_{max} = 10$
PM = 5

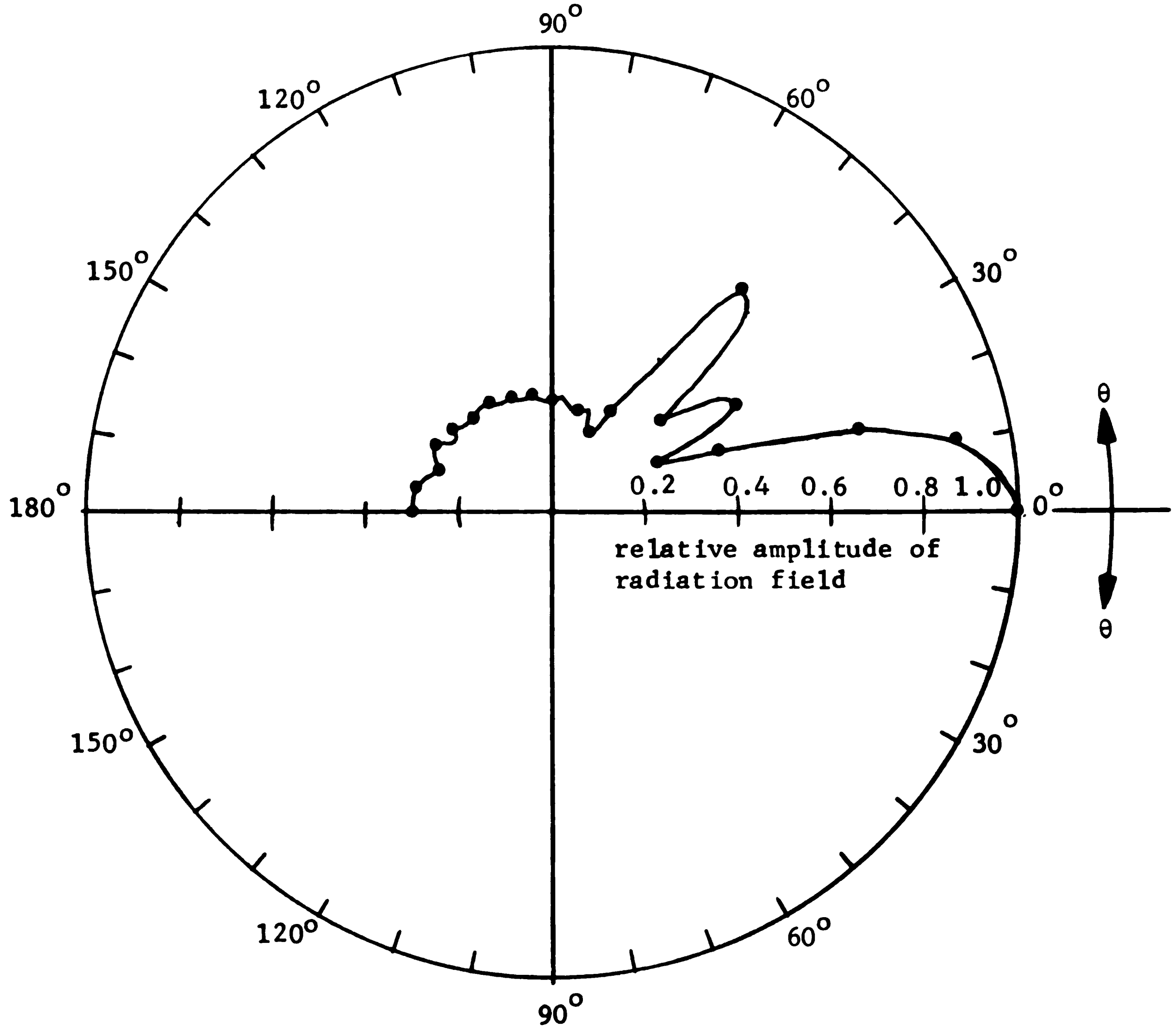

Figure 4.23. E-plane radiation field pattern of a twenty-five element, waveguide-backed slot array.

4.5.4 Frequency Dependence of a Yagi-Uda Slot Array:

Finally, the radiation and circuit properties of a ten-element, waveguide-backed, Yagi-Uda slot array are investigated as a function of its excitation frequency. The results of this section are used to ascertain the operating bandwidth for this array.

Figure (4.24) indicates the E-plane radiation field patterns of this array, with all the array dimensions indicated in meters. It is observed that the radiation field deteriorates very rapidly as frequency is varied from a center frequency of 3.0 GHz to 2.6 GHz or 3.4GHz. The pattern beam-width of this array is identified as approximately 400MHz.

Figure (4.25) indicates the variation of input admittance to the driven element of the same Yagi-Uda slot array as a function of its excitation frequency. This admittance curve has the same behavior as determined by Nyquist and Mathur (25) by a direct numerical solution. It is observed that B_o increases monotonically in the frequency range $2.0\text{GHz} < f < 3.7\text{GHz}$ and drops to a lower value for frequencies greater than 3.7GHz, while G_o has a peak at 3.20GHz and again a sharper peak at 3.8GHz. In the frequency range $2.8\text{GHz} < f < 3.2\text{GHz}$, the input admittance passes through resonance, and presents a relatively low input conductance which can provide a near match to practical transmission lines.

$a = 0.06$ m
$b = 0.03$ m
$c = 0.4$ m
$\Gamma_1 = -1.0$
$\Gamma_2 = 0.0$

$h_1 = 0.025$ m
$h_2 = 0.024$ m
$h_3 - h_{10} = 0.02$ m
$(\Delta z)_{ref} = 0.025$ m
$(\Delta z)_{dir} = 0.020$ m

$\Omega = 2\ell n(4h_2/\epsilon) = 10.6$
$n_{max} = m_{max} = 10$
$PM = 5$

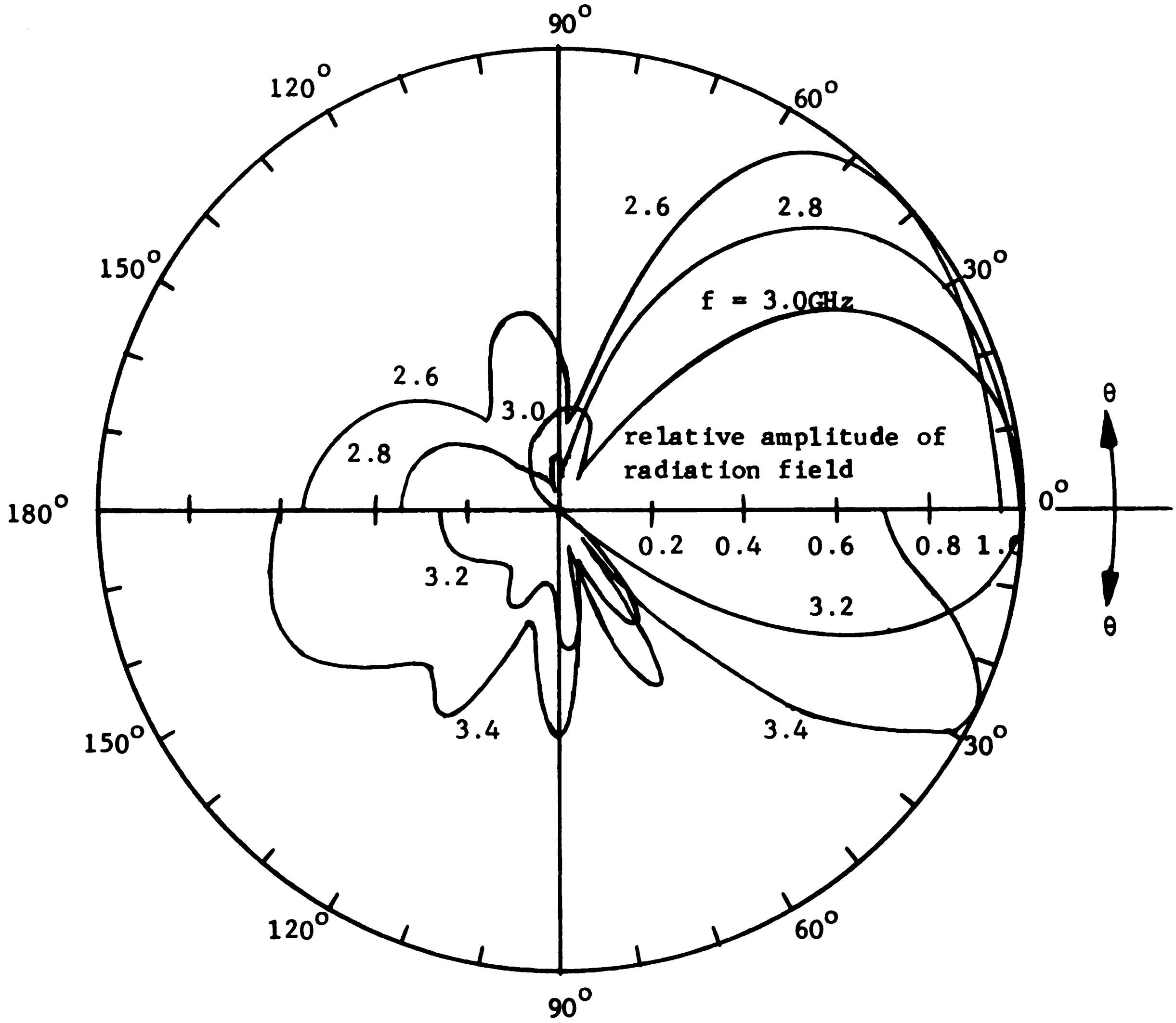

Figure 4.24. Frequency dependence of the E-plane radiation field pattern of a ten-element, waveguide-backed, Yagi-Uda slot array.

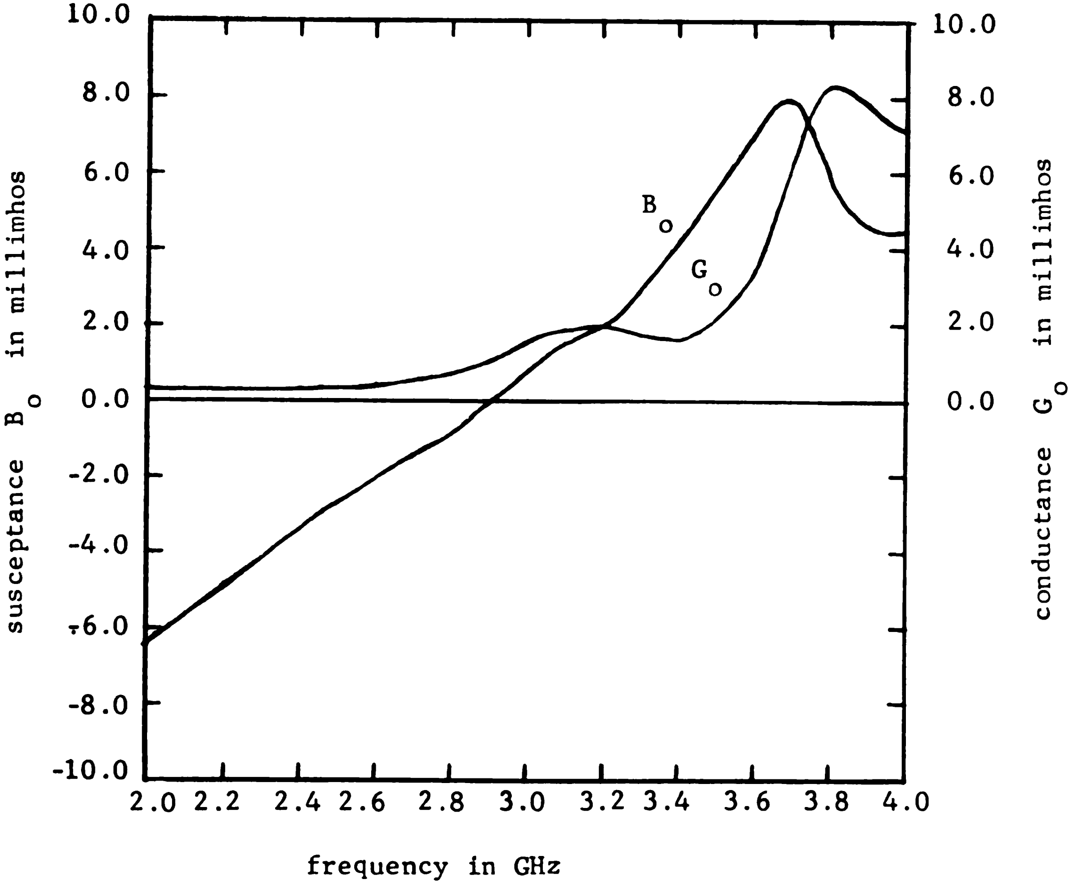

$a = 0.06$ m
$b = 0.03$ m
$c = 0.4$ m
$\Gamma_1 = -1.0$
$\Gamma_2 = 0.0$
$\Omega = 2\ell n(h_2/\epsilon) = 10.6$
$(\Delta z)_{ref} = 0.025$ m
$n_{max} = m_{max} = 10$
PM = 5
$h_1 = 0.025$ m
$h_2 = 0.024$ m
$h_3 - h_{10} = 0.020$ m
$(\Delta z)_{dir} = 0.02$ m

Figure 4.25. Input admittance to the driven element of a ten-element, Yagi-Uda waveguide-backed slot array.

CHAPTER 5

EXPERIMENTAL INVESTIGATION OF WAVEGUIDE-BACKED SLOT ARRAYS

5.1 Introductory Remarks:

In this chapter, the results of an experimental investigation on the waveguide-backed slot array are presented and in some instances correlated with the theoretical-numerical solution described in Chapters 3 and 4. Typical relative amplitude and phase distributions of the slot fields (at $x = a/2$) in the array aperture, E-plane ($\varphi = -\pi/2$) radiation patterns and input impedances were measured for both the Yagi-Uda type slot array (excited by impressed current of coaxial line feed) and the array excited by a dominant mode incident wave in the backing waveguide. Similar measurements were made for a ten-element Yagi-Uda slot array with backing waveguide width at its maximum (a/λ_o = max.) and the waveguide (interior) side of the array covered by microwave absorber to simulate the theoretically complementary strip dipole (and hence equivalent cylindrical dipole) array.

Section 5.2 describes the anechoic chamber and experimental set up. Section 5.3 presents the results for an eight-element waveguide backed array excited by a TE_{10} mode incident wave and compares these results with theoretical ones obtained using the numerical solution described in Chapter 3. Section 5.4 presents the results for a ten-element, waveguide-backed, Yagi-Uda array excited by means of impressed currents and compares these results to the theoretical ones obtained using the approximate analytical solution presented in Chapter 4. Section 5.4 presents a summary of the experimental and theoretical results and attempts to explain the discrepensies that exist between them.

5.2 Anechoic Chamber and Experimental Set-up:

The experimental arrangement consists basically of an anechoic chamber constructed with an aluminum image or ground plane forming one of its walls. Experimental measurements are made upon the slot array which is cut in the ground plane backed by a waveguide of adjustable width, and subsequently radiates into the chamber. The purpose of the anechoic chamber is to simulate a free half-space environment. A photograph of the experimental anechoic chamber and the slot array with its near field probing system is shown in Figure (5.1). Figure (5.2) displays a photograph of instrumentation involved for making various measurements in this experiment. Figure (5.3) indicates the complete experimental set up, including the anechoic chamber and the inter-connection of all the instrumentation which was used. The backing waveguide was provided with movable side walls such that the width "a" of the waveguide could be adjusted as shown in Figures (5.2) and (5.3).

The anechoic chamber (dimensions of 8 ft. wide, 6 ft. height, and 6 ft. deep) was constructed from appropriately covered wooden frames. Its interior was completely covered by an aluminum ground plane on one wall and with B.F. Goodrich type VHP-8 microwave absorbers covering the remaining three walls as well as the floor and the ceiling.

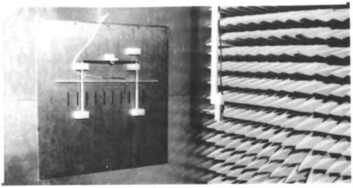

Figure 5.1a. Photograph of slot array cut in ground plane and mounted in anechoic chamber (with near-field probing system and dipole receiving antenna).

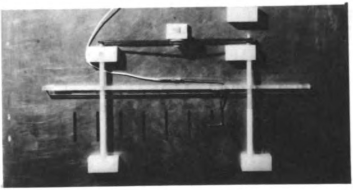

Figure 5.1b. Photograph showing close-up view of the slot array and the coaxial near-field probing system used to measure the aperture field along the array and the slot field distributions.

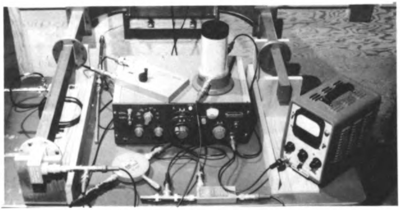

Figure 5.2. Photograph of various microwave instrumentation (and part of the backing waveguide system) used in making measurements on the waveguide-backed slot array.

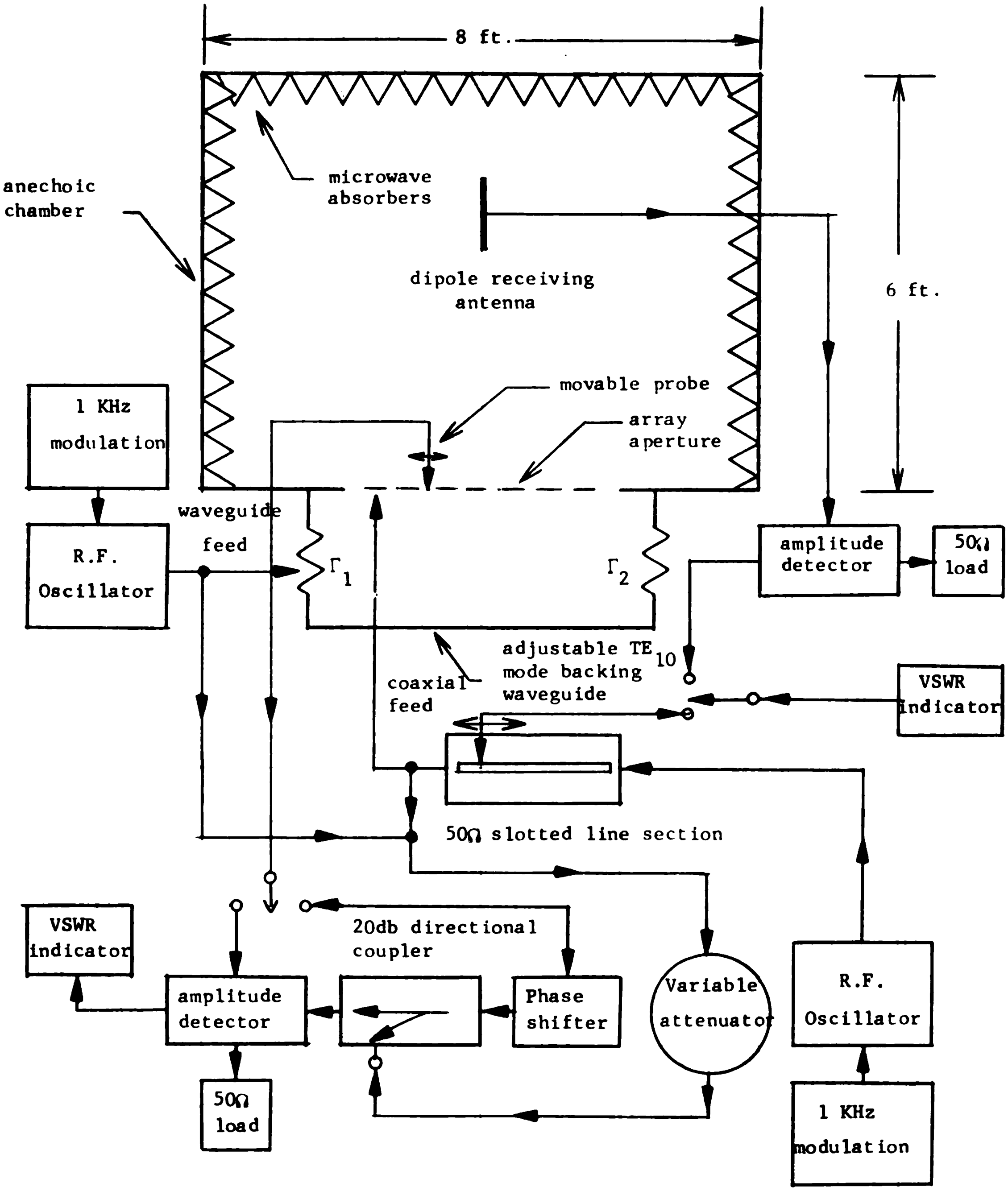

Figure 5.3. Anechoic chamber and block diagram of experimental set-up.

Figure (5.2) indicates the waveguide system that is used to excite a TE_{10}-mode wave in the backing waveguide and provide terminations at its ends as well as the coaxial system used to excite (maintain an impressed current in the driven element of) the Yagi-Uda type slot array. The latter arrangement is also shown (in its view from inside the anechoic chamber) in Figure (5.1b). As shown in Figure (5.2), two ninety-degree waveguide bends are used at either of the terminal-ends of the backing waveguide, followed by two waveguide tapers to reduce the waveguide dimensions from (9.525 cm. × 4.445 cm.) I.D. for the adjustable backing waveguide to (7.2136 cm. × 3.4036 cm.) I.D., the latter being the standard S-band waveguide dimensions. This particular backing waveguide size allows appropriate guided wavelength adjustment for its TE_{10} dominant mode wave and the center frequency of its band for single, dominant mode propagation is approximately 2.5 GHz. At the terminal end of the array, the taper is followed by a standard S-band matched load (to effect a reflection coefficient of $\Gamma_2 = 0$), while at the initial (input) end the taper is preceeded by a S-band waveguide slotted-line section with a waveguide probe; the input end of the slotted section is connected to an R.F. Oscillator.

In the case of coaxial system excitation, as shown in Figure (5.3), the R.F. Oscillator was connected through a 50-ohm coaxial, slotted-line to a 50-ohm adjustable airline followed by a section of 50-ohm solid-jacketed cable (micro-coax). The 50-ohm solid-jacketed cable passes through the ground plane (through a hole just below the backing waveguide) and along a channel cut on the inside of the ground plane which terminates adjacent to the center of slot number 2.

The center conductor of the solid-jacketed cable extends across this slot at its mid-point. The outer conductor of the coaxial calbe lies in (and is soldered to) the ground plane channel while its center conductor passes transversely across the center of the slot and is soldered to its opposite side to make a good electrical contact. The details of the coaxial feed are indicated in Figure (5.1).

Figure (5.1) also indicates a coaxial, near-zone, electric-field probe that can be moved horizontally as well as vertically to measure the relative amplitudes and phases of the slot fields (voltages) as well as the slot field distributions in individual array elements.

A movable, resonant-length receiving dipole was provided to monitor the radiation field (E-plane) maintained by the slot array, and was located a radial distance 106 cm from the center of the array (which is approximately 8.83 λ_o at 2.50 GHz). The length of the adjustable, coaxial air-line was adjusted such that the total line length (solid-jacketed cable plus air-line) was approximately $\frac{\lambda_o}{2}$ such that its input impedance (measured by using conventional slotted line techniques) was approximately equal to that of the driven element of the array. A block diagram of the equipment arrangement used in this experimental set up is shown in Figure (5.3).

The slot lengths, widths, and spacings in the experimental 10-element array are as follows

$$h_1 = 3.0 \text{ cm} \qquad w = 2\epsilon = 0.4 \text{ cm} \qquad (\Delta z)_{12} = 3.0 \text{ cm}$$

$$h_2 = 2.88 \text{ cm} \qquad \frac{h_2}{\epsilon} = 14.4 \text{ cm}$$

$$h_3 - h_{10} = 2.64 \text{ cm} \qquad \Omega = 2\ell n\left(\frac{4h_2}{\epsilon}\right) = 8.1 \qquad (\Delta z)_{pq} = 4.0 \text{ cm}$$

$$\ldots \text{ for } \; p \neq 1, \; q \neq 1$$

while the cross-sectional dimensions of the adjustable backing waveguide are a = 5.28 to 8.9 cm and b = 3.6 cm.

An excitation frequency of 2.5 GHz (corresponding to a free-space wavelength of $\lambda_o = 12.0$ cm) was used throughout the experiment. The width of the backing waveguide was varied manually (utilizing adjustable feed screws attached to the movable plates). Electrical dimensions corresponding to the physical ones given above are therefore

$$h_1 = 0.25\ \lambda_o \qquad w = 2\epsilon = 0.3333\ \lambda_o \qquad (\Delta z)_{12} = 0.25\ \lambda_o$$

$$h_2 = 0.24\ \lambda_o \qquad \frac{h_2}{\epsilon} = 1.2\ \lambda_o \qquad (\Delta z)_{pq} = 0.33\ \lambda_o$$

$$h_3 - h_{10} = 0.22\ \lambda_o \qquad \Omega = 2\ell n\left(\frac{4h_2}{\epsilon}\right) = 8.1 \qquad \ldots \text{ for } p \neq 1,\ q \neq 1$$

$$a = 0.22\ \lambda_o \text{ to } 0.74\ \lambda_o,\ b = 0.3\ \lambda_o .$$

The standing-wave-ratio (SWR) on the transmission system (waveguide or coaxial) driving the slot array was measured for both types (incident waveguide mode or impressed current) of array excitation; input impedances were not explicitly obtained. Since the input terminal plane of the waveguide-excited array has an arbitrary location, the input impedance is not well defined and therefore only the input SWR was measured for comparison with the theoretically predicted results. The impressed currents which excite the Yagi-Uda array are maintained by the relatively long ($\approx 2.66\ \lambda_o$) section of solid-jacketed cable which is very lossy at 2.5 GHz. Due to the difficulty of determining the electrical length and the attenuation and phase constants of this lossy line section with sufficient accuracy, it was found nearly impossible to transform the measured impedances looking into the line section to those antenna input impedances at the input point of the driven array element. Only the SWR on the 50-ohm air-line slotted section which was terminated by the input to the lossy feeder line are therefore, presented here and compared with the theoretically predicted values.

5.3. Measurements on Waveguide-Backed Slot Array Excited by a Dominant-Mode Incident Wave:

An eight-element, waveguide-backed slot array (using elements 3-10 of the experimental set up described in the last section with elements 1 and 2 covered by conducting tape) excited by a TE_{10} dominant-mode incident wave was investigated experimentally. The slot voltage distributions, the relative amplitudes and phases of the slot voltages in the elements along the array aperture, and the E-plane radiation patterns were measured. Measurements on the ten-element experimental slot array were not made since the lengths of the elements 1 and 2 were different from those of elements 3-10 and the presence of the coaxial feeder cables in slot number 2 of the array (which is to be used in the Yagi-Uda slot array measurements) will significantly load that slot and affect its field distribution. Therefore, to achieve an eight-element array of equal-length slots, the first two elements were covered by conducting aluminum tape to reduce their aperture fields to zero. Slots 3-10 of the experimental set up now forms the required 8-element, waveguide-backed slot array with each slot of half-length $h/\lambda_o = 0.22$ and an element spacing of $(\Delta z)/\lambda_o = 0.33$. The width of each slot is $\frac{\lambda_o}{30}$, at an operating frequency of 2.5 GHz; the thickness parameter is $\Omega = 2\ln(\frac{4h}{\epsilon}) = 8.1$.

Figure (5.4) indicates the relative amplitudes and phases of slot voltages in the elements of the 8-element array for various backing waveguide widths "a"; both measured experimental results and the results obtained analytically by the numerical solution (as outlined in Chapter 3) are presented. It is observed from Figure (5.4a) that the relative amplitudes of measured slot voltages (dashed lines) in slots 1 through 5 agree quite well with the theoretically predicted results (solid lines) for a backing-waveguide of width $a/\lambda_o = 0.6$. Near the end of the array, the comparison is relatively poor. This can be explained in two ways. First, in the experiment, when $a/\lambda_o < 0.74$ the movable plates that vary the backing-waveguide width present a discontinuity at the input and output ends of the array, while in the analytical solution both Γ_1 and Γ_2 were assumed to be zero. Secondly, the numerical results from the analytical solution are not absolutely accurate since they were computed using only 10-partitions along the slot axes and only five terms were retained in each of the double Fourier series when evaluating G^i. The standing-wave due to the terminal-end effect is, however, apparent in both experimental and theoretical results. For $a/\lambda_o = 0.505$, the agreement between the theoretically predicted and experimentally measured amplitude distributions is relatively poor although the general trends agree. This is probably due to the fact that the TE_{10} mode in the backing-waveguide is near cut off and its reflections at the discontinuities mentioned above becomes critical.

Figure (5.4b) indicates very good agreement between the theoretically predicted results and experimentally measured ones for the relative phases of slot voltages in the elements along the array

$b = 0.3\lambda_o$ $h = 0.22\lambda_o$ $n_{max} = m_{max} = 5$

$\Gamma_1 = \Gamma_2 = 0.0$ $\Omega = 2\ln(4h/\epsilon)$ $PM = 5$

$\Delta z = \lambda_o/3$ $= 8.1$ $MM = 10$

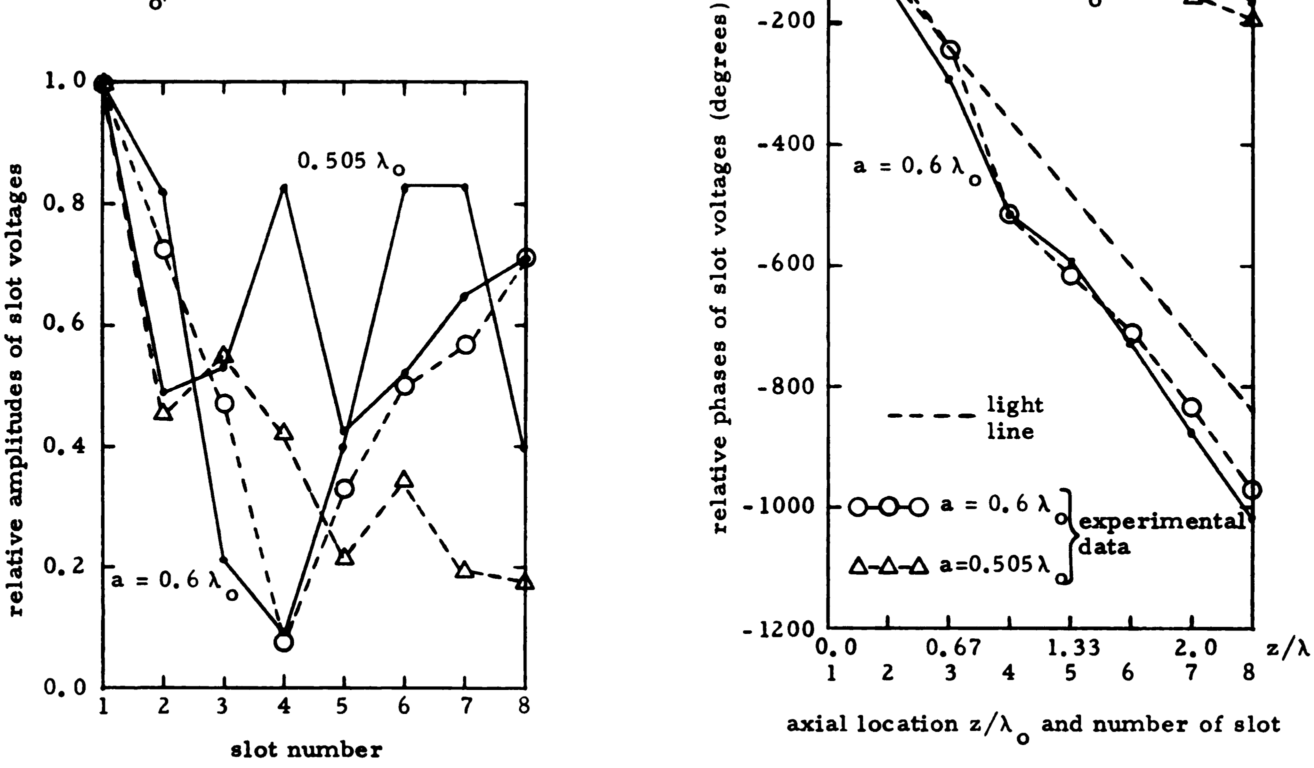

a. Amplitudes of slot voltages.

b. Phases of slot voltages.

Figure 5.4. Comparison of theoretical and experimental amplitudes and phases of slot voltages in the elements of a 8-element array for various backing waveguide widths.

aperture. It is observed that for $a/\lambda_o = 0.505$ a fast wave is excited in the array aperture while a slow wave is excited when $a/\lambda_o = 0.6$. This confirms the feasibility for varying the phase velocity of the traveling wave aperture field by adjusting the waveguide width. The slow wave for $a/\lambda_o = 0.6$ is expected to produce endfire radiation, while off-endfire radiation is expected for the fast wave obtained with $a/\lambda_o = 0.505$.

Figure (5.5) indicates a comparison between experimentally measured and theoretically predicted slot field amplitude distributions for several individual elements of the array. They are observed to compare very closely, being essentially sinusoidal distributions in each case.

Figure (5.6), which indicates the theoretical and experimental E-plane radiation field pattern for $a/\lambda_o = 0.505$ and 0.6 confirms the above predicted nature of the radiation fields. Again, the agreement between theoretical and experimental results is very good for $a/\lambda_o = 0.6$ although the endfire radiation is obtained, the lobe at $\theta = 0^o$ is not the main beam of the radiation pattern, the latter being at $\theta = 48^o$. This behavior is due to the fact that in the experimental set up $(\Delta z)/\lambda_o = 0.33$ is relatively large. In Chapter 3 (section 3.5) it was demonstrated that to achieve endfire radiation from the main beam, an optimum slot spacing is $(\Delta z)/\lambda_o = 0.1$. Therefore, an off-endfire main beam radiation for $(\Delta z)/\lambda_o = 0.33$ is expected. The experimental slot spacing of $(\Delta z)/\lambda_o = 0.33$ was originally chosen for the Yagi-Uda array design, and could not be readily modified. It was also pointed out in Chapter 3 that by changing the width of the backing waveguide (a/λ_o) it is possible to achieve beam scanning.

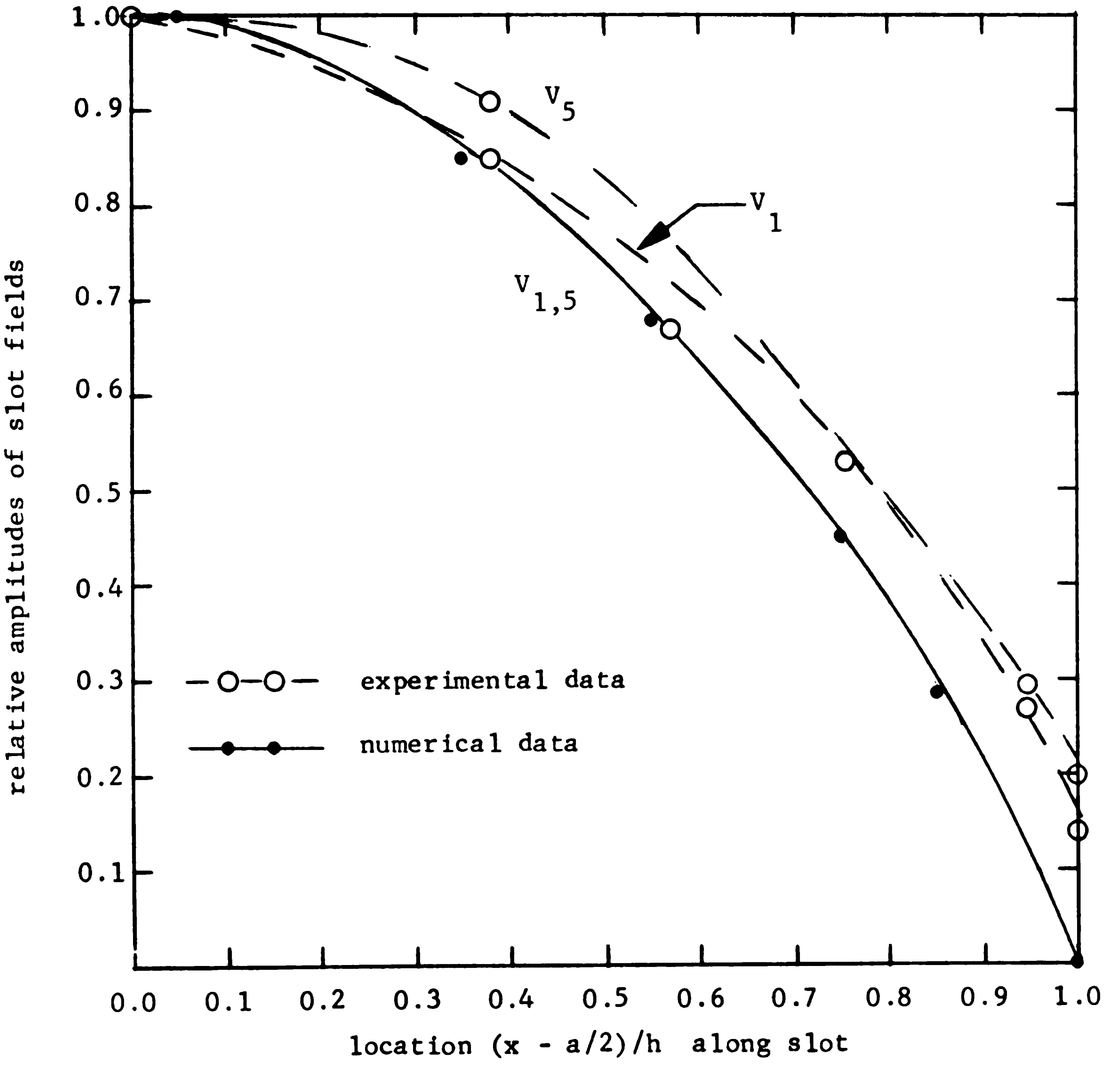

$a = 0.6\ \lambda_o$

$b = 0.3\ \lambda_o$

$\Gamma_1 = \Gamma_2 = 0.0$

$h = 0.22\ \lambda_o$

$\Omega = 2\ell n(4h/\epsilon) = 8.1$

$(\Delta z) = 0.33\ \lambda_o$

$n_{max} = m_{max} = 5$

PM = 5

MM = 10

$I_1 = (1 + j0)$ AMPS

$I_2 - I_8 = 0$ AMPS

Figure 5.5. Slot field distributions in the elements of a 8-element, waveguide-backed, slot array.

$b = 0.3\,\lambda_o$

$\Gamma_1 = \Gamma_2 = 0$

$h = 0.22\,\lambda_o$

$\Omega = 2\ln(4h/\epsilon) = 8.1$

$h/\epsilon = 14.4$

$n_{max} = m_{max} = 5$

$PM = 5$

$MM = 10$

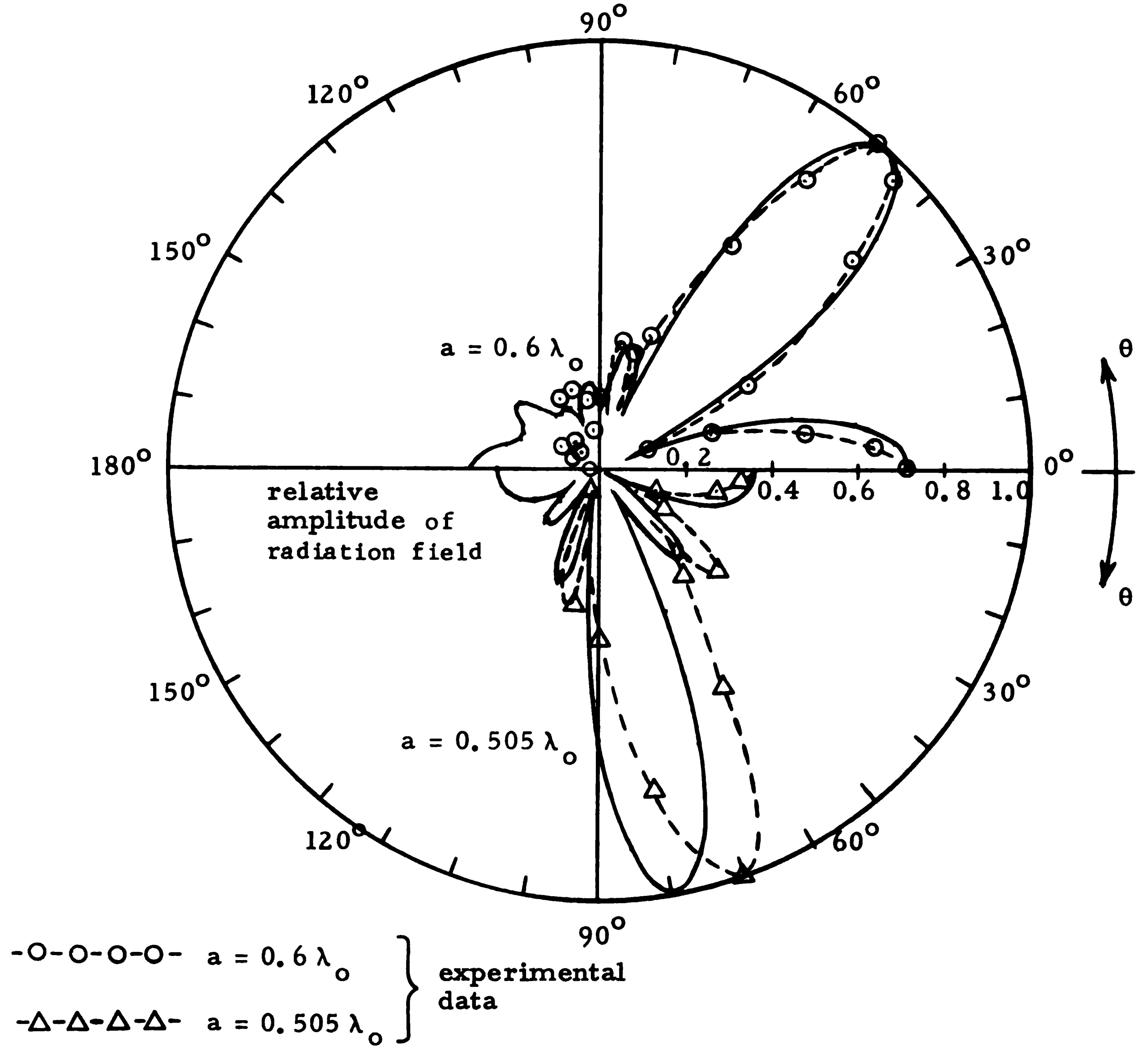

Figure 5.6. Theoretical and experimental radiation patterns for a 8-element slot array with two different backing waveguide widths.

This is confirmed in Figure (5.6). The main beam shifts from $\theta = 48^o$ for $a/\lambda_o = 0.60$ to $\theta = 80^o$ (70^o for experimental results) for $a/\lambda_o = 0.505$. It should be noted that near cutoff ($a/\lambda_o = 0.505$) the E-plane radiation pattern has the same shape for both in numerical results and experimental measurements even though an angular shift is evident between the two patterns. This shift is likely due to the difficulty in precisely adjusting a/λ_o experimentally; a slight error results in a modified aperture field phase velocity.

Table (5.1) investigates the circuit properties of the eight-element, waveguide-backed slot array with dominant-wave excitation. It is observed that the SWR produced by the array load on the driving waveguide is not excessively high, even at $a/\lambda_o = 0.505$ where the width of the array's backing waveguide places it near cutoff for the dominant TE_{10} mode wave; a reasonably good match (at the input terminal of the array) is therefore indicated between the driving waveguide and the antenna system for various widths of the backing waveguide (scan angles). As mentioned earlier, the input impedances to this array depends upon the choice of input terminal plane, and are thus somewhat arbitrary. For this reason, only the driving waveguide SWR's computed from the corresponding input impedances are presented. A favorable comparison between theoretical and experimentally measured SWR's is indicated.

5.4. Measurements on Yagi-Uda, Waveguide-Backed Slot Array:

In this section, a ten-element, waveguide-backed Yagi-Uda slot array is investigated. The array of ten transverse slots (cut in a large ground plane and backed by a waveguide) consists of a driven element, one reflector and eight directors. The reflector

a/λ_o	0.505	0.6
$(SWR)_{EXP}$	6.3	1.45
$(SWR)_{THY}$	5.0	2.1

Table 5.1. Experimental and theoretical driving waveguide SWR (8-slot array) for two backing waveguide widths ($b = 0.3\lambda_o$, $h=0.22\lambda_o$, $\Gamma_1 = \Gamma_2 = 0$, $\Omega = 2\,\ell n(4h/\epsilon) = 8.1$).

length is $h_1/\lambda_o = 0.25$, the driven element length is $h_2/\lambda_o = 0.24$, while all directors (slots 3 to 10) have the same length $h_D/\lambda_o = 0.22$. The reflector is situated $0.25\ \lambda_o$ in front of a short-circuited end of the backing waveguide ($\Gamma_1 = 0$) and $0.25\ \lambda_o$ in back of the driven element, while the spacing between the driven slot and all adjacent directors is $(\Delta z)_{dir}/\lambda_o = 0.33$. The end of the waveguide at the terminal end of the array is terminated in a matched load. By removing the backing waveguide, this array becomes complementary to a ten-element, Yagi-Uda array of equivalent cylindrical dipoles. The width parameter (Ω) for slot 2 is equal to the value $\Omega = 2\ell n(4h_2/\epsilon) = 8.10$.

Figure (5.7) indicates the experimentally measured and theoretically calculated (new array theory as described in Chapter 4) results for a ten-element Yagi-Uda slot array radiating into free-space on either side of the ground plane. Significant array parameters are shown in the top left-hand corner of the figure. Figure (5.7a) compares the relative amplitudes of slot voltages against slot number for experimental data (dotted lines) and theoretical results (solid lines). The theoretical results are obtained for both $\Omega = 2\ell n(4h_2/\epsilon) =$ 10.6 and 8.10. It is observed that the experimental data ($\Omega = 8.10$) and the theoretical results (for $\Omega = 8.10$) do not agree well, while theoretical results for $\Omega = 10.6$ follow the experimental ones relatively well. Since, from the results presented in Chapter 4 (comparison with published King-Sandler theory) it is clear that the new array theory predicts accurate results for narrow slots ($\Omega = 10.6$), it can be concluded that the new array theory cannot accurately predict the array behavior for wider slots ($\Omega = 8.10$, for instance). This is due to the fact that the peaking properties of the kernels

$h_1 = 0.25\ \lambda_o$ $(\Delta z)_{ref} = 0.25\ \lambda_o$ MM = 20

$h_2 = 0.24\ \lambda_o$ $(\Delta z)_{dir} = 0.33\ \lambda_o$

$h_3 - h_{10} = 0.22\ \lambda_o$ $n_{max} = m_{max} = 10$

$G^i = G^o$ PM = 5

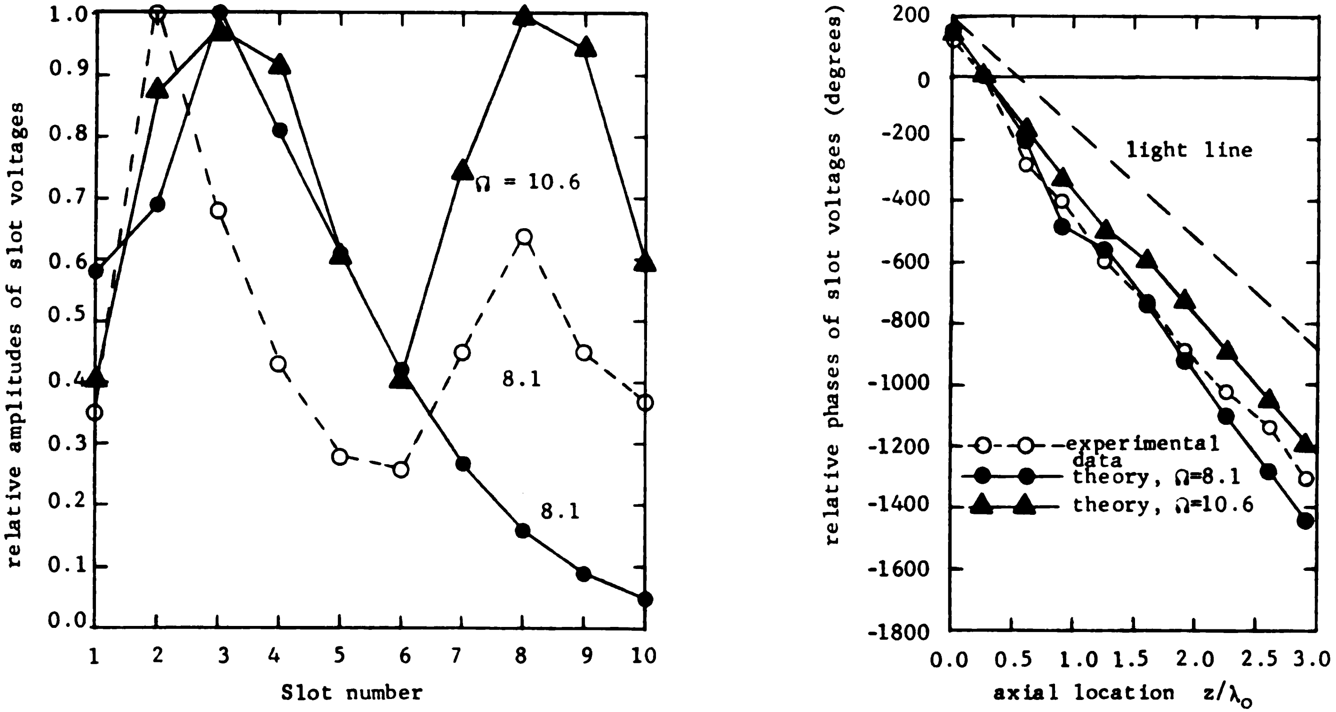

a. Amplitudes of slot voltages.

b. Phases of slot voltages

Figure 5.7. Comparison of theoretical and experimental amplitudes and phases of slot voltages in the elements of a ten-element Yagi-Uda slot array.

in the system of integral equations (upon which the approximate array theory is based) no longer exist with the behavior described in Chapter 4. It is therefore expected that the results of experimental measurements will not correspond well with the theoretical results for $\Omega = 8.10$ but might compare more closely with those for $\Omega = 10.6$.

Figure (5.7b) indicates a progressive phase delay for the field along the array aperture. It is seen from the figure that a slow wave is excited in the array aperture for all cases and that experimentally measured and theoretically predicted results are in good agreement. These aperture fields should lead to an endfire E-plane radiation field pattern.

Figure (5.8) indicates the E-plane radiation field pattern of this array. As noted above, the experimental and the theoretical results (for $\Omega = 10.6$) agree very well while for $\Omega = 8.1$, the theoretical results predict a backfire pattern with a main lobe maximum at $\theta = 180^\circ$ rather than at $\theta = 0^\circ$. This can be explained by the fact that due to the excessively slow aperture field wave and its particular amplitude distribution the phases of the slot voltages excited in the array are such that they produce a field maximum in the $\theta = 180^\circ$ direction instead of at $\theta = 0^\circ$. This assertion is confirmed by a simple calculation. Again, the non-validity of new theory for wide slots with $\Omega = 8.1$ and its relative accuracy at $\Omega = 10.6$ is confirmed.

Figure (5.9) indicates the relative amplitudes and phases of slot fields along the same Yagi-Uda slot array backed by a waveguide of width $a/\lambda_o = 0.6$. All other array parameters are the same as those of the array described above. The agreement between experimentally

$h_1 = 0.25\ \lambda_o$
$h_2 = 0.24\ \lambda_o$
$h_3 - h_{10} = 0.22\ \lambda_o$

$(\Delta z)_{ref} = 0.25\ \lambda_o$
$(\Delta z)_{dir} = 0.33\ \lambda_o$
$G^i = G^o$

$n_{max} = m_{max} = 10$
PM = 5
MM = 20

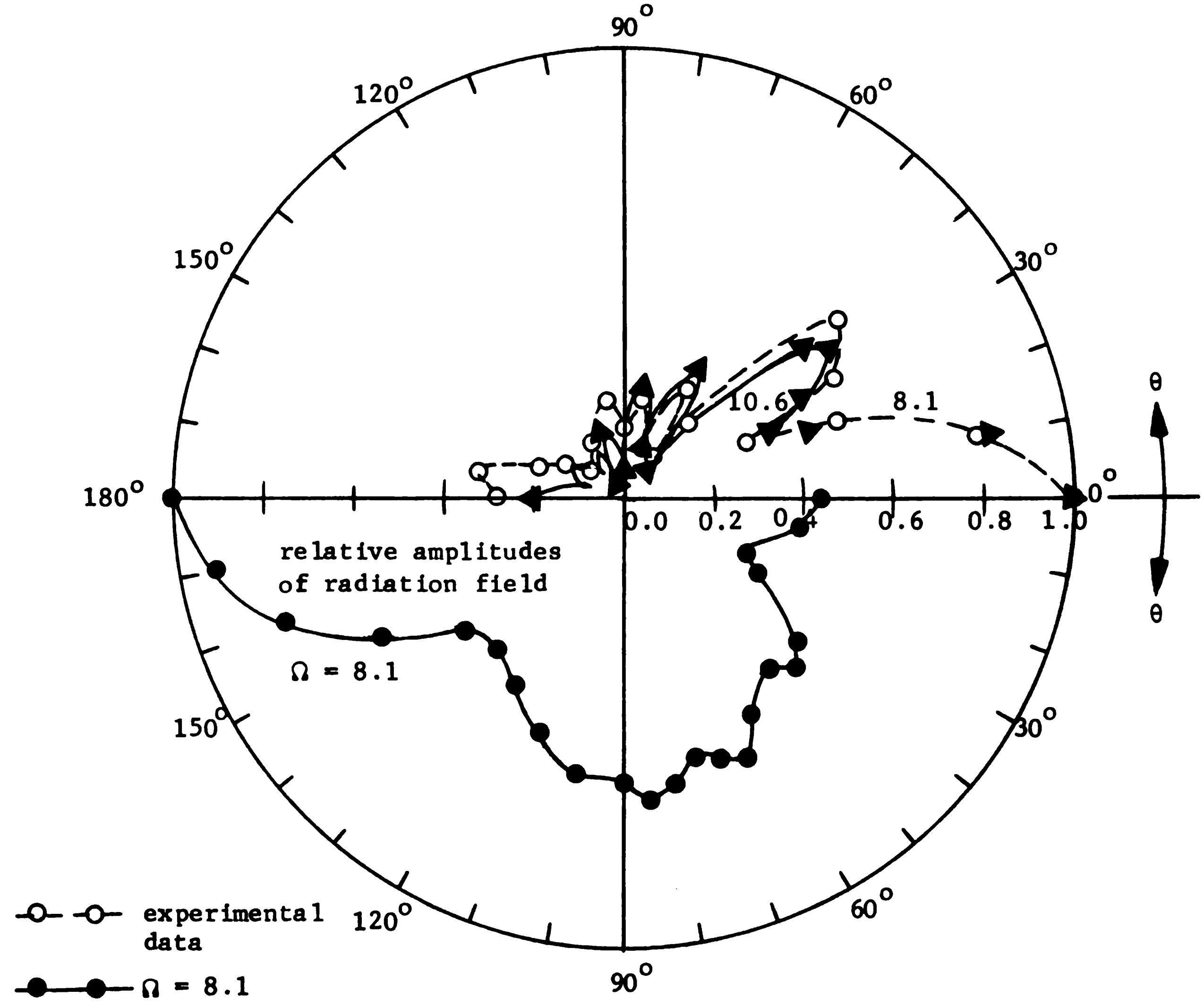

Figure 5.8. Theoretical and experimental radiation patterns for a ten-element, Yagi-Uda slot array.

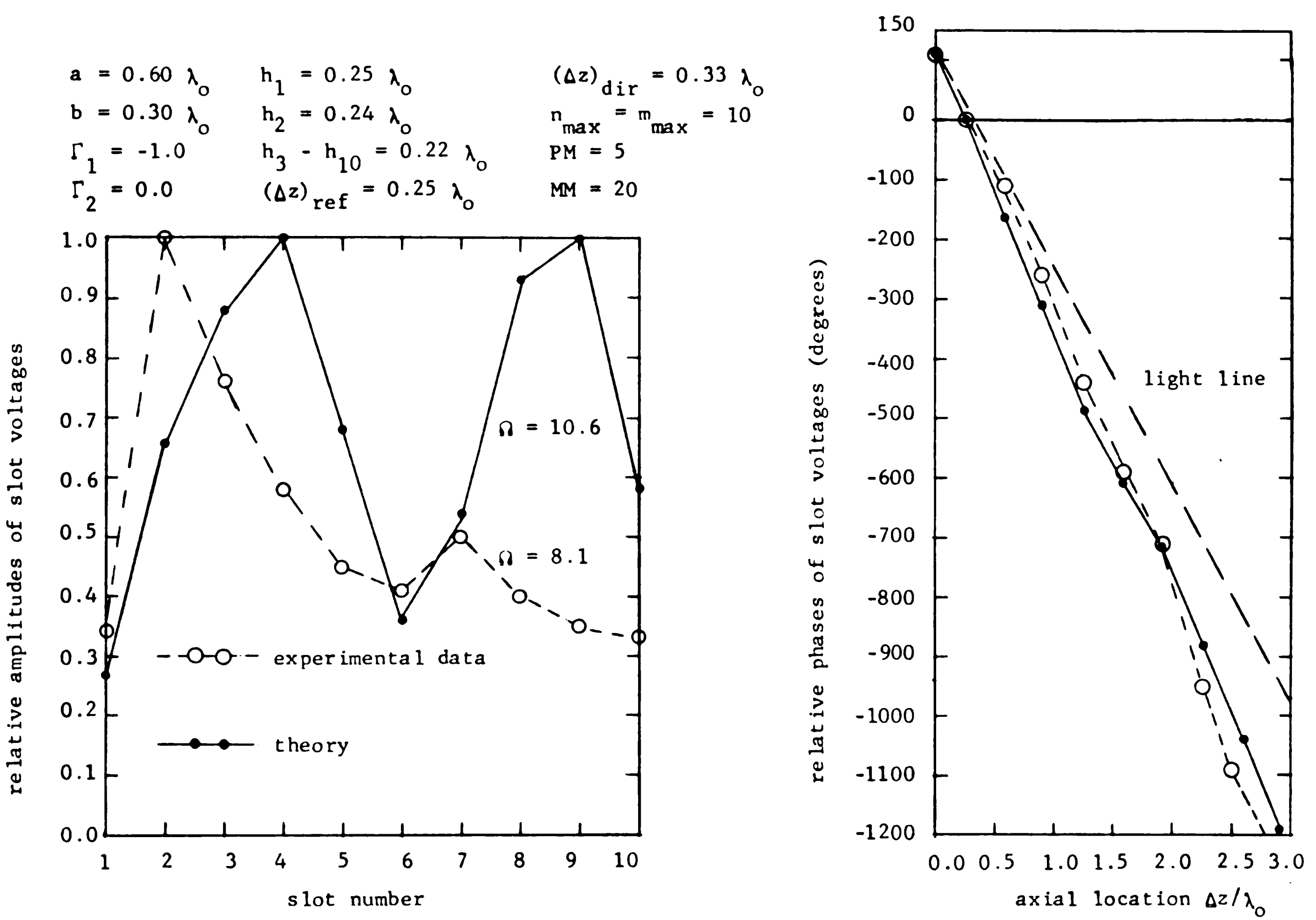

a. Amplitudes of slot voltages.

b. Phases of slot voltages.

Figure 5.9. Comparison between theoretical and experimental relative amplitudes and phases of slot voltages in the elements of a ten-element, waveguide-backed, Yagi-Uda slot array.

measured and theoretically predicted amplitude distributions (for $\Omega = 10.6$) in Figure (5.9a) is not very good; the deviation near the end of the array can be explained by reflections from the waveguide adjusting plates as discussed in section 5.3. Figure (5.9b) indicates the relative phases of slot voltages against slot locations. It is observed that experimental and theoretical results agree well and indicate a slow wave along the array aperture.

Figure (5.10) indicates a comparison between experimentally measured and theoretically predicted slot field amplitude distributions for several individual elements of the array. They are observed to compare quite closely, being essentially sinusoidal distributions in each case. Some discrepancies (for example in the plot for slot number 1) that exist between theoretical and experimental results are probably due to unavoidable experimental errors.

Figure (5.11) compares the experimental and theoretical E-plane radiation field patterns for the above array. The agreement between theory and experiment is quite good. This further confirms the conclusion that the new array theory accurately predicts the array behavior for narrow slots ($\Omega \geq 10.6$) while for wider slots ($\Omega = 8.10$) the theory fails to predict accurate results.

Finally, the circuit properties of the Yagi-Uda slot array are investigated in Tables (5.2) and (5.3). Experimental and theoretical values for the input admittance could not be compared directly due to uncertainties in the values of the attenuation and phase constants of the lossy coaxial feeder line and its exact electrical length. Since the theoretically predicted admittances for the Yagi-Uda array without waveguide backing were found to agree with

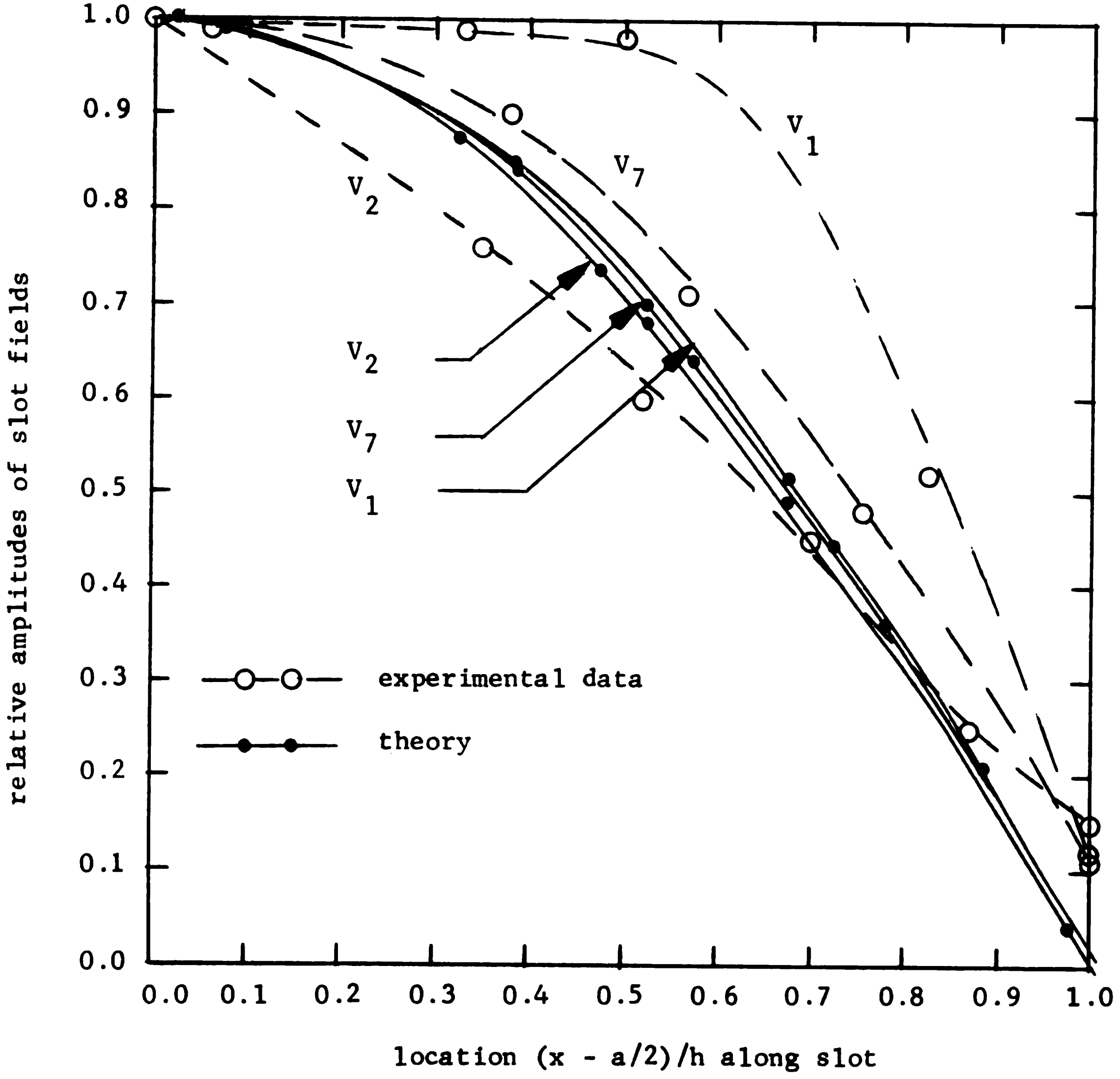

$a = 0.6\ \lambda_o$

$b = 0.3\ \lambda_o$

$\Gamma_1 = -1.0,\ \Gamma_2 = 0.0$

$\Omega = 2\ell n(4h_2/\epsilon) = 8.1$

$h_1 = 0.25\ \lambda_o$

$h_2 = 0.24\ \lambda_o$

$h_3 - h_{10} = 0.22\ \lambda_o$

$(\Delta z)_{ref} = 0.25\ \lambda_o$

$(\Delta z)_{dir} = 0.33\ \lambda_o$

$n_{max} = m_{max} = 10$

PM = 5

MM = 20

$I_2 = (1 + j0)$ AMPS

$I_{1,3\text{-}10} = 0$ AMPS

Figure 5.10. Slot field distributions in the elements of a 10-element, waveguide-backed, Yagi-Uda slot array.

$a = 0.6\ \lambda_o$

$b = 0.3\ \lambda_o$

$\Gamma_1 = -1.0$

$\Gamma_2 = 0.0$

$h_1 = 0.25\ \lambda_o$

$h_2 = 0.24\ \lambda_o$

$h_3 - h_{10} = 0.22\ \lambda_o$

$(\Delta z)_{ref} = 0.25\ \lambda_o$

$(\Delta z)_{dir} = 0.33\ \lambda_o$

$n_{max} = m_{max} = 10$

PM = 5

MM = 20

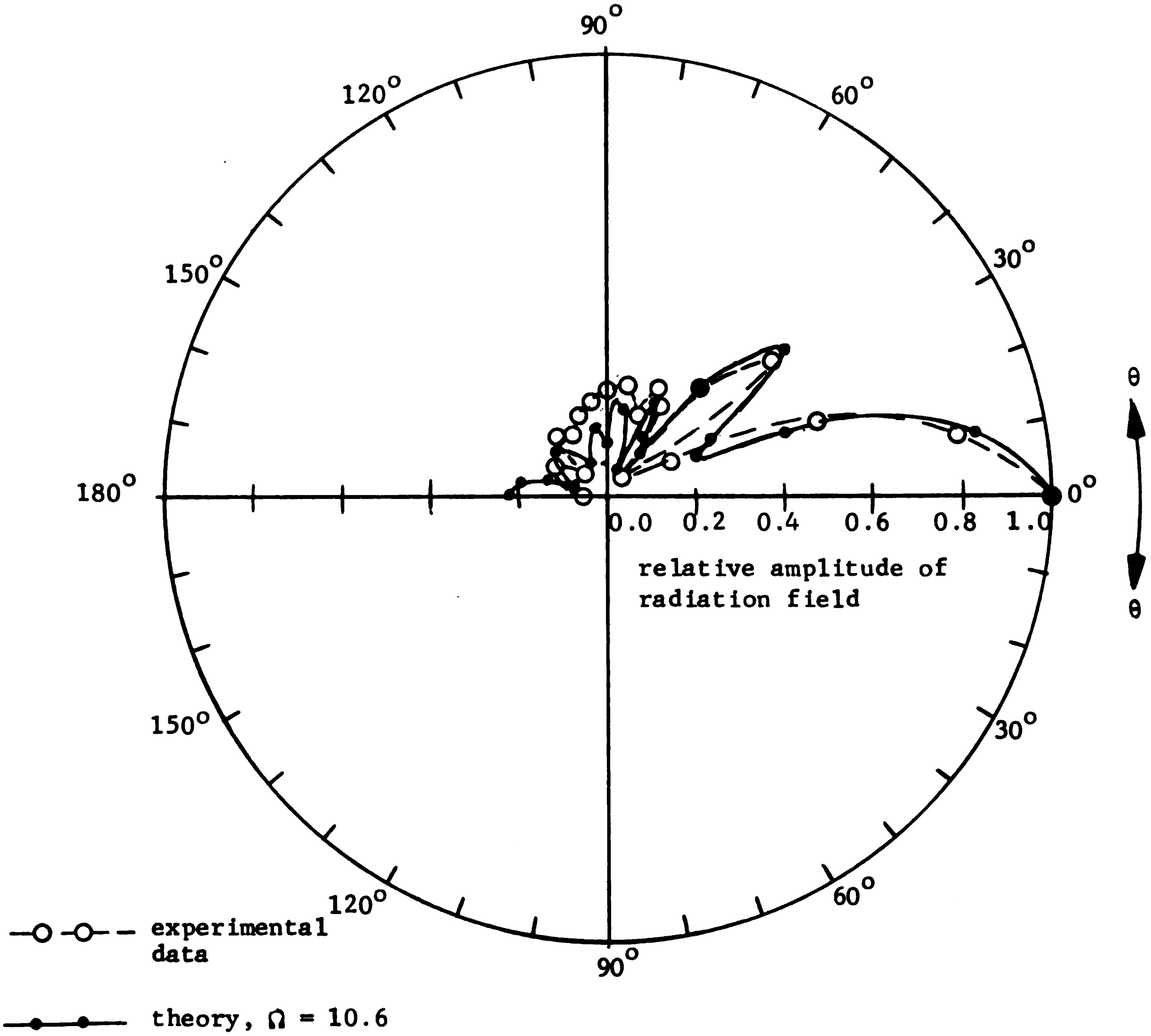

Figure 5.11. Theoretical and experimental radiation patterns for a ten-element, waveguide-backed, Yagi-Uda slot array.

$\Omega = 2\ln(4h_2/\epsilon)$	8.1	10.6
$(SWR)_{THY}$	14.0	10.5
$(SWR)_{EXP}$	7.0	-

Table 5.2. Experimental and theoretical SWR's maintained by a 10-element, waveguide-backed, Yagi-Uda slot array ($a = 0.6\ \lambda_o$, $b = 0.3\ \lambda_o$, $h_1 = 0.25\ \lambda_o$, $h_2 = 0.24\ \lambda_o$, $h_D = 0.22\lambda_o$, $(\Delta z)_{ref} = 0.25\ \lambda_o$, $(\Delta z)_{dir} = 0.33\ \lambda_o$, $\Gamma_1 = -1.0$, $\Gamma_2 = 0.0$) on its 50-ohm coaxial exciting system.

$\Omega = 2\ln(4h_2/\epsilon)$	8.1	10.6
$(SWR)_{THY}$	12.0	11.0
$(SWR)_{EXP}$	9.25	-

Table 5.3. Experimental and theoretical SWR maintained by a 10-element, Yagi-Uda slot array ($G^i = G^o$, $h_1 = 0.25\ \lambda_o$, $h_2 = 0.24\ \lambda_o$, $h_D = 0.22\ \lambda_o$, $(\Delta z)_{ref} = 0.25\ \lambda_o$, $(\Delta z)_{dir} = 0.33\ \lambda_o$) on its 50-ohm coaxial exciting system.

published results from the King-Sandler(12) array theory (and experiments) the experimental measurements were concluded to be faulty. Thus only the SWR maintained on a 50-ohm coaxial air-line section by the load impedance consisting of the input impedance to the lossy feeder line was considered. These results for the array with and without waveguide backing are presented in Tables (5.2) and (5.3). For the reasons noted earlier, the theoretical SWR's for $\Omega = 10.6$ compare best with experimental measurements for a slot array with $\Omega = 8.1$.

CHAPTER 6

SUMMARY AND CONCLUSIONS

A numerical and an approximate analytical method are applied in a theoretical investigation of the circuit and radiation properties of a waveguide-backed slot antenna array. The voltages excited in elements (slots) of this array are determined as the solution to a coupled system of integral equations by this numerical-approximate analytical approach. In terms of these slot voltages the radiation field maintained by the array as well as its input impedance (or admittance) to the driven element are subsequently evaluated. An experimental investigation of the waveguide-backed slot array was also conducted. The results of the analytical solution and those from the experiment compared favorably. It was clearly demonstrated that the results from the approximate analytical solution, when reduced to several special cases, compared favorably with previously published results. A comparison of analytical results for the special cases with the experimental data was again good.

A basic theory for the waveguide-backed slot array was formulated in Chapter 2. The EM boundary value problem is formulated theoretically in terms of a system of Hallén-type integral equations for the unknown voltaged induced in the array elements (slots). In deriving this system of integral equations, the slots were assumed to be thin and narrow such that the longitudinal components of the

slot field could be neglected. The slot field was then related to the slot voltages utilizing a quasi-static field approximation valid for narrow slots. The system of integral equations takes into account two modes of array excitation: first by an incident, dominant TE_{10}-mode wave in the backing waveguide, and secondly by means of impressed currents maintained in one (or more) of the slots. The general expressions for the radiation field maintained by the as yet unknown slot voltages are presented in the last section of Chapter 2.

Chapter 3 presents a numerical solution to the coupled system of Hallén-type integral equations for the array excited by the incident TE_{10}-mode wave. By expanding the unknown (induced) slot voltages in a series of pulse functions and subsequently point-matching the integral equations, the unknown expansion coefficients are evaluated. The input impedance to the backing waveguide was evaluated as the ratio of total transverse electric field (incident and scattered by the slots) associated with the TE_{10}-mode wave to the total transverse magnetic field of the same wave at an arbitrarily located terminal plane. The radiation field maintained by the slot array is evaluated in terms of the (now determined) coefficients for pulse functions series expansions of the slot fields.

Section 3.6 presents all the numerical results calculated by the point-matching numerical solutions for the array with TE_{10}-mode excitation. These results include relative amplitude and phase distributions of the slot voltages excited in the array elements as well as the E-plane and H-plane radiation fields maintained by the array for various array parameters. The circuit properties of this array, as described by the backing waveguide standing wave ratio, were also investigated.

It is found from the numerical results that voltage amplitude distributions in the elements of the waveguide backed slot array, excited by a dominant TE_{10}-mode wave in the backing waveguide, are very nearly sinusoidal along the slot axes; this suggests the feasibility of applying an extension of the King-Sandler dipole array theory to this problem. The relative phases of slot voltages were found to be a sensitive function of various slot spacings, $(\Delta z)/\lambda_o$, slot lengths, h/λ_o, and the backing waveguide width, a/λ_o. It can be concluded from the results presented in section 3.6 that optimal array parameters, to achieve directive end-fire radiation, were $a/\lambda_o = 0.6$, $(\Delta z)/\lambda_o = 0.1$ and $h/\lambda_o = 0.22$ for a slot width specified by $\Omega = 2\ell n(4h/\epsilon) = 10.6$. While one can achieve some degree of beam-scanning capability by departing from various of these optimal dimensions, it is found that by suitably changing a/λ_o the main lobe of the E-plane radiation field pattern can be scanned from a near broadside orientation for $a/\lambda_o = 0.505$ (near cutoff for TE_{10}-mode wave) to an endfire orientation for $a/\lambda_o = 0.70$. The backing waveguide SWR was found to be minimized for $h/\lambda_o = 0.22$, $\Delta z/\lambda_o = 0.10$ and $a/\lambda_o = 0.70$.

Chapter 4 presents an approximate analytical solution for the waveguide-backed slot array excited by impressed currents in one or more of its elements. This solution is an extension of the King-Sandler dipole array theory. For a ten-element array it is necessary to invert a matrix of order (10 X 10), whereas in the direct numerical solution described above a matrix of order at least (100 X 100) must be inverted to obtain adequate accuracy for the same array. Thus, utilizing the approximate analytical solution results in a considerable saving in computational time. (For example, average computational times for a 10-element, waveguide-backed slot array, using numerical and new array theory are 528 seconds and 215.5 seconds respectively.) This new approximate theoretical solution was tested by considering several special cases. It was observed that this theory predicts correct results for a single slot radiator (cut in an infinite ground plane) with either unbounded free-space on both sides or a backing cavity behind one side of the slot. Results for this case were compared to those for a complementary dipole in free-space and previously published theoretical and experimental results for a single, cavity-backed slot. The new array theory also predicts the correct results for an eight director (ten-element) Yagi-Uda slot array (cut in a ground screen with unbounded free-space on either side), which is complementary to a Yagi-Uda dipole array. It is also observed (by comparison with Galej's variational results) that this theory cannot predict correct slot voltage amplitude distributions for slots backed by shallow cavities, as indeed one might expect to be the case.

The optimal dimensions for a five-element Yagi-Uda, waveguide-backed slot array to produce a directive, endfire radiation field were determined to be a director element spacing of $(\Delta z)_{dir}/\lambda_o = 0.25$ and a director half-length of $h_D/\lambda_o = 0.20$ for a backing waveguide of width $a/\lambda_o = 0.6$. For a ten-element Yagi-Uda slot array, the above parameters are essentially unchanged except for $(\Delta z)_{dir}/\lambda_o$ which is now optimized as 0.30. This value of director element spacing compares quite favorably with the optimal spacing of director elements in a Yagi-Uda array of cylindrical dipoles. It was found that a large standing-wave component was always present in the aperture field of the array for relatively large director lengths, resulting in significant back radiation (large back lobe in the E-plane radiation field pattern of the array).

A ten-element, waveguide-backed slot array with all elements of equal length and the first element excited by an impressed current was also investigated. This array was expected to simulate the array investigated in Chapter 3. However, the optimal array parameters were found to closely resemble those of the Yagi-Uda type slot array rather than those of the array excited by a TE_{10}-mode incident wave, indicating that the mode of excitation of the array significantly changes its behavior and its optimum element spacings. It was observed that a large standing wave component in the relative amplitude distribution of slot fields along the array invariably results in a large back lobe in its E-plane radiation field pattern.

Investigating the input admittance to the driven elements of five- and ten-element Yagi-Uda slot arrays, it was observed that the admittance passes through resonance when the driven-element length lies between 0.22 λ_o to 0.23 λ_o. This resonant admittance presents a relatively low input conductance, which can provide a near match to practical transmission lines. The variation of input admittance for a ten-element slot array is quite similar to that for an isolated slot cut in a ground plane located in an otherwise unbounded space.

The frequency dependence of the E-plane radiation field for a ten-element Yagi-Uda slot array is investigated in section 4.5.4. This investigation reveals that the E-plane field pattern degrades rapidly as frequency is varied from a center frequency of 3.0 GHz to 2.6 GHz or 3.4 GHz. Therefore, the pattern band-width of the array appears to be approximately 400 MHz. The dependence of input admittance to the driven element as a function of frequency indicates a resonance near the center frequence of 3.0 GHz.

In all the results summarized above it was noted that the E-plane radiation field patterns have sharper main lobes (narrower beam widths) as the number of array elements is increased. A twenty five-element waveguide-backed slot array maintains a radiation pattern having a much sharper main lobe and a relatively low back lobe (if $h/\lambda_o = 0.20$) compared to the pattern for a ten-element array.

Chapter 5 indicates a comparison between various experimental results and theoretical predictions for both the dominant-mode-wave excited, waveguide-backed slot array and the arrays excited by impressed currents. The experimental and theoretical results for an eight-element waveguide-backed slot array excited by a TE_{10}-mode incident wave agree very favorably. The analytical predictions for the Yagi-Uda slot array do not agree as well with the experimental results. This can be explained by the observation that the new, extended King-Sandler array theory cannot predict accurate results for wide slots ($\Omega = 8.1$) such as those used in the experimental array.

In conclusion, the direct, numerical point-matching solution to the system of coupled integral equations for the slot voltages appears to provide an accurate analytical means to investigate both the radiation and circuit properties of waveguide-backed slot arrays. The new, approximate solution for the waveguide-backed Yagi-Uda slot array provides an efficient but somewhat less accurate means to analytically examine its radiation and circuit properties. It was found that beam-scanning can be achieved with a waveguide-backed slot array excited by an incident, dominant TE_{10}-mode, by varying the backing waveguide width. No such scanning capability can be achieved with the Yagi-Uda, waveguide-backed slot array excited by an impressed current in its driven element. The new, extended King-Sandler theory provides an analytical solution for a finite waveguide-backed slot array and also provides sufficient computational efficiency to allow calculations for large arrays within reasonable time limits.

REFERENCES

REFERENCES

(1) Burton, R.W. and R.W.P. King, "An experimental investigation of currents on a Yagi array of slot antennas on planar and curved surfaces," IEEE Trans. Ant. Prop. AP-14, 4, 451-454 (July 1966).

(2) Mailloux, R.J., "Excitation of a surface wave along an infinite Yagi-Uda array," IEEE Trans. Ant. Prop. AP-13, 5, 719-724 (September 1965).

(3) Mailloux, R.J., "The long Yagi-Uda array," IEEE Trans. Ant. Prop. AP-14, 2, 128-137 (March 1966).

(4) Coe, R.J. and G. Held, "A parasitic slot array," IEEE Trans. Ant. Prop. AP-12, 1, 10-16 (January 1964).

(5) Hyneman, R.F., "Closely-spaced transverse slots in rectangular waveguide," IRE Trans. Ant. Prop. AP-7, 4, 335-341 (October 1959).

(6) Elliott, R.S., "Serrated waveguide - part I: theory," IRE Trans. Ant. Prop. AP-5, 5, 270-275 (July 1957).

(7) Kelly, K.C. and R.S. Elliott, "Serrated waveguide - part II: experiment," IRE Trans. Ant. Prop. AP-5, 5, 276-283 (July 1957).

(8) Galejs, J., "Admittance of a rectangular slot which is backed by a rectangular cavity," IEEE Trans. Ant. Prop. AP-11, 2, 119-126 (March 1963).

(9) Galejs, J., "Hallen's method in the problem of a cavity backed rectangular slot antenna," Radio Science (J. Res. of NBS), 67D, 2, 237 (March-April 1963).

(10) Harrington, R.F., "Matrix methods for field problems," Proc. IEEE 55, 136-149 (February 1967).

(11) King, R.W.P. and S.S. Sandler, "The theory of broadside arrays," IEEE Trans. Ant. Prop. AP-12, 3, 269-275 (May 1964).

(12) King, R.W.P., R.B. Mack, and S.S. Sandler, " Array of cylindrical dipoles," Cambridge, Chapter 6, 181-232 (1968).

(13) Silver, S., "Microwave antenna theory and design," Dover Publications, Inc., New York, Chapter 9, 291-293 (1965).

(14) Collin , R.E., "Foundations for Microwave Engineering," McGraw Hill Book Co., Chapters 2 and 3, 11-143 (1966).

(15) Hong, M.H., D.P. Nyquist, and K.M. Chen, "Investigation of open-cavity radiators and backfire antennas part I: open-cavity antennas," AFCRL report, AFCRL-70-0361, (July 1970).

(16) Jackson, J.D., "Classical Electrodynamics," John Wiley and Sons, Inc., New York, Chapter 9, 268-308, (1967).

(17) Harrington, R.F., "Field computation by moment methods," The Macmillan Company, New York (1968).

(18) Booker, H.G., "Slot aerials and their relation to complementary wire aerials," J. IEE (London), 93, Pt. IIIA, 620-626 (1946).

(19) King, R.W.P. and C.W. Harrison Jr., "Antennas and Waves: A Modern Approach," The M.I.T. Press, Cambridge, Mass., Chapter 13, 657-688 (1969).

(20) Collin , R.E. and F.J. Zucker, "Antenna theory part I," McGraw Hill Book Co., (1969).

(21) King, R.W.P. and T.T. Wu, "Currents, charges and near fields of cylindrical antennas," Radio Science J. of Res. NBS/USNC-URSI, 69D, 3, 429-445 (March 1965).

(22) Watson, G.N., "A treatise on the theory of Bessel functions," 2nd ed., Cambridge Univ. Press, Cambridge, Eng., (1952).

(23) Abramowitz, M. and I.A. Stegun, "Handbook of mathematical functions," Dover Publications, Inc., New York, 495-499 (1965).

(24) King, R.W.P., "The theory of linear antennas," Harvard Univ. Press, Cambridge, Mass., 141-204 (1956).

(25) Nyquist, D.P. and S.P. Mathur, "Analysis of a parallel array of waveguide or cavity backed rectangular slot antennas," presented at the 1972 USNC/URSI-IEEE Spring Meeting, Washington, D.C., (April 13-15, 1972).

APPENDICES

APPENDIX I

APPROXIMATE EVALUATION OF AN IMPROPER INTEGRAL

The double integral

$$I = \int_{x_{km}-\Delta x_k/2}^{x_{km}+\Delta x_k/2} \int_{z_k-\Delta z/2}^{z_k+\Delta z/2} \frac{e^{-jk_oR_{km}}}{2\pi R_{km}} \, dz'dx' \qquad (I.1)$$

where

$$R_{km} = \sqrt{(x_{km} - x')^2 + (z_k - z')^2} \, ,$$

and Δx_k and Δz are small quantities (i.e., $k_o\Delta x_k \ll 1$ and $k_o\Delta z \ll 1$), is improper since its integrand has a singularity when $x' = x_{km}$ and $z' = z_k$. This integral can be evaluated analytically as outlined below.

Since $k_oR_{km} \ll 1$ in this case, by expanding the exponential into a power series and retaining only its leading two terms, equation (I.1) can be approximated as

$$I \approx \int_{x_{km}-\Delta x_k/2}^{x_{km}+\Delta x_k/2} \int_{z_k-\Delta z/2}^{z_k+\Delta z/2} \frac{(1 - jk_oR_{km})}{2\pi R_{km}} \, dz'dx'$$

or

$$I \approx \int_{x_{km}-\Delta x_k/2}^{x_{km}+\Delta x_k/2} \int_{z_k-\Delta z/2}^{z_k+\Delta z/2} \frac{1}{2\pi R_{km}} \, dz'dx' - \frac{jk_o(\Delta x_k)(\Delta z)}{2\pi} \, . \qquad (I.2)$$

If the change of variables $u = x_{km} - x'$ and $v = z_k - z'$ is made, equation (I.2) can be rewritten as or

$$I \approx \frac{2}{\pi}\{\frac{-jk_o(\Delta x_k)(\Delta z)}{4} + \frac{\Delta z}{2}\ \ell n[(\frac{\Delta x_k}{\Delta z}) + \sqrt{1 + (\frac{\Delta x_k}{\Delta z})^2}] +$$

$$\frac{\Delta x_k}{2}\ \ell n[(\frac{\Delta z}{\Delta x_k}) + \sqrt{1 + (\frac{\Delta z}{\Delta x_k})^2}]\}. \qquad (I.6)$$

APPENDIX II

EVALUATION OF DEFINITE INTEGRALS

Consider the integral

$$I_1 = \int_{z_k-\epsilon}^{z_k+\epsilon} \frac{e^{\pm\gamma_{nm}(z_k+z')}}{\sqrt{\epsilon^2 - (z' - z_k)^2}}\, dz' \qquad \text{(II.1)}$$

where $\gamma_{nm} = \alpha_{nm} + j\beta_{nm}$, and α_{nm} and β_{nm} are constants.

Let the following change of variables be made,

$$(z' - z_k) = \epsilon \cos \theta,$$

then $dz' = -\epsilon \sin \theta\, d\theta$, and equation (II.1) can be rewritten as

$$I_1 = \int_0^{\pi} \frac{e^{\pm\gamma_{nm}(2z_k + \epsilon \cos \theta)}}{\epsilon \sin \theta}\, \epsilon \sin \theta\, d\theta$$

or

$$I_1 = e^{\pm 2\gamma_{nm} z_k} \int_0^{\pi} e^{\pm\gamma_{nm}\epsilon \cos \theta}\, d\theta\ . \qquad \text{(II.2)}$$

Expression (II.2) can be evaluated for complex γ_{nm} but here it will be evaluated for the following two special cases:

(a) γ_{nm} pure real i.e., $\beta_{nm} = 0$, and

(b) γ_{nm} pure imaginary i.e., $\alpha_{nm} = 0$.

<u>Case (a)</u>: $\gamma_{nm} = \alpha_{nm} + j0$, then

$$I_1 = e^{\pm 2\alpha_{nm} z_k} \int_0^\pi e^{\pm \alpha_{nm} \epsilon \cos \theta} \, d\theta \, . \tag{II.3}$$

From Watson (22), it is observed that

$$\int_0^\pi e^{\pm x \cos \theta} \, dx = \pi \, I_o(x),$$

where $I_o(x)$ is the modified Bessel function of the first kind of zeroth order with argument x. Thus, letting $x = (\alpha_{nm}\epsilon)$, expression (II.3) becomes

$$I_1 = e^{\pm 2\alpha_{nm} z_k} [\pi \, I_o(\alpha_{nm}\epsilon)]. \tag{II.4}$$

<u>Case (b)</u>: $\gamma_{nm} = 0 + j\beta_{nm}$, then

$$I_1 = e^{\pm j2\beta_{nm} z_k} \int_0^\pi e^{\pm j\beta_{nm}\epsilon \cdot \cos \theta} \, d\theta \, . \tag{II.5}$$

Again, by Watson (22), it is observed that

$$\int_0^\pi e^{jx \cos \theta} \, d\theta = \pi \, J_o(x),$$

where $J_o(x)$ is the Bessel function of the first kind of zeroth order with argument x. It must be noted, however, that $J_o(x)$ is an even function of x such that $J_o(x) = J_o(-x)$. Therefore

$$\int_0^\pi e^{\pm jx \cos \theta} = \pi \, J_o(x),$$

and expression (II.5) becomes

$$I_1 = e^{\pm j2\beta_{nm} z_k} [\pi \, J_o(\beta_{nm}\epsilon)]. \tag{II.6}$$

Consider the following definite integral

$$I_2 = \int_{z_k-\varepsilon}^{z_k+\varepsilon} \frac{e^{\pm\gamma_{nm}|z_k - z'|}}{\sqrt{\varepsilon^2 - (z_k - z')^2}}\, dz' , \tag{II.7}$$

where $\gamma_{nm} = \alpha_{nm} + j\beta_{nm}$, and α_{nm} and β_{nm} are constants. Making the following change of variables

$$z_k - z' = \varepsilon \cos \theta$$

then $-dz' = -\varepsilon \sin \theta \, d\theta$, and expression (II.7) can be rewritten as

$$I_2 = \int_0^{\pi} \frac{e^{\pm\gamma_{nm}|\varepsilon \cos \theta|}}{\varepsilon \sin \theta} \cdot \varepsilon \sin \theta \, d\theta$$

or

$$I_2 = 2\int_0^{\pi/2} e^{\pm\gamma_{nm}\varepsilon \cos \theta}\, d\theta \, . \tag{II.8}$$

Expression (II.8) can be evaluated for the following two cases:

(a) γ_{nm} pure real i.e., $\beta_{nm} = 0$, and

(b) γ_{nm} pure imaginary i.e., $\alpha_{nm} = 0$.

<u>Case (a)</u>: $\gamma_{nm} = \alpha_{nm} + j0$, then

$$\begin{aligned} I_2 &= 2\int_0^{\pi/2} e^{\pm\alpha_{nm}\varepsilon \cos \theta}\, d\theta \\ &= 2\int_0^{\pi/2} \cosh(\alpha_{nm}\varepsilon \cos \theta)d\theta \pm 2\int_0^{\pi/2} \sinh(\alpha_{nm}\varepsilon \cos \theta)d\theta . \end{aligned} \tag{II.9}$$

From the Handbook of Mathematical Functions (23):

$$2\int_0^{\pi/2} \sinh(x \cos \theta)d\theta = \pi\, L_o(x), \text{ and}$$

$$2\int_0^{\pi/2} \cosh(x \cos \theta)d\theta = \pi\, I_o(x),$$

where $L_o(x)$ is the modified Struve function of zeroth order with argument x and $I_o(x)$ is the modified Bessel function of the first kind of zeroth order with argument x. Therefore, expression (II.9) can be written as

$$I_2 = \pi[I_o(\alpha_{nm}\varepsilon) \pm L_o(\alpha_{nm}\varepsilon)] \; . \qquad \text{(II.10)}$$

Case (b): $\gamma_{nm} = 0 + j\beta_{nm}$, then

$$I_2 = 2\int_0^{\pi/2} e^{\pm j\beta_{nm}\varepsilon \cos\theta}\, d\theta ,$$

or

$$I_2 = 2\int_0^{\pi/2} \cos(\beta_{nm}\varepsilon \cos\theta)d\theta \pm 2j\int_0^{\pi/2} \sin(\beta_{nm}\varepsilon \cos\theta)d\theta . \qquad \text{(II.11)}$$

From Handbook of Mathematical Functions (23):

$$2\int_o^{\pi/2} \sin(x \cos\theta)d\theta = \pi\, H_o(x), \text{ and}$$

$$2\int_o^{\pi/2} \cos(x \cos\theta)d\theta = \pi\, J_o(x),$$

where $H_o(x)$ is the Struve function of zeroth order with argument x, and $J_o(x)$ is the Bessel function of zeroth order with argument x. Using the above results, expression (II.11) can be written as

$$I_2 = \pi[J_o(\beta_{nm}\varepsilon) \pm jH_o(\beta_{nm}\varepsilon)] \; . \qquad \text{(II.12)}$$

In summary,

$$I_1 = \int_{z_k-\epsilon}^{z_k+\epsilon} \frac{e^{\pm\gamma_{nm}(z_k+z')}}{\sqrt{\epsilon^2-(z'-z_k)^2}}\,dz' = \begin{cases} \pi e^{\pm 2\alpha_{nm}z_k} I_o(\alpha_{nm}\epsilon) \ldots \text{ for } \gamma_{nm}=\alpha_{nm}+j0, \\ \\ \pi e^{\pm j2\beta_{nm}z_k} J_o(\beta_{nm}\epsilon) \ldots \text{ for } \gamma_{nm}=0+j\beta_{nm}, \end{cases}$$

and

$$I_2 = \int_{z_k-\epsilon}^{z_k+\epsilon} \frac{e^{\pm\gamma_{nm}|z_k-z'|}}{\sqrt{\epsilon^2-(z_k-z')^2}}\,dz' = \begin{cases} \pi[I_o(\alpha_{nm}\epsilon) \pm L_o(\alpha_{nm}\epsilon)] \ldots \text{ for } \gamma_{nm}=\alpha_{nm}+j0, \\ \\ \pi[J_o(\beta_{nm}\epsilon) \pm jH_o(\beta_{nm}\epsilon)] \ldots \text{ for } \gamma_{nm}=0+j\beta_{nm}. \end{cases}$$